KU LEUVEN

ARENBERG DOCTORAL SCHOOL
FACULTY OF SCIENCE

Aquifer Thermal Energy Storage under different hydrochemical and hydrogeological conditions

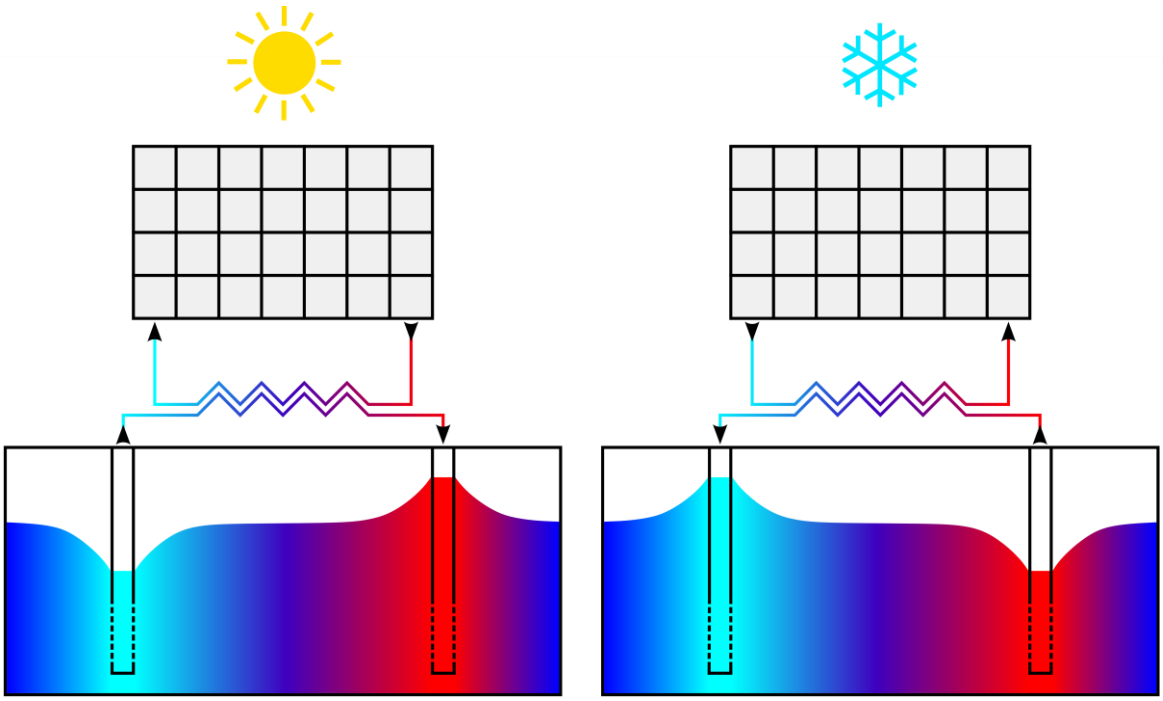

Mathias Possemiers

Supervisors:
Prof. Dr. Okke Batelaan
Prof. Dr. Ir. Marijke Huysmans

Dissertation presented in partial fulfilment of the requirements for the degree of Doctor of Science

December 2014

Aquifer Thermal Energy Storage under different hydrochemical and hydrogeological conditions

Mathias Possemiers

Examination committee:

Prof. Dr. Noël Vandenberghe, *chairman*

Prof. Dr. Okke Batelaan, *supervisor*

Prof. Dr. Ir. Marijke Huysmans, *co-supervisor*

Prof. Dr. Philippe Muchez

Prof. Dr. Ir. Alain Dassargues

Département ArGEnCo, Université de Liège

Dr. Boris van Breukelen

Department of Earth Sciences, VU Amsterdam

Dr. Simon Six

Afdeling Winning en Leefmilieu, De Watergroep

Dissertation presented in partial fulfilment of the requirements for the degree of Doctor of Science

December 2014

Uitgegeven in eigen beheer, Mathias Possemiers, Heverlee.

ISBN nummer: 978-90-8649-770-6

Wettelijk depotnummer: D/2014/10705/78

ISSN 0250-7803

Aardkundige Mededelingen 44

Dankwoord

Zo'n vier jaar geleden kreeg ik een telefoontje van Marijke en een mailtje van Okke met de vraag of ik bij hen een doctoraat zou willen starten. Ik had op dat moment al enkele maanden een boeiende job, wat de keuze niet gemakkelijk maakte. Na een aantal dagen twijfelen, besloot ik dan toch naar Leuven terug te keren. Ik heb hierbij erg veel bijgeleerd en heb dan ook (bijna) nog geen moment spijt gehad van deze keuze…

Eerst en vooral wil ik dan ook mijn promotoren Prof. Okke Batelaan en Prof. Marijke Huysmans bedanken voor deze kans. Bedankt voor het vertrouwen, in het begin door me de vrijheid te geven mijn eigen onderzoek te definiëren en doorheen het project door me mijn eigen weg in het onderzoek te laten vinden. Okke wil ik graag bedanken voor de mogelijkheid die ik kreeg om hem te bezoeken in Adelaide aan Flinders University, mijn onderzoek te kunnen presenteren op congressen in Wenen en Perth, en de cursus Reactive Transport Modeling te volgen in Rome. Marijke wil ik graag bedanken voor haar meer dagelijkse begeleiding, wanneer ze nog als postdoc in onze bureau zat, maar ook daarna met haar wekelijkse bezoekjes vanuit Brussel.

Ik wil ook graag de andere leden van mijn doctoraatsjury: Prof. Noël Vandenberghe, Prof. Alain Dassargues, Prof. Philippe Muchez, Boris van Breukelen en Simon Six bedanken voor hun interesse in mijn onderzoek. Hun constructieve opmerkingen hebben in grote mate bijgedragen tot dit proefschrift.

In het bijzonder wil ik verder Jos Van Steenwinkel en Yves Meyus bedanken, voor het begrip wanneer ik al na een half jaar AGT verliet, voor het aanbrengen van onderzoeksideeën en voor me in het kader van dit doctoraat te betrekken in IFTech projecten. Bedankt ook om me steeds als "één van jullie" te zijn blijven zien en voor het vertrouwen om me straks opnieuw bij AGT te laten beginnen.

Een groot deel van mijn onderzoek leunt sterk op gegevens die door anderen werden verzameld. Ik bedank Jos Van Steenwinkel en Ywan Dejonghe (VMM) voor het aanleveren van de noodzakelijke gegevens. Simon Six (De Watergroep), Karel De Mey (PIDPA) en Benno Drijver (IFTechnology) wil ik graag bedanken voor hun inbreng in verband met de uitdagingen in verband met KWO. Hun input in het begin van dit doctoraatsproject heeft mee de weg bepaald die dit onderzoek is ingeslagen. Verder bedank ik Vincent Post (Flinders University) voor de waardevolle inbreng met betrekking tot de reactieve transport modellen en Koen Zuurbier (KWR Watercycle Research Institute) voor het verstrekken van de aangepaste versie van PHT3D en voor de hulp met enkele modelkwesties. Rieko wil ik graag bedanken voor zijn hulp met de kwantificatie van de mineralen met XRD en Wouter Vienne bedank ik voor de aangename samenwerking op het terrein. Een dikke merci ook aan Ria en Petra voor het regelen van alle administratie.

Ik bedank alle collega's in het Geo-instituut voor de aangename middag- en koffiepauzes. In het bijzonder bedank ik hier mijn jaargenoten Katrijn, Tom en Jorik voor de 9 onvergetelijke jaren in Leuven. Ik wil ook graag Koen T. bedanken voor de goede samenwerking rond de oefenzittingen van geologie en GAS I voor de eerste bachelor studenten. Wim en Koen V. bedank ik graag voor de aangename samenwerking op de jaarlijkse Luxemburg excursie: jullie (en een onvermijdelijke Bofferding) maakten het verbeteren van notaboekjes tot laat op de avond best verteerbaar. Met mijn meest constante bureaugenootje Benedicta deelde ik niet alleen dezelfde deadlines maar ook een promotor in Australië. Bene, bedankt voor jouw steun en aanstekelijke lach!

Ine en Christian wil ik graag bedanken voor de toffe tijd in Adelaide, van de lunchpauzes met 'vegan pies' tot de uitstapjes in het weekend. Ine, bedankt om me op sleeptouw te nemen met jullie autootje naar McLaren Vale en Goolwa, en voor de fietstocht naar Belair NP.

Graag wil ik hier nog mijn familie en vrienden bedanken voor de afleiding die ze me boden, maar ook voor de steun waarop ik steeds kon rekenen. In het bijzonder wil ik mijn ouders bedanken omdat ze mij steeds alle

mogelijkheden hebben gegeven. Mama, Papa en Benjamin, bedankt ook voor de goede thuis. Mijn schoonouders, Rita en Eddy wil ik graag bedanken voor de goede zorgen doorheen de werkweek gedurende de laatste twee jaar. Tenslotte wil ik Elke bedanken om me steeds te motiveren, voor het begrip en geduld wanneer ik iets minder geduldig was of wanneer iets niet zo goed lukte. Schat, ik kijk uit naar de toekomst, met binnenkort onze verhuis naar ons eigen huisje en onze trouw op 30 mei!

Abstract

Energy storage techniques are receiving a growing interest because renewable energy is not always available when needed. One of these energy storage technologies is Aquifer Thermal Energy Storage (ATES). In an ATES system the thermal energy available at the surface is seasonally stored in an aquifer through injection and extraction of groundwater. During summer, cool groundwater is extracted from the cold well(s) for cooling purposes. Through this process the water is heated after which it is injected in the warm well(s). During winter this system is reversed and the stored warm water is extracted for heating purposes. The cooled water is then re-injected into the cold well(s). In this way, warm and cold zones arise around the ATES wells in the subsurface and a seasonal storage of thermal energy is created.

The increasing number of ATES systems leads to concerns by drinking water companies and environmental regulators about the long term impacts of ATES systems on groundwater quality. Additionally, only a small part of the subsurface in Flanders meets the optimal conditions for ATES, i.e. the presence of a thick, reasonable homogeneous aquifer. Therefore, the question is posed whether ATES is also feasible in less favorable conditions such as aquifers with varying redox conditions or aquifers characterized by sedimentary heterogeneity. The possibility to install ATES systems in such suboptimal conditions would largely increase the applicability of ATES in Flanders.

In the first part of the study, the influence of ATES on groundwater chemistry is assessed by means of a literature review and a comparison of groundwater quality monitoring data at seven ATES systems with ambient groundwater quality values from 69 monitoring wells in Flanders. The seven evaluated Aquifer Thermal Energy Storage (ATES) systems are positioned in key aquifers, which contain major groundwater resources for the region. The results of the analysis of the hydrochemical data confirm that the small temperature differences ($\Delta T \leq 10$) at which the ATES systems operate do not influence the concentrations of the main chemical constituents. Mixing of shallow with deeper groundwater during ATES operation, on the other hand, can alter groundwater quality. So, an integrated design of ATES systems taking into account the groundwater chemistry is very important, especially in phreatic aquifers and in the vicinity of public drinking water supply well fields.

Well clogging due to iron (hydr)oxide precipitation is a widespread problem in aquifers with varying redox conditions from which the performance of ATES wells may also suffer. The interactions between physical and chemical processes during ATES operation are, however, not well understood. In the second part of the study, the reactive transport modeling code PHT3D is used to assess the effects of alternating pumping by ATES systems near the redox boundary on the precipitation of iron hydroxides for two cases in Flanders. Results show that in both investigated cases, initial mixing plays an important role in the development of $Fe(OH)_3$ precipitation around the wells. The models further predict that even small temperature differences have a significant effect on the $Fe(OH)_3$ concentration. Avoiding the mixing of oxygen/nitrate rich water with iron rich water remains the best strategy to prevent well clogging.

Recent model studies indicate that meter-scale heterogeneities in the hydraulic conductivity field introduce considerable uncertainty in the distribution of thermal energy around an ATES system and can lead to a reduction in the thermal recoverability. In the third part of the study, the influence of centimeter-scale clay drapes on the efficiency of a doublet ATES system and the distribution of the thermal energy around the ATES wells is quantified. Multiple-point geostatistical simulation of edge properties is used to incorporate the clay drapes in the models. The results show that clay drapes have an influence both on the distribution of thermal energy in the subsurface and on the efficiency of an ATES system. The distribution of the thermal energy is determined by the strike of the clay drapes, with the major axis of anisotropy parallel to the clay drape strike. The clay drapes have a negative impact on ATES efficiency in the models without a hydraulic

gradient. In the models with a hydraulic gradient, however, the presence of clay drapes has a positive influence on the efficiency of the ATES system. It is recommended to incorporate small scale heterogeneities in heat transport models to get a better estimate on ATES efficiency and distribution of thermal energy.

To conclude, the results of this thesis show that the groundwater quality changes induced by ATES are rather small. However, phreatic aquifers are more vulnerable and especially near drinking water production sites, an integrated ATES design, taking the groundwater chemistry into account, is indispensable. Each feasibility study for ATES in aquifers with varying redox conditions should incorporate an analysis of the hydrochemistry at several depths. In this way, the well screen setting can be optimized and the risk of well clogging due to iron (hydr)oxide precipitation is reduced. A good insight in the heterogeneity of an aquifer is indispensable for a proper positioning of ATES wells, as even small scale sedimentary features can have a large impact on the distribution of thermal energy and on the efficiency of an ATES system.

Samenvatting

Aangezien hernieuwbare energie niet altijd beschikbaar is wanneer nodig, is er een stijgende interesse in de opslag van deze energie. Eén van de energieopslagtechnieken is koude-warmte opslag (KWO). Bij KWO wordt de thermische energie die beschikbaar is aan de oppervlakte opgeslagen in een aquifer door middel van injectie en extractie van grondwater. In de zomer kan op die manier koel grondwater worden opgepompt van de koude bron(nen) voor koeling. Hierbij warmt dit water op, waarna het wordt geïnjecteerd in de warme bron(nen). In de winter wordt dit systeem omgedraaid en wordt het opgeslagen warme water opgepompt voor verwarmingsdoeleinden. Het afgekoelde water wordt vervolgens opnieuw geïnjecteerd in de koude bron(nen). Op deze manier ontstaan er warme en koude zones rond de KWO putten in de ondergrond en wordt een seizoensgebonden opslag van thermische energie gecreëerd.

Het stijgende aantal KWO systemen leidt tot ongerustheid bij drinkwaterbedrijven en milieu-instanties over de langetermijneffecten van KWO op de grondwaterkwaliteit. Verder beantwoord slechts een klein deel van de ondergrond in Vlaanderen aan de optimale condities voor KWO, namelijk de aanwezigheid van een dikke, redelijk homogene aquifer. Daarom rijst de vraag of KWO ook mogelijk is in suboptimale condities zoals in aquifers met variërende redox omstandigheden of in aquifers gekenmerkt door sedimentaire heterogeniteit. De mogelijkheid om KWO systemen in zulke omstandigheden te installeren, zou de toepasbaarheid van KWO in Vlaanderen immers sterk verhogen.

In het eerste deel van deze studie wordt de invloed van KWO op de grondwaterkwaliteit onderzocht door middel van een literatuurstudie en een vergelijking van de grondwaterchemie in zeven KWO installaties, met de grondwaterchemie in 69 peilbuizen in Vlaanderen. De zeven geëvalueerde KWO systemen bevinden zich in belangrijke aquifers met grote grondwatervoorraden voor de regio. De analyse van de hydrochemische data bevestigt dat de kleine temperatuursverschillen ($\Delta T \leq 10$) waarmee de KWO systemen werken, geen significante invloed hebben op de concentraties van de chemische hoofdelementen. Het mengen van ondiep met dieper grondwater tijdens KWO werking, kan echter wel een invloed hebben op de grondwaterchemie. Een geïntegreerd ontwerp van KWO systemen, rekening houdend met de plaatselijke grondwaterchemie is dus onmisbaar, vooral in freatische aquifers en in de nabijheid van sites voor drinkwaterproductie.

Putverstopping veroorzaakt door ijzer-(hydr)oxide neerslag is een veelvoorkomend probleem in aquifers met variërende redoxcondities, waaronder ook KWO putten kunnen lijden. De interactie tussen fysische en chemische processen tijdens KWO zijn echter niet goed begrepen. In het tweede deel van deze studie wordt de code voor reactief transport, PHT3D, gebruikt om de effecten van KWO systemen nabij de redoxgrens op de neerslag van ijzerhydroxiden te kunnen beoordelen. Hiervoor werden twee sites gekozen met verschillende redoxcondities. De resultaten tonen aan dat in beide gevallen, het initieel mengen een belangrijke rol speelt bij de ontwikkeling van $Fe(OH)_3$ neerslag rond de putten. De modellen voorspellen verder dat zelfs kleine temperatuursveranderingen een significant effect hebben op de $Fe(OH)_3$ concentratie. Het vermijden van het mengen van zuurstof/nitraatrijk water met ijzerrijk water blijft dan ook de beste manier om putverstopping te vermijden.

Recente modelstudies geven aan dat groot-schalige (m) heterogeniteit in doorlatendheid een aanzienlijke onzekerheid in de distributie van thermische energie rond KWO systemen met zich meebrengt en eveneens kan leiden tot een vermindering in efficiëntie. In het derde deel van deze studie wordt de invloed van kleinschalige (cm) kleilaagjes op de efficiëntie van een doublet KWO systeem en op de distributie van de thermische energie rond KWO putten gekwantificeerd. Om de kleilaagjes in de modellen te implementeren, werd de methode van ‘multiple-point geostatistical simulation of edge properties’ gebruikt. De resultaten tonen aan dat kleilaagjes een invloed hebben op zowel de distributie van thermische energie in de

ondergrond als op de efficiëntie van een KWO systeem. De distributie van de thermische energie wordt bepaald door de strekking van de kleilaagjes, waarbij de grootste anisotropie-as parallel is aan de strekking van de kleilaagjes. De kleilaagjes hebben verder een negatieve invloed op KWO efficiëntie in de modellen zonder hydraulische gradiënt. In de modellen met een hydraulische gradiënt echter, heeft de aanwezigheid van kleilaagjes een positieve invloed op de efficiëntie van het KWO systeem. Het wordt daarom aanbevolen om kleinschalige heterogeniteit in warmtetransport modellen in te bouwen om zo een betere inschatting te kunnen maken van de efficiëntie van KWO systemen en van de distributie van thermische energie in de ondergrond.

De resultaten van deze thesis tonen dus aan dat de veranderingen in grondwaterkwaliteit, die worden veroorzaakt door KWO, relatief klein zijn. Freatische aquifers zijn echter meer kwetsbaar en vooral in de buurt van waterwingebieden is een geïntegreerd KWO ontwerp, dat rekening houdt met de grondwaterchemie, onmisbaar. Verder zou elke haalbaarheidstudie voor KWO in aquifers met variërende redox omstandigheden, een analyse van de grondwaterchemie op verschillende dieptes moeten inhouden. Op die manier kan de positie van de putfilters worden geoptimaliseerd en wordt het risico op putverstopping door ijzer(hydr)oxides verkleind. Een goed inzicht in de heterogeniteit van de aquifer is onmisbaar voor een correcte plaatsing van de KWO putten. Zelfs kleinschalige sedimentaire structuren kunnen immers een grote impact hebben op de distributie van thermische energie en op de efficiëntie van een KWO systeem.

List of Abbreviations

A_{pyr}/V	Ratio of pyrite surface area to solution volume
ASR	Aquifer Storage and Recovery
ATES	Aquifer Thermal Energy Storage
BTES	Borehole Thermal Energy Storage
c_a	Volumetric heat capacity of the aquifer (matrix and water)
C_{H+}	Proton concentration
C_{NO3-}	Concentration of nitrate
C_{O2}	Dissolved oxygen concentration
COD	Chemical Oxygen Demand
CPU	Central Processing Unit
c_s	Specific heat capacity of the solid phase
CTES	Cavern Thermal Energy Storage
c_w	Specific heat capacity of water
CW	Cold well
D_m	Molecular diffusion coefficient
D_{m_temp}	Thermal diffusion coefficient
DO	Dissolved Oxygen
DOC	Dissolved Organic Carbon
Eh	Oxidation-reduction potential
GWHP	Groundwater Heat Pump
H	Well screen length
K	Equilibrium constant
K_{d_temp}	Thermal distribution coefficient
K_h	Horizontal hydraulic conductivity
K_v	Vertical hydraulic conductivity
l_v	Liter bulk volume
l_w	Liter pore water
mbs	Meters below surface
MMOC	Modified Method of Characteristics

n	Porosity of the aquifer
Q	Well discharge
RAM	Random-access Memory
SR	Saturation Ratio
STES	Seasonal Thermal Energy Storage
T_c	Groundwater temperature
TIC	Total Inorganic Carbon
T_{ref}	Reference temperature
TVD	Total Variation Diminishing
UTES	Underground Thermal Energy Storage
V	Volume of water that is injected in one storage phase
VOCs	Volatile Organic Compounds
WW	Warm well
XRD	X-ray diffractometry
ΔH	Enthalpy of reaction
ΔT	Temperature difference
λ_e	Bulk thermal conductivity of the aquifer
ρ	Bulk density
ρ_w	Density of water

Contents

List of Figures

List of Tables

Chapter 1

Introduction

1.1 Background

Environmental concerns and an increasing pressure on fossil fuels cause a rapidly growing interest in renewable energy. The renewable energy sources are biomass, geothermal energy, hydropower, ocean power, solar energy and wind energy. Hydropower, ocean power and wind energy are used for electricity production, whereas the other energy sources can be used for both electricity production and direct heating. Biomass, additionally can be used for the production of biofuel (IEA, 2014). Next to these energy technologies, energy storage gets more and more attention since renewable energy is not always available when needed the most. Energy storage therefore contributes to a more efficient use of these fluctuating renewable energy sources (Gao et al., 2009). Electricity can be stored in batteries, as chemical energy but also as potential energy in elevated water reservoirs. Thermal energy can be stored as heat and cold, both on the short term (day-night) and on the long term (season). Short term energy storage is commonly used, e.g., warm water is prepared by a solar water heater, stored and used when needed or ice is made at night, when electricity is cheap and used during the day to cool the air in buildings. Seasonal Thermal Energy Storage (STES) allows heat and cold to be used months after it was stored. The most common STES technology is Underground Thermal Energy Storage (UTES). In UTES, the subsurface is used as storage medium for heat and cold. UTES technologies can be subdivided in three main variants, ATES (Aquifer Thermal Energy Storage), BTES (Borehole Thermal Energy Storage) and CTES (Cavern Thermal Energy Storage).

In Aquifer Thermal Energy Storage (ATES), also called groundwater heat pumps (GWHP), open loop ground source heat pumps or open systems, the groundwater and aquifer material act as a storage medium for thermal energy (Meyer and Todd, 1973). An ATES system typically consists of one or more extraction and injection wells (Figure 1.1). During summer, cool groundwater is extracted from the cold well(s). By means of a heat exchanger, the thermal energy is transferred to cool the building. Through this process, the water is heated after which it is injected in the warm well(s). During winter, this system reverses and

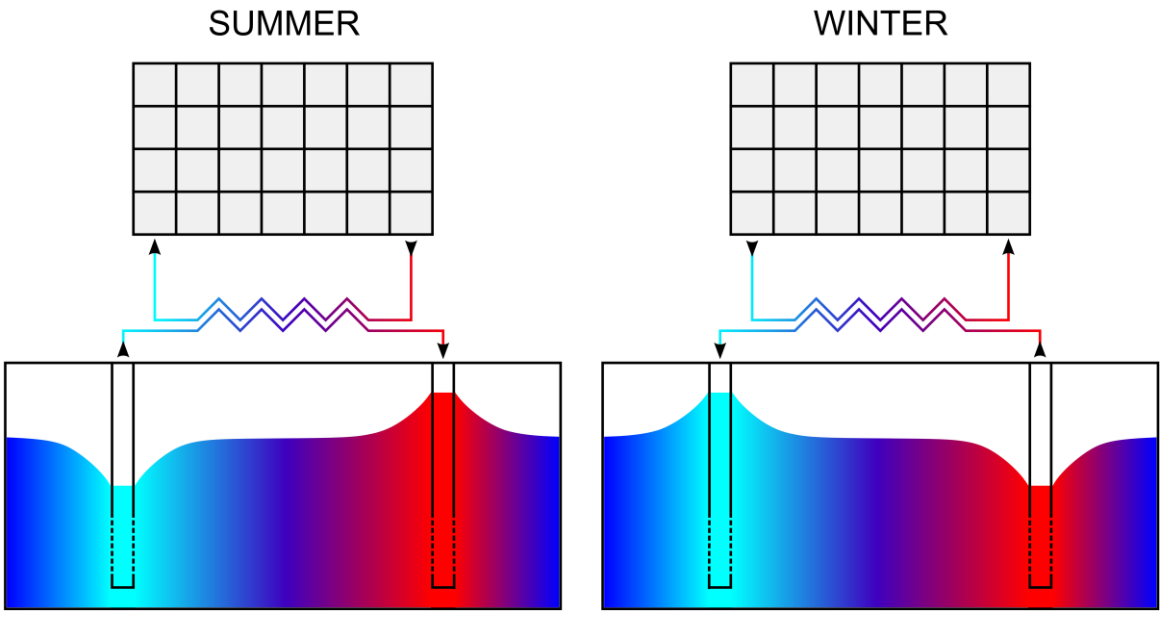

Figure 1.1 ATES principle. In the summer cool groundwater is extracted from the aquifer (cold well) and by means of a heat exchanger, the cold is delivered to the building (passive cooling). Through this process the water is heated after which it is injected back in the aquifer at the warm well. In the winter this system is reversed and the stored warm water is extracted. Via a heat exchanger this heat is extracted at the evaporator of the heat pump after which it is further heated by the compressor and finally it is delivered to the building via the condenser of the heat pump. The cooled groundwater is then re-injected into the cold well. In summer, this cooled water can then be re-used. This process creates a cycle of seasonal thermal energy storage.

the stored warm water is extracted. Via a heat exchanger the thermal energy is extracted at the evaporator of a heat pump and is delivered to the building via the condenser of the heat pump at a higher temperature level, suitable for comfort heating. The cooled groundwater is then re-injected into the cold well(s). During summer, this cooled water can then be re-used. This process creates a cycle of seasonal thermal energy storage. Most ATES systems operate with only small temperature differences (ΔT<15°C) between the warm (<20°C) and the cold (ca. 5°C) wells in shallow aquifers with an ambient groundwater temperature of about 11° to 12 °C. Variants of ATES systems are mono-well systems and recirculation systems. In a mono-well the borehole is equipped with two wells with different well screen settings. The warm water is stored and extracted via the upper well screen; the cold water is stored and extracted via the lower well screen. In a recirculation system the flow direction is not reversed. A recirculation system is thus either used for cooling or for heating purposes. When used for cooling, cold water is injected during winter to avoid aquifer warming. When used for heating, warm water is injected during summer to avoid aquifer cooling.

In Borehole Thermal Energy Storage (BTES), also called closed loop ground source heat pumps (GSHP) or closed systems, the thermal energy is stored and recovered with a closed hydraulic circuit consisting of one or more boreholes with vertical heat exchangers. BTES systems generally require more boreholes to deliver the same power compared to ATES (Bonte, 2013). The heat exchangers consist of plastic tubes wherein a fluid (commonly a water-glycol mixture) is circulated and absorbs the thermal energy (heat and cold) from the ground. In addition to vertical heat exchangers also horizontal closed systems and energy piles are used. In horizontal closed systems, the heat exchangers are installed horizontally in trenches of about 1 m depth. In energy piles, the heat exchangers are embedded in the foundation piles of buildings (Mustafa Omer, 2008).

Cavern Thermal Energy Storage (CTES) is a technique which can only be used in a few places as it is applied in flooded mines or other man-made chambers (Michel, 2009).

The choice between one of these UTES variants is strongly determined by the subsurface characteristics. For the application of ATES an aquifer must be present that can provide a sufficient flow rate and a good water quality to avoid corrosion and clogging of the wells and piping. As no groundwater is extracted during BTES operation, the requirements for the subsurface are less strict than for ATES, but a high thermal conductivity is desirable. The higher the thermal conductivity, the less meters of borehole and heat exchangers have to be installed which determines the total cost of a BTES installation. CTES can only be used at a limited number of locations, e.g. old mining areas.

This research project is focused on ATES. Worldwide, the number of ATES systems has been continuously increasing over the last 15 years and is expected to increase further in the future. In the Netherlands, the number of ATES systems has grown from around 29 installations in 1995 to around 1800 in 2012 (Bonte, 2013). Similar growth rates are reported in other European countries like Switzerland, Sweden and Germany (Sanner et al., 2003), in China (Gao et al., 2009) and in the US (Lund and Bertani, 2010), both for ATES and associated thermal energy storage systems such as Borehole Thermal Energy Storage (BTES) (Bayer et al., 2012; Bonte et al., 2011b; Hähnlein et al., 2013; Lund et al., 2004, 2011; Rybach, 2010). In the northern part of Belgium (Flanders), there are much less ATES systems operational (about 20 large systems (>250 kW) in 2011), but a growing demand is expected.

This evolution from only a few ATES systems to a much greater density of such systems poses several practical as well as scientific questions and challenges. The first challenge associated with an increasing number of ATES systems in Flanders is the concern of public drinking water companies (e.g. De Watergroep, PIDPA) and environmental regulators such as the Flemish Environment Agency (VMM) about the impact of ATES systems on groundwater quality. As more installations appear, they will inevitably be placed in the vicinity of public drinking water supply well fields. A second challenge in Flanders is that only a small part of the subsurface meets the optimal conditions for

ATES: i.e. the presence of a thick, geologically and geochemically homogeneous aquifer. This raises the question whether ATES is also cost-effective and reliable in geologically or geochemically heterogeneous aquifers, such as aquifers with varying redox conditions and aquifers characterized by fine scale sedimentary structures.

1.2 Research objectives and questions

Based on these challenges, this study has three main objectives. The first objective is to determine the impact of existing ATES systems on the groundwater quality on the long term. The second objective is to assess iron (hydr)oxide precipitation around ATES wells in phreatic aquifers. The third and last objective is to determine the effect of small scale sedimentary features (clay drapes) on the distribution of thermal energy and the efficiency of an ATES system. In order to reach these objectives, the following research questions and sub-questions should be answered:

1. What is the impact of existing ATES systems on groundwater quality on the long term?
   - What does the international literature report on the effects of ATES on groundwater quality?
   - Do the small temperature differences (<10°C) at which the ATES systems in Flanders operate have an influence on groundwater quality?
   - Does mixing of shallow with deeper groundwater have an influence on groundwater quality?

2. What is the effect of alternating pumping by ATES systems near the redox boundary on the precipitation of iron (hydr)oxides?
   - What is the extent and location of the precipitation?
   - What is the impact of temperature, well screen setting and flow rate on the precipitation?
   - Can reactive transport modeling help in determining the effects?

3. Do centimeter-scale clay drapes have an effect on heat transport around ATES wells?
   - What is the effect of clay drapes on the distribution of thermal energy around the wells?
   - What is the effect of clay drapes on the recovered temperatures and the efficiency of an ATES system?

1.3 Outline of the thesis

These research questions will be answered in the following chapters and are finally discussed in the last chapter.

Chapter 2 relates to research question 1. It presents a literature review on the influence of ATES on groundwater chemistry, illustrated with new groundwater quality monitoring data of seven Aquifer Thermal Energy Storage systems situated in Flanders, which are compared with the ambient groundwater quality values measured in 69 monitoring wells and the Flemish drinking water standard.

Chapter 3 relates to research question 2. It addresses the problem of iron (hydr)oxide precipitation at Aquifer Thermal Energy Storage (ATES) wells. Using reactive transport modeling the effects of alternating pumping by ATES wells on the precipitation of iron hydroxides is assessed for two case studies with different redox conditions.

Chapter 4 relates to research question 3. It presents a heat transport modeling study to investigate the effect of clay drapes on the distribution of thermal energy around ATES wells and the impact that these small scale clay drapes have on the efficiency of an ATES system.

Chapter 5 synthesizes the results and conclusions. This final chapter further lists some recommendations for future research.

Chapter 2

Influence of Aquifer Thermal Energy Storage on groundwater quality: A review illustrated by seven case studies from Belgium

Modified from: Possemiers, M., Huysmans, M., Batelaan O. 2014. Influence of Aquifer Thermal Energy Storage on groundwater quality: A review illustrated by seven case studies from Belgium. Journal of Hydrology: Regional Studies 2: 20-34. DOI: 10.1016/j.ejrh.2014.08.001

2.1 Introduction

Because of the large growth in the demand for Aquifer Thermal Energy Storage, ATES systems are expected to be installed increasingly in the vicinity of drinking water production sites and protected nature areas. This leads to concerns by environmental regulators and drinking water companies about the environmental impacts of ATES installations, such as hydrological, thermal, chemical and microbiological impacts (Arning et al., 2006; Bonte et al., 2011a; Brielmann et al., 2011, 2009; Brons et al., 1991; Griffioen and Appelo, 1993; Hall et al., 2008; Zhu et al., 2011). In addition, according to EU environmental policy, these impacts should be minimized so that no detrimental effects can occur (EU-WFD, 2000).

This study presents a review of published research about the interaction between ATES and groundwater chemistry. This review is illustrated by a new hydrochemical dataset from seven ATES systems in Flanders.

2.2 Influence of ATES on groundwater chemistry: a review

To assess the effect of the storage of thermal energy on the groundwater chemistry a literature review was conducted. The possible impacts of ATES were divided into the effects caused by changes in temperature and the effects caused by mixing different groundwater qualities.

2.2.1 Temperature effects

As a result of reactions between groundwater and the surrounding aquifer material, groundwater contains a wide variety of dissolved chemical constituents in various concentrations. Temperature changes can cause alteration of groundwater chemistry as temperature plays a very important role in the solubility of minerals, reaction kinetics, oxidation of organic matter, redox processes and sorption-desorption of anions and cations (Arning et al., 2006; Brons et al., 1991; Griffioen and Appelo, 1993; Holm et al., 1987; Hoyer et al., 1994; Sowers et al., 2006).

Mineral equilibria

Most research on this topic is focused on operational aspects such as scaling due to mineral precipitation at higher temperatures (>60°C) (Arning et al., 2006; Griffioen and Appelo, 1993; Holm et al., 1987; Palmer and Cherry, 1984). The goal of these studies was to predict and prevent problems of clogging caused by the effect of temperature changes on mineral equilibria. Therefore, most research on the effect of temperature on the solubility of minerals in aquifers was focused on the solubility of minerals responsible for clogging. At a thermally balanced ATES system, solutes resulting from dissolved minerals are transported between wells. A mineral can dissolve in one well and precipitate in the other well and vice versa. At temperatures higher than 60°C, silicates for example will dissolve, resulting in high Si concentrations at the warm well and precipitation of silicates (e.g. talc, quartz) at the cold well. For carbonates on the other hand (e.g. $CaCO_3$ and $FeCO_3$), precipitation will occur at the warm well and dissolution will occur at the cold well (Brons et al., 1991; Griffioen and Appelo, 1993; Holm et al., 1987; Hoyer et al., 1994; Jenne et al., 1992; Perlinger et al., 1987; van Oostrom et al., 2010).

The effect on mineral equilibria is smaller for ATES systems at lower temperatures. A geochemical modeling study on the effects of heating and cooling at a heat storage system in aquifers, shows that heating of groundwater from 10 to 50 °C significantly reduces porosity and permeability by calcium precipitation (Palmer and Cherry, 1984). In practice, however, calcium precipitation does not occur when the temperature rise is limited (Drijver, 2011). Different temperatures are mentioned in the literature, varying from 50 °C (Heidemij, 1987), 40 to 60 °C (Snijders, 1994, 1991) and 60 to 70 °C (Knoche et al., 2003). The fact that no precipitation occurs despite significant oversaturation is attributed to the presence of inhibitors (e.g. phosphates, organic acids). Furthermore, these temperatures are still significantly higher than the temperature range (5 to 20°C) of most current ATES systems.

Hartog et al. (2013) showed with the Van 't Hoff equation that there is a limited impact for such small temperature changes in ATES systems with an underground thermal balance, as the effect of temperature on equilibrium constants is opposite for temperature increases and decreases. In a study on the effect of the discharge of cooling water into groundwater, differences in groundwater temperature (8.7 – 17.8 °C) did not result in detectable changes in groundwater chemistry and were smaller than seasonal changes in the shallow groundwater (Brielmann et al., 2009). In another study on the effect of rising groundwater temperature (from 10°C to 20°C in 10 years) due to a thermal imbalance at a low temperature ATES system, no significant changes in time were found for pH, conductivity and the considered anion and cation concentrations (Sowers et al., 2006). According to the available literature the effect of low temperature (<25°C) ATES systems on mineral equilibria is expected to be limited.

Kinetics

Many of the reactions that occur in groundwater systems are however not determined by chemical equilibria but by kinetic processes (Appelo and Postma, 2005). Examples of kinetically controlled reactions in groundwater systems are weathering reactions of silicates and redox reactions (van Oostrom et al., 2010). ATES field tests at high temperatures (40 – 100°C) for example showed that K-feldspar weathering progresses faster around the warm well then around the cold well (Holm et al., 1987; Perlinger et al., 1987). Prommer and Stuyfzand (2005) demonstrated that redox reactions in groundwater are affected by small temperature differences. In their study, surface water with a variable temperature (2 - 23 °C) was injected during two years. Differences in breakthrough in the monitoring wells indicated that the oxidation of pyrite and organic matter by oxygen and nitrate proceeds significantly faster at higher temperatures. When the ATES system is in thermal balance, however, no significant temperature effects are expected from the Arrhenius equation when $\Delta T < 20^{o}C$. If there is an unbalance in energy input and output in the ATES system, or if the temperature differences are larger ($\Delta T > 20^{o}C$), the effects of the temperature on kinetics increases due to the exponential dependence of reaction rates on temperature (Hartog, 2011).

Organic matter

Laboratory research (Brons et al., 1991) into the effect of temperature on organic matter in aquifers demonstrated that at temperatures above 45°C organic carbon is mobilized resulting in an increased chemical oxygen demand (COD) of the groundwater. The ability of the remaining organic matter to adsorb organic micro pollutants or trace elements may hereby decrease (TCB, 2009; van Oostrom et al., 2010). Two more recent studies (Bonte et al., 2013b; Jesußek et al., 2012) reported increased concentrations of DOC with increasing temperature in a laboratory setting. It was shown that the occurrence and rate of nitrate, sulfate and iron reduction are strongly dependent on temperature. At 70°C, a change in sediment sorption behavior for cations and organic acids was assumed based on changes in pH, Mg and K concentration. At 10°C to 40°C, on the other hand, no clear changes of pH, total inorganic carbon (TIC) and the major cations occurred. Incubation experiments have shown that when organic acids and orthophosphates are present, a strong oversaturation of the carbonates is possible because of precipitation inhibition. An increase in temperature leads, at the one hand, to a reduced solubility of calcium and magnesium carbonates (carbonate precipitation) and, on the other hand, carbonate precipitation is inhibited by mobilization of dissolved organic carbon. The calcium content in groundwater is therefore less influenced by temperature than expected solely based on equilibrium reactions (Griffioen and Appelo, 1993).

Redox processes

Jesußek et al. (2012) showed with their column experiments that temperatures of 25°C and above lead to the mobilization of organic carbon and an increase in microbial activity. The increased availability of organic carbon combined with a higher microbial activity causes the redox zoning to shift towards more reducing conditions. Since the occurrence and rate of nitrate, iron and sulfate reduction are dependent on the redox conditions a temperature increase

can have a strong influence on these processes. The findings of this study predict that at temperatures of 25°C and higher, the usability of groundwater as drinking and process water can be impaired by reducing metal oxides and thus possibly releasing heavy metals from the sediment.

The column experiments performed by Bonte et al. (2013a, 2013b) showed that water quality was not affected when anoxic aquifer sediments were subjected to lower temperature (5°C) than in-situ temperature (11°C). But at 25°C, the concentration of As was significantly increased and at 60°C also significant effects on the pH, dissolved organic carbon (DOC), P, K, Si, Mo, V, B and F were observed. The same experimental setup was used to determine the effect of temperature variations (5-80°C) on redox processes and associated microbial communities (Bonte et al., 2013a). Both the hydrochemical and microbiological data showed that a temperature increase from the in situ 11°C to 25°C caused a shift from iron-reducing to sulfate-reducing and methanogenic conditions. A further temperature increase to more than 45°C resulted in the emergence of a thermophilic microbial community specialized in fermentation and sulfate reduction.

Sorption - desorption

Natural or contaminant organic components in groundwater can adsorb to sedimentary components, in particular organic material. In addition, groundwater composition is influenced by cation-exchange on clay minerals and oxides. A hydrogeochemical reactive transport model (PHREEQC) using the results from previously described column experiments (Bonte et al., 2013a, 2013b) revealed that sorption of anions decreases with temperature whereas sorption of cations increases with temperature (Bonte, 2013). Results showed that As and B are desorbed in the centre of the warm water plume and mobilized towards the fringe of the warm water plume and the centre of the cold water plume where these solutes become resorbed. According to Chiang et al. (2001), sorption of chlorinated methanes (carbon tetrachloride (CCl_4), chloroform ($CHCl_3$), methylene chloride (CH_2Cl_2)) also depends on temperature. Sorption of these VOCs decreases with increasing temperature. From about 8°C to 16°C, this decrease is about 10%. Since cation-exchange in aquifers takes place competitively on clay minerals, oxides and organic matter, each with other exchange properties, the derivation of thermodynamic constants per cation is difficult. Research showed that at room temperature K^+, Cs^+ and NH_4^+ are more strongly adsorbed than Ca^{2+}, Mg^{2+} and Na^+. This difference however decreases with rising temperature. Further, divalent cations adsorb stronger with increasing temperature than the monovalent Na^+ (Appelo et al., 1990; Drijver and Willemsen, 2004). Because of the stronger adsorption of Ca^{2+} at increasing temperatures, the precipitation of calcite at higher temperatures will be reduced to some extent (TNO, 1990). Additionally, Griffioen and Appelo (1993) noted that ammonium (NH_4^+) and divalent iron (Fe^{2+}) preferably desorb upon an increase of the temperature (van Oostrom et al., 2010).

2.2.2 Mixing

Besides the effect of temperature on geochemical processes within an ATES system, mixing will also have an influence on groundwater chemistry. Although this process is not specific for ATES (e.g. return dewatering), it may be an important factor for changes in groundwater chemistry (van Oostrom et al., 2010). Groundwater often presents concentration gradients with depth, even within the same aquifer (Bonte et al., 2011b). The more heterogeneous the aquifer and the more reactive the sediment, the more pronounced the stratification of groundwater (Hartog et al., 2002).

Gradients

The expected impact of mixing depends on the type of gradient over which mixing occurs (TCB, 2009): redox gradient, chloride gradient, pH gradient or contamination gradient. Redox gradients are caused by redox reactions occurring within groundwater and by the interaction of groundwater with the sediment. It is common practice to avoid mixing of oxygen and nitrate rich shallow groundwater with deeper iron containing groundwater. Mixing of waters with these and other contrasting redox

conditions may result in the formation of gas phases (N_2, CO_2), formation of biomass and precipitation of oxides (FeOOH, MnOOH) which can all lead to well clogging and are thus operationally undesirable. In addition, changes in redox conditions can induce oxidation of reduced minerals (e.g. pyrite) or reduction of oxides (e.g. Fe-oxides) whereby trace elements and metals can be mobilized (Descourvières et al., 2010). Another type of gradient is a fresh-salt water gradient or chloride gradient. In addition to the effect of salinity on the usability of groundwater, the increased ionic strength will have an effect on mineral equilibria. Further, cations may be desorbed from exchanger sites by the higher sodium levels in saline/brackish water. A third type of gradient is a pH- or groundwater hardness gradient. Mixing of sources of groundwater with a different hardness can lead to dissolution of calcite (Sanz et al., 2011). In addition to the presence of calcite in aquifer sediments, also the CO_2 partial pressure has an influence on the pH and hardness of the groundwater (Appelo and Postma, 2005). Mixing of groundwater with different CO_2 partial pressure and equal temperature leads to an undersaturation of calcite. In the model study of Palmer et al. (1992), the possible effects of CO_2 gas pressure changes on the calcium balance in ATES systems are described. At equal temperature, a reduction in CO_2 partial pressure can lead to precipitation of calcite. These effects are also observed during lab experiments with 14 Dutch groundwater samples (Willemsen and Appelo, 1985). Finally, the transport of contaminants to the deeper groundwater can be accelerated by mixing processes. For contaminants where the degradation depends on redox conditions, mixing can create either more or less favorable conditions for degradation (van Oostrom et al., 2010; Zuurbier et al., 2013).

The extent to which ATES systems mix different groundwater types depends on the screen length, sealing practice and water quality distribution in the aquifer surrounding the well screens. To achieve the desired flow rates, water is often extracted over a large portion of the aquifer. Where water quality differences are present over the screen length, mixing may lead to changes in groundwater composition around the ATES wells. The effects of mixing in the extraction wells are comparable to the effects observed in drinking water wells, including clogging. However, the effects in the extraction wells of an ATES system are expected to be smaller since drinking water wells only produce groundwater and, therefore continuously pull water quality transition zones towards the wells. ATES wells on the other hand usually switch pumping direction twice a year, so that the main share of the water that is pumped has already been pumped and mixed in the previous season. As a consequence drinking water wells have a much higher probability to mix different types of groundwater. In ATES systems on the other hand, the pumped, mixed groundwater is re-injected into the aquifer in a nearby well, which is (usually) not the case for drinking water wells. Geochemical changes related to the injection of water are discussed in the context of Aquifer Storage and Recovery (ASR) (Descourvières et al., 2010; Prommer and Stuyfzand, 2005; Pyne, 2005). In ASR systems, often oxic (surface) water is injected into anoxic aquifers and the geochemical effects are therefore larger than for ATES systems in which (mixed) water from the same aquifer is re-injected. In the storage volume, the native water is replaced by the injected water, and a new hydrochemical and geochemical equilibrium will be installed over time.

A field and modeling study in the Netherlands (Bonte et al., 2013c) showed that ATES operation results in homogenization of the natural redox zoning in the aquifer, which may trigger secondary reactions such as mobilization of trace elements and organic carbon. However, the results of the investigated site showed that the observed concentration changes are sufficiently small to keep groundwater suitable for drinking water production from a chemical point of view.

The mixing of shallow groundwater, more influenced by human activity, with deeper, less influenced groundwater by ATES operation however implies that the risk of pollution of a public drinking water supply well field nearby can be increased.

Mixing processes

Three types of mixing can be distinguished (Figure 2.1). First there is the initial mixing of different groundwater types withdrawn over the well screen length at the ATES startup. This process determines the initial composition of the ATES water. In presence of vertical heterogeneity in hydraulic conductivity, this hydraulic conductivity will determine the contribution of the different groundwater types to the mixed ATES water. Secondly there is a continuous inflow and replacement of a portion of the ATES water by ambient groundwater. The importance of this mixing type is determined by the regional groundwater flow rate, compared to the ATES discharge and recharge rate. Again the hydraulic conductivity over the depth range is important because it will determine the flow paths of the inflowing ambient water. Thirdly, mixing will occur at the interface between the injected mixed water from the ATES and the surrounding groundwater by dispersion processes. These processes will be especially important when there is sufficient contrast between the composition of the mixed water in the ATES and the ambient groundwater (Dinkla et al., 2012). In addition to these three types, the water balance of the ATES system is also important for mixing. A yearly imbalance between extraction and injection will lead to some extra initial mixing each year.

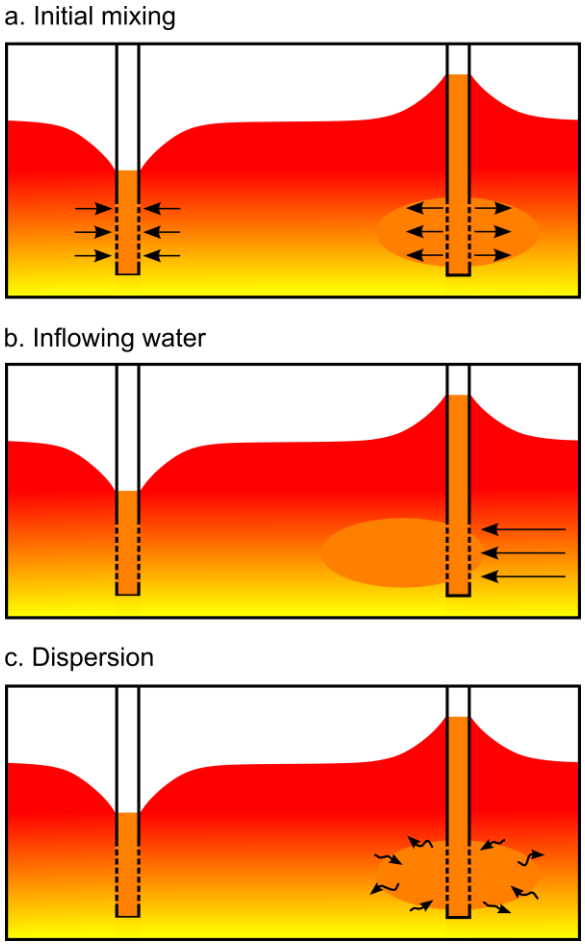

Figure 2.1 Mixing processes; **a**: initial mixing process; **b**: continuous inflow and replacement of a portion of the ATES water by ambient groundwater; **c**: dispersion processes.

2.2.3 Conclusions

Based on literature, ATES may have an impact on groundwater quality in two different ways. On the one hand, extraction, mixing and injection of shallow groundwater with deeper groundwater over a large well screen length can have an important influence on groundwater quality. For example, mobilization of trace elements and organic carbon can be induced by changing the natural redox conditions and contaminants can be introduced in deeper pristine groundwater. The temperature changes (<15°C) handled in current ATES systems, on the other hand, seem to have hardly any effect on the chemistry of the main chemical constituents in the groundwater. But redox sensitivity to small changes in temperature (Prommer and Stuyfzand, 2005) and especially the increased mobility of arsenic observed in laboratory experiments (Bonte et al., 2013b) show that further research and monitoring are necessary.

2.3 Materials and Methods

The groundwater chemistry around seven ATES installations in Flanders is evaluated (Figure 2.2). The selected ATES systems are located in several key aquifers, which represent major groundwater resources for the region.

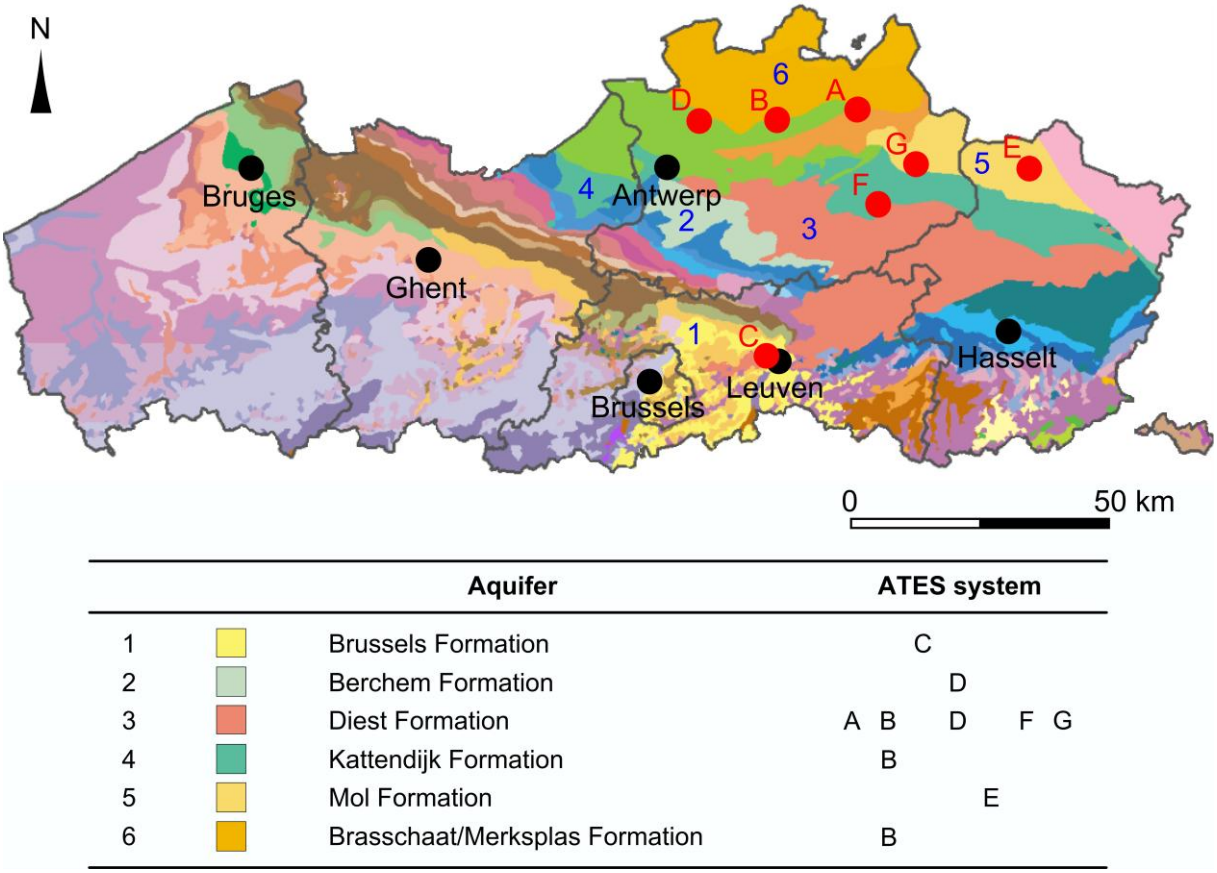

		Aquifer	ATES system
1		Brussels Formation	C
2		Berchem Formation	D
3		Diest Formation	A B D F G
4		Kattendijk Formation	B
5		Mol Formation	E
6		Brasschaat/Merksplas Formation	B

Figure 2.2 Tertiary subcrop map of Flanders with the designation of the used aquifers and locations of the studied ATES systems (red dots) (adapted from DOV, 2014).

In Flanders, the main chemical constituents of groundwater in the cold and warm wells of all ATES systems are reported at least once a year to the environmental authorities in the context of their environmental permit. The ambient groundwater composition is measured once a year by the VMM (Flemish Environment Agency) in their monitoring wells (Monitoring Network 1 - Primary Groundwater Monitoring Network). The available time series (four to eight years) of the groundwater chemistry in the ATES wells are investigated for seven ATES systems and compared with the time series of the ambient values in the used aquifer. For this study, an inventory was made of all monitoring wells in the used aquifer in a 10 km radius around each of the seven ATES systems. The time series of the monitoring data for the different solutes in all ATES wells were analyzed using linear regression analysis to determine if the data series show significant trends. For that purpose, statistical hypothesis testing was conducted on the slope of the regression line. The null hypothesis of zero slope was evaluated at 5% significance level.

The different aquifers studied (Figure 2.2) are described below in chronological order. The *Brussels Formation* is an early Middle Eocene shallow marine sand deposit in central Belgium. The Brussels Sands occur in a 40 km wide SSW-NNE oriented zone in central Belgium. These sands fill an approximately 120 km long and 40 km wide embayment which ended in the north of the Province of Antwerp in the Eocene North Sea. The base of the sands is characterized by two central major SSW-NNE trending troughs and several minor troughs with the same orientation. The Brussels Sands consist of unconsolidated quartz sands with variable percentages of feldspar, flint, glauconite, lime and heavy minerals (Gulinck and Hacquaert, 1954). The groundwater in the aquifer is of $CaHCO_3$ type (Stuyfzand, 1986) because of the presence of lime in the Brussels Sands and the layers above. At several locations the most shallow part of the aquifer has suffered of increased concentrations in

nitrate, chloride and sulfate correlated with antropogenic activity (Peeters, 2014).

The *Berchem Formation* is an early Miocene shallow marine sand deposit in the north of Belgium. The Berchem Formation consists of green to black, fine to medium grained, often slightly clayey, very glauconitic sand. The sand is rich in shells which appear dispersed in the sediment or concentrated in subhorizontal layers. At some locations however, the sand can be decalcified.

The *Diest Formation* is deposited in the late Miocene during a large transgression. In erosive trenches, the deposit can be more than 100 meters thick. The Diest Formation consists of grey-green to brownish glauconitic coarse sands wherein sandstone layers often occur. The unit contains almost no fossils, except very locally.

The *Kattendijk Formation* is deposited in the early Pliocene. The Kattendijk Sands consist of dark grey to green-grey, fine to medium grained, slightly clayey glauconitic sand. Shells appear dispersed in the sand but also concentrated in one or more layers.

The late Pliocene *Mol Formation* is a white coarse to medium grained sand deposit. It sometimes contains lignite and clay lenses. Locally the lower part is slightly glauconitic (Laga et al., 2001).

Both the *Brasschaat and Merksplas Formation* are late Pliocene estuarine deposits occurring in the northern Campine area. The Merksplas Formation consists of a grey medium to coarse grained sand with glauconite and wood fragments. The sands contain shell fragments in the lower part and occasionally gravel. The Brasschaat Formation is a dominantly sandy complex with a grain size distribution ranging from very fine to medium grained sand. Beside typical minerals such as micas and glauconite, the unit also contains vegetation remains, peat and wood fragments. The Merksplas and Brasschaat Formations are partly lateral facies (Gullentops et al., 2001).

The Formations of Berchem, Diest, Kattendijk, Mol, Merksplas and Brasschaat together form the Neogene Aquifer. The natural groundwater composition of this aquifer is characterized by low levels of chloride (<25 mg/l). The composition of the groundwater is further determined by the oxidation of organic matter creating a strong vertical variation in groundwater quality. Pyrite oxidation occurs in the shallow groundwater introducing high amounts of sulfate (to 100 mg/l) and iron (>50 mg/l). Deeper in the aquifer these concentrations decrease due to sulfate reduction. In the infiltration areas the groundwater is mostly of $CaSO_4$, $FeSO_4$, CaMix or NaCl type. Deeper in the aquifer the groundwater becomes of $CaHCO_3$ type. In the deepest parts of the aquifer $MgHCO_3$ and $NaHCO_3$ groundwater types occur (Coetsiers et al., 2014, 2004; Stuyfzand, 1986).

2.4 Results and Discussion

For several ATES systems (A, E, F, G) (Appendix A - Figs. A1, A5-A7), the samples from the cold and warm well(s) were taken only once a year in the same season. Therefore the effect of temperature on the groundwater quality could not be determined for these systems, as the extracted water always originates from the same well. When sampling during winter, water extracted from both the warm and cold well originates from the warm bubble, when sampling during summer, the sampled water from both wells originates from the cold bubble. For other ATES systems however, water was sampled once or twice a year in different seasons (B, C, D) (Appendix A - Figs. A2-A4), whereby water originating from both the cold and warm bubble was displayed in the time series. Comparing the quality of the water extracted from the cold well during summer (cold bubble) with the quality of the water extracted from the warm well during winter (warm bubble) shows no larger differences than between the samples from the same season over time.

Figure 2.3 shows a chart summarizing the data of the ATES systems and the ambient values compared with the Flemish drinking water standard. The chart shows upward or downward trends for some of the considered species for several of the investigated ATES systems. The measured values however stay well within the drinking water standard for calcium, sodium,

magnesium, sulfate and chloride. For the pH, manganese, iron and ammonium the analyses for several ATES systems show values outside the drinking water standard. This is especially the case for iron and ammonium where for all ATES systems, except respectively one (C) and two systems (C and E), values above the drinking water standard are reported. However, for most of these cases the ambient values measured in the VMM monitoring network are also outside the drinking water standard, and thus likely caused by the aquifer characteristics (e.g. mineralogy, organic matter content). In addition to the drinking water standard, the groundwater guidelines were also given. Comparing to these guidelines, the measured values are only outside the limits for iron in system B and ammonium in systems A, B, D, F and G. Both parameters can be easily corrected by treatment of the raw water.

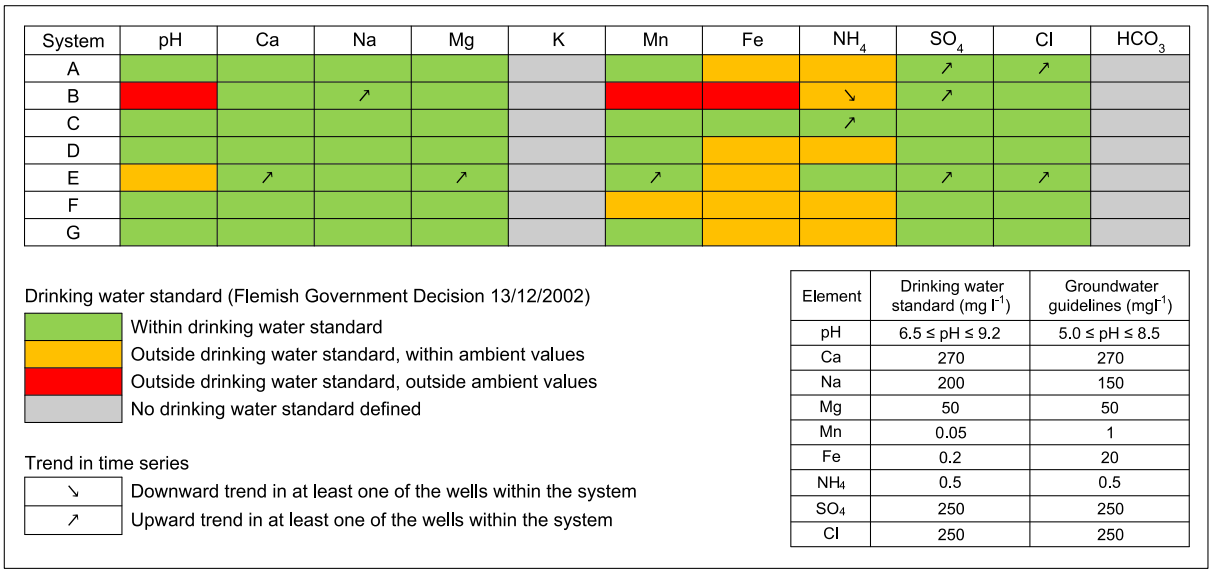

Figure 2.3 Summary chart of the data from all 7 investigated ATES systems. The time series of the monitoring data for the different solutes (Figure A.1 - A.7) as well as the p-values used to determine the significance of the trends (Table A.1) are presented in Appendix A.

Therefore, we focus further on ATES system B where the values for pH, manganese and iron are outside the drinking water standard as well as outside the window of the ambient values (Figure 2.4). For these three parameters no upward trend in the values is measured since the beginning of the monitoring of the system in 2004. On the other hand, there is a slightly upward trend in sulfate concentration (Figure A.2). This trend combined with the high iron and low pH possibly indicates ongoing FeS_2 oxidation. As no data from before ATES installation are available, no comparison can be made between the undisturbed groundwater and the ATES water.

At different ATES systems, upward and downward trends in the concentration of several species are recorded. The results for system E for example show that the concentrations of several species indicate a slightly upward trend (Figure 2.3). Comparison with the trends measured in the corresponding monitoring wells (Figure 2.5), however, shows that also in the monitoring wells upward and downward trends are present. The observed trends in the ATES system can therefore be caused by ATES operation, but also by the same processes causing the trends in the monitoring wells.

For sodium, sulfate and chloride, upward trends are recorded in respectively one (B), three (A, B and E) and two (A and E) ATES systems (Figure 2.3), which can be caused by contamination of the groundwater with fertilizers (sulfate) and road de-icing salt (sodium and chloride). Here the contribution of the ATES operation also cannot be demonstrated as the concentrations in the monitoring wells show upward trends in some cases as well. However ATES operation can negatively contribute to the introduction of these contaminations at larger depth in the

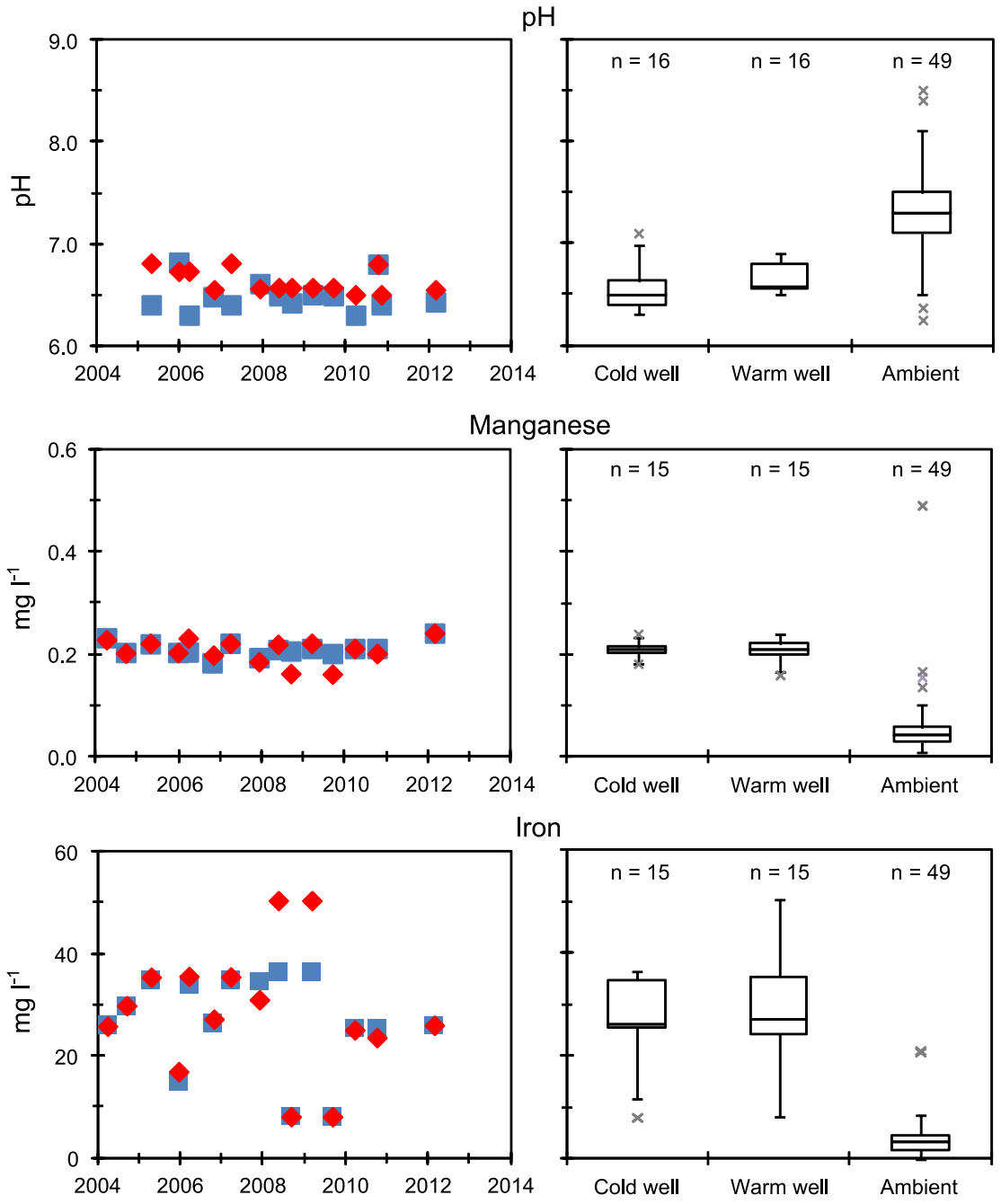

Figure 2.4 Time series of the reported concentrations in ATES system B for pH, Mn and Fe in the cold well (blue squares) and warm well (red rhombuses) and box plots of the ATES data and the ambient data reported from the monitoring wells in the considered aquifer in a 10 km radius around the ATES system.

aquifer by mixing shallow groundwater with deeper groundwater. For system A, this mixing effect is confirmed by comparing the data from different shallow monitoring wells (<10 mbs) with data from the nearest deep monitoring well (monitoring well 1-0261 with well screen from 80 to 82 mbs). For the shallow monitoring wells the concentrations are between 24 and 217 mg/l for sulfate and between 20 and 218 mg/l for chloride whereas for the deep monitoring well the concentration of chloride is maximally 11 mg/l and for sulfate stays below detection limit (<1 mg/l). The upward trends recorded in system B can also be explained by mixing the higher concentrations in the shallow part of the aquifer with the deeper groundwater. At the near deep monitoring well (monitoring well 1-1104b with well screen from 64 to 68 mbs), maximal values are 12 mg/l and 9 mg/l, and at the shallow monitoring wells (<10 mbs) the maximal

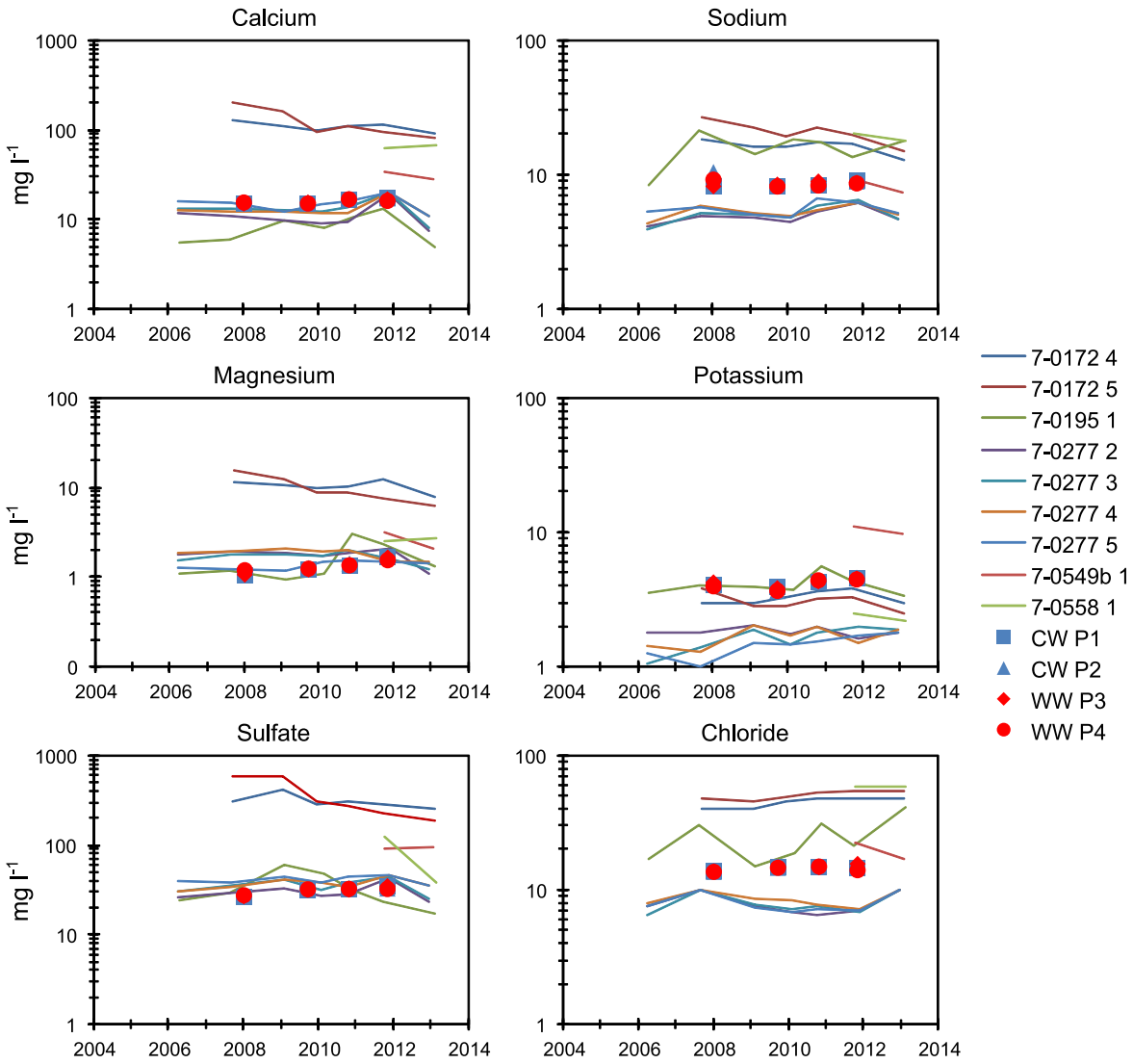

Figure 2.5 Time series of the reported concentrations in ATES system E for Ca, Na, Mg, K, SO_4 and Cl in the two cold wells (blue symbols) and two warm wells (red symbols) and the time series of the reported concentrations in the nine monitoring wells in the considered aquifer in a 10 km radius around the ATES system (line graphs).

values are 37 mg/l and 160 mg/l for sodium and sulfate, respectively. For system E, however, the upward trends for sulfate and chloride cannot be explained by mixing shallow with deeper groundwater as the concentrations in nearby monitoring wells are sometimes higher in the deep wells than in the shallow wells.

The nitrate concentration in the ATES waters of systems A, B, D, E, F and G comes rarely above the detection limit and when above detection limit it stays far below the drinking water standard of 50 mg/l (e.g. maximally 2.6 mg/l in system D). An exception is ATES system C where the nitrate concentration is much higher and often above drinking water standard (Figure 2.6). The reason is that the Brussels Sands aquifer at this location is a phreatic aquifer, low in organic matter content in which the groundwater remains oxidized to a large depth. Therefore the aquifer is vulnerable to nitrate contamination especially when shallow, by fertilization nitrate rich groundwater is pumped, mixed with deeper groundwater and injected back in the other well during the ATES operation. Figure 2.6 shows that no trend in the concentration time series is recorded, as a result it can be assumed that the deviation from the ambient values is explained by initial mixing of groundwater during development of the wells and in the beginning of ATES operation. This mixing effect is confirmed by data from more

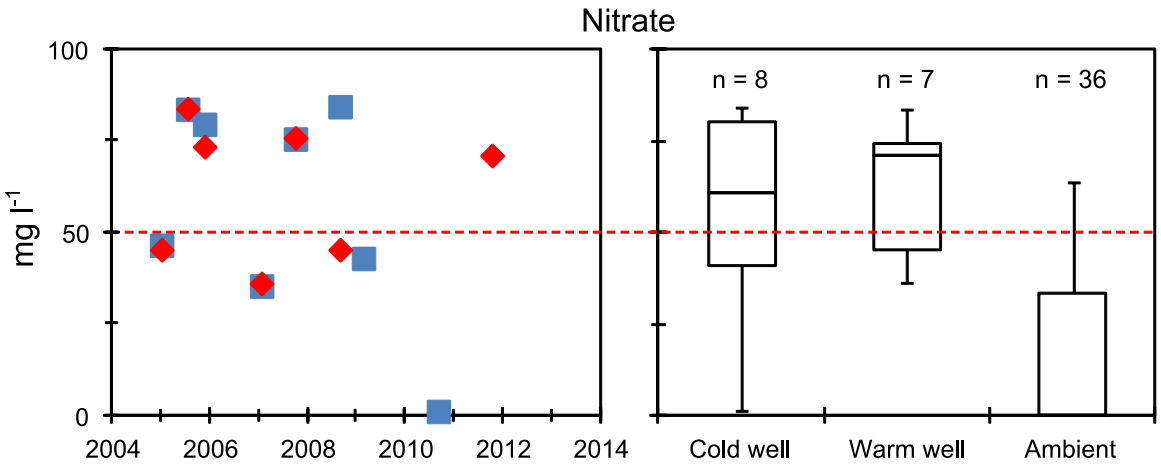

Figure 2.6 Time series of the reported concentrations in ATES system C for NO_3 in the cold well (blue squares) and warm well (red rhombuses) and box plots of the ATES data and the ambient data reported from the monitoring wells in the considered aquifer in a 10 km radius around the ATES system. The red dashed line represents the drinking water standard for nitrate (50 mg/l).

shallow monitoring wells in the vicinity of system C, where nitrate concentrations of about 50 mg/l occur, in contrast to the nearby deep monitoring well (2-0073) where the maximal measured nitrate concentration is 2 mg/l.

2.5 Conclusions

No temperature influence on the groundwater quality is recorded for the ATES systems in Flanders. This is in accordance with the results from other studies and could be expected as these ATES systems operate with small temperature differences ($\Delta T \leq 10$) and within a narrow temperature range (about 6°C to 16°C). As was already stated in the research of Bonte et al. (2013c, 2011b) groundwater vulnerability in the deeper part of the aquifer is increased by injecting shallow groundwater, which is more influenced by human activity, over the whole length of the well screen. The largest risk hereby exists for phreatic aquifers, which are less protected against contamination. This can lead to a deteriorated quality of the water pumped in a nearby public drinking water supply well field, especially when the well screens of the drinking water wells are situated deeper than the screens of the ATES wells. The results of this study suggest however that the quality changes at the investigated sites are rather small, so that there is no immediate risk for the drinking water supply in these cases. When mixing of shallow groundwater with deeper groundwater occurs, it is clear that the changes in the water composition are made in the beginning of ATES operation or even while developing the wells as no further deterioration of groundwater quality was monitored in the investigated ATES systems. It can be concluded that both the design of the ATES system (depth and length of well screens) and the site specific conditions (groundwater quality, land-use and possible input of contaminants) will play an important role in the impact the ATES system will have on the groundwater quality. Therefore an integrated design of the ATES system taking into account the local groundwater chemistry will be indispensable, especially for future ATES systems in the vicinity of public drinking water supply well fields.

As the natural groundwater flow can have an important impact on the monitoring of the groundwater quality around an ATES system, it is important to adapt each monitoring campaign to the local conditions. Further, the groundwater should be monitored in each phase of ATES operation. Minimally one sample should be taken from the cold well during summer and from the warm well during winter. The moment of sampling is different for the possible geochemical changes that are related to temperature changes and for changes related to mixing. For a maximal impact of temperature changes, the samples should be taken approximately halfway the season because that

water had the longest residence time in the warm and the cold bubble (because of thermal retardation) and was influenced the most. To investigate the effect of mixing different groundwater compositions, the samples should be taken near the end of the heating/cooling season since attracting shallower groundwater (more impacted by human activity) is most likely near the end of the season. To be able to assess the possible impact of mixing groundwater, information on the groundwater composition at several depths is needed. Depending on the situation it may be necessary to sample a number of piezometers at different depths. When these piezometers are not available it may be necessary to install these piezometers. It is recommended to sample in nearby monitoring wells downstream the groundwater flow direction, taking into account bubble drift and bubble size. In this way a comparison can be made between the water quality in the ATES wells and the water quality in other parts of the thermal plumes. Finally it is important that the groundwater is passed through a 0.45 µm filter before sampling and acidification. In this way underestimation of iron and manganese concentrations is avoided.

Although very important in the impact assessment of ATES on the groundwater quality, trace elements and microbiology are not included in this study as the focus of this study was to evaluate the impact of ATES on the groundwater quality on the long term and no trace element and microbiological data are available from the beginning of the different ATES operations. Therefore future work should focus on the monitoring of trace elements (e.g. As) and microbiology in ATES and monitoring wells, so that an analysis of the evolution of these parameters over time can be made.

Chapter 3

Reactive transport modeling of redox processes to assess $Fe(OH)_3$ precipitation around Aquifer Thermal Energy Storage wells in phreatic aquifers

Modified from: Possemiers, M., Huysmans, M., Batelaan, O., Van Steenwinkel, J. (in review) Reactive transport modeling of redox processes to assess clogging of Aquifer Thermal Energy Storage (ATES) wells in phreatic aquifers.

3.1 Introduction

Precipitation of iron (hydr)oxide is well known to reduce the performance of wells by clogging (Bustos Medina et al., 2013; Houben, 2001, 2006, 2004, 2003; Houben and Weihe, 2010; van Beek and Kooper, 1980; van Beek, 2010). The formation of iron (hydr)oxide precipitates can result from mixing oxygen/nitrate rich with iron rich groundwater. This can be caused by injecting water with a different redox condition than the ambient water in the aquifer, which occurs during e.g. Aquifer Storage and Recovery (ASR) (Prommer and Stuyfzand, 2005; Wallis et al., 2011). It can also be caused by capturing water from above the redox boundary together with water from below the redox boundary during groundwater abstraction. The redox boundary discussed in this chapter is defined as the transition between oxygen/nitrate rich and iron rich groundwater. The precipitation percolating into the ground contains dissolved gases from the atmosphere such as carbon dioxide, nitrogen and oxygen. As this water percolates to the groundwater table, it often takes up nitrate from the soil. The main sources of nitrate are vegetation and fertilizers. At greater depth, the groundwater often contains dissolved iron originating from partial oxidation of pyrite, from dissolution of Fe(2) bearing minerals or from reductive dissolution of iron oxides (Appelo and Postma, 2005; Miotliński, 2008; Postma et al., 1991). The percolation depth of dissolved oxygen (and nitrate) will strongly depend on the reduction capacity of the aquifer material (van Beek, 2010). Installing well screens over or near the redox boundary will cause mixing of oxygen/nitrate rich water with iron rich water during extraction and injection (Figure 3.1). The dissolved oxygen (and nitrate) comes into contact with the dissolved iron, which will result in precipitation of iron (hydr)oxides and can cause well clogging (Brown and Misut, 2010; Houben, 2006; IFTechnology, 2006; Kohfahl et al., 2008; van Beek, 2012; van Beek et al., 2012).

$$4Fe^{2+} + O_2 + 10\,H_2O \leftrightarrow 4Fe(OH)_3 + 8H^+ \quad (3.1)$$

Furthermore the reduced zone of the aquifers often contains pyrite and/or glauconite, which are oxidized and dissolved under the influence of the more oxygen rich captured and injected

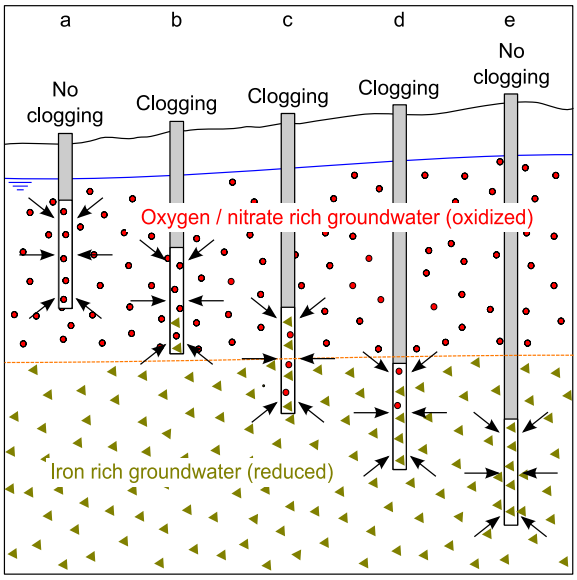

Figure 3.1 The redox boundary is the transition between oxygen/nitrate rich and iron rich groundwater. **a**: well screen installed entirely in the oxidized part of the aquifer, no iron (hydr)oxide precipitation; **b**: bottom of the filter close to the redox boundary, iron rich groundwater is attracted to the well screen, possible iron (hydr)oxide precipitation; **c**: well screen installed over the redox boundary, oxygen/nitrate rich and iron rich groundwater are attracted and mixed, possible iron (hydr)oxide precipitation; **d**: top of the well screen is installed close to the redox boundary, oxygen/nitrate rich groundwater is attracted to the well screen, possible iron (hydr)oxide precipitation; **e**: well screen installed entirely in the reduced part of the aquifer, no iron (hydr)oxide precipitation.

water, providing additional dissolved iron in the groundwater (Prommer and Stuyfzand, 2005). However, mixing oxygenated water with iron rich water does not always have to be detrimental. With the technique of in situ iron removal, oxygenated water is injected in a reduced aquifer to allow water to be extracted with a lower than initial iron content. In this case, no well clogging occurs, as the iron hydroxides precipitate at a larger distance from the well where the iron concentration in the ground water is not diminished by exchange and sorption (Appelo and de Vet, 2003; Appelo et al., 1999; van Halem et al., 2012, 2011, 2010).

This chapter focuses on the issue of precipitation of iron hydroxide at ATES wells. Generally, ATES is applied in relatively thick sandy aquifers under either oxidized or reduced conditions, well above or below the redox

boundary, in order to prevent the risk of well clogging. The exact processes around extraction and injection wells are not well understood and therefore the precautionary principle of staying far away from the redox boundary when applying ATES is followed. In this way, the development of ATES in phreatic aquifers is potentially hampered. Therefore it is necessary to better understand the interaction between physical and chemical processes in phreatic aquifers during ATES operation. A useful tool for this is reactive transport modeling, whereby both physical and chemical processes can be incorporated and modeled. The capability to quantify the reactivity of natural reductants, such as pyrite and glauconite is also important for other applications such as the application of ATES in contaminated aquifers (Zuurbier et al., 2013), artificial recharge (Prommer and Stuyfzand, 2005), in situ bioremediation (Eckert and Appelo, 2002; Hartog et al., 2002; Prommer et al., 2000; Thullner and Schäfer, 1999), treatment of nitrate contaminated groundwater (Engesgaard and Kipp, 1992; Postma et al., 1991), dewatering and drinking water production.

The main goal of this study is to identify the extent and location of the precipitation and the effect of temperature and mineralogy to determine possible measures that can avoid or reduce the risk of well clogging during ATES operation. Hence, the reactive transport code PHT3D (Prommer and Post, 2010) is used to assess the effects of alternating pumping by ATES systems near the redox boundary on the precipitation of iron hydroxides and the potential clogging of the wells. The groundwater chemistry and mineralogy in the developed conceptual models is based on, but differs from the natural situation. The models are instructive in understanding the processes around ATES wells near the redox boundary. The presented results, however, should not be viewed quantitatively.

3.2 Materials and Methods

3.2.1 Field Sites and Investigation Program

Two case studies in Flanders are selected. In the first case the potential of ATES is investigated in a thick phreatic sandy aquifer (Brussels Sands) with a deep redox boundary in Leuven. In the second case the applicability of ATES is investigated in a shallow clay-rich sand layer (Berchem Sands) with a very shallow redox boundary in Antwerp. In both cases, the redox conditions play an important role in the feasibility of an ATES system.

The first site is located on a hill west of the centre of Leuven (Figure 3.2). On this location, there is already an ATES system in operation since 1996. In 2011, however, an additional well was installed for the existing ATES system. In this context, an evaluation of the redox conditions was conducted. A thick, 60 m sandy aquifer is available here for the application of ATES. Under the Quaternary loam deposits, the aquifer consists of Diest Sands, Sint-Huibrechts-Hern Sands, Lede Sands, and Brussels Sands, respectively. At the bottom, the aquifer is delimited by the clays of the Ieper Group. The well screen is positioned just above the clay layer, entirely in the permeable Brussels Sands (52 to 67 mbs). The hydraulic head at rest is about 33 mbs, so that there is a 34 m thick saturated zone. The redox boundary is located at around 64 mbs, at the bottom part of the well screen. This is based on the color differences observed in the drilling samples and on analysis of mineralogy. Above 64 mbs the sediments have an orange-brown color, whereas below 64 mbs, the sediments have a green-gray color. Below 64 mbs pyrite is present, which is a strong reducing agent (Figure 3.3).

The second site is located in the south of the city of Antwerp (Figure 3.2). The evaluation of the redox conditions here was conducted in the framework of a feasibility study for an ATES system for a new office building. At this site, only 24 m of sandy layers is available above a thick clay layer. Beneath the Quaternary loam, sand, pebbles and shell fragments, the aquifer consists of the clayey glauconitic sands of the Kattendijk and Berchem Formation respectively.

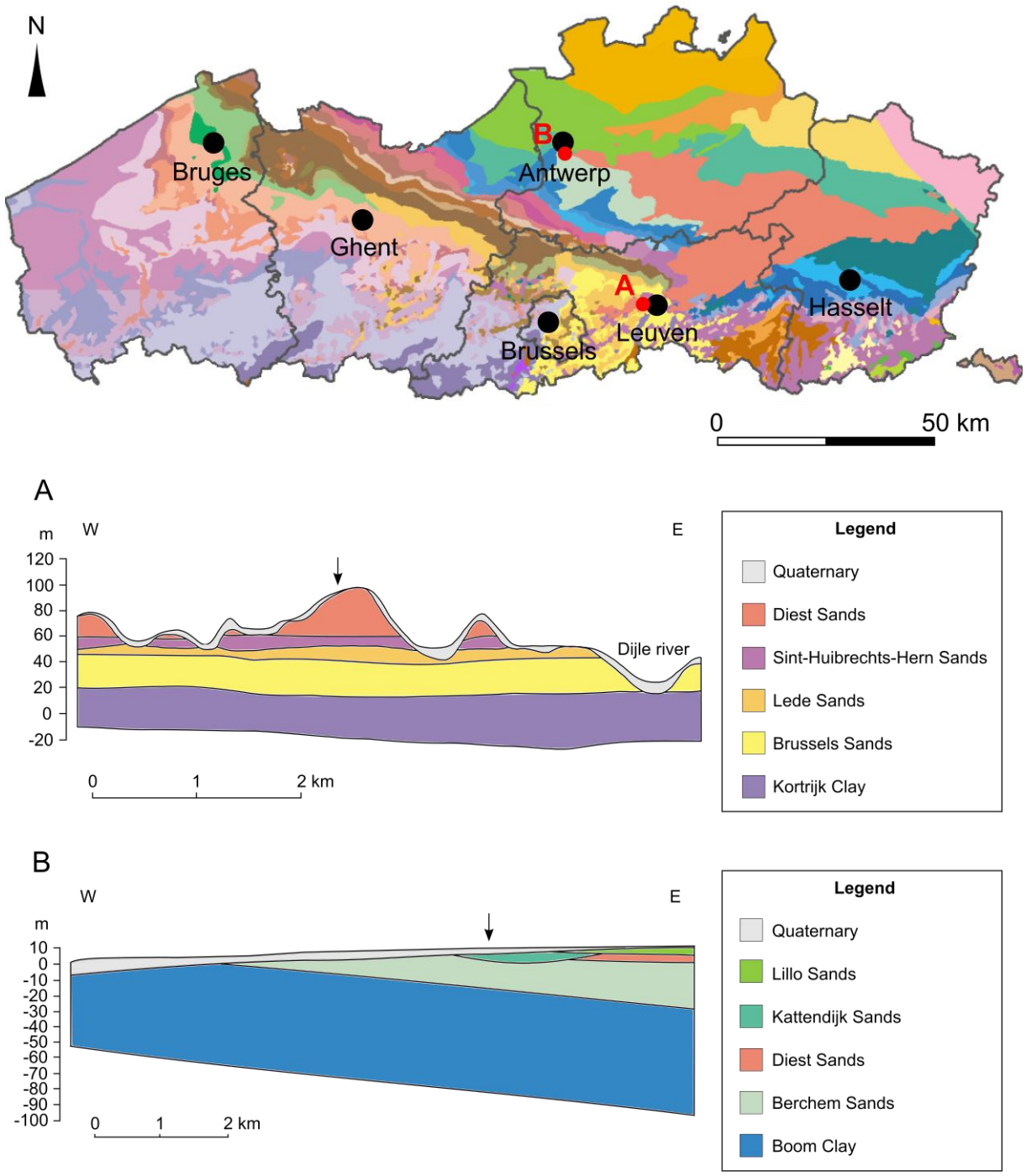

Figure 3.2 Tertiary subcrop map of Flanders indicating the position of the investigated sites and geological sections through the study areas. Sections A and B represent the geology for the Leuven case and Antwerp case respectively, the arrows represent the approximate places of the sites on the profiles (adapted from DOV, 2014).

At the bottom, the aquifer is delimited by a thick clay layer, the Boom Clay. A test well and several monitoring wells were drilled at this location. The well screen of the test well is positioned just above the clay layer (14 to 24 mbs). In addition, two other boreholes were drilled at this site, the first borehole was equipped with four monitoring wells (well screens: 4 to 5, 9 to 10, 14 to 15 and 19 to 20 mbs) and the second borehole was equipped with a well screen from 19 to 20 mbs. The hydraulic head at rest is 6 mbs, which results in a saturated zone of 18 m. The exact position of the redox boundary could not be determined, although the aquifer is definitely reduced at 9 mbs (3 m below the water table), derived by iron (4.6 mg/l) and nitrate (<0.9 mg/l) concentrations measured in the monitoring well

at 9 to 10 mbs (Table 3.2) This means that the redox boundary occurs minimum 5 m above the top of the well screen (Figure 3.3).

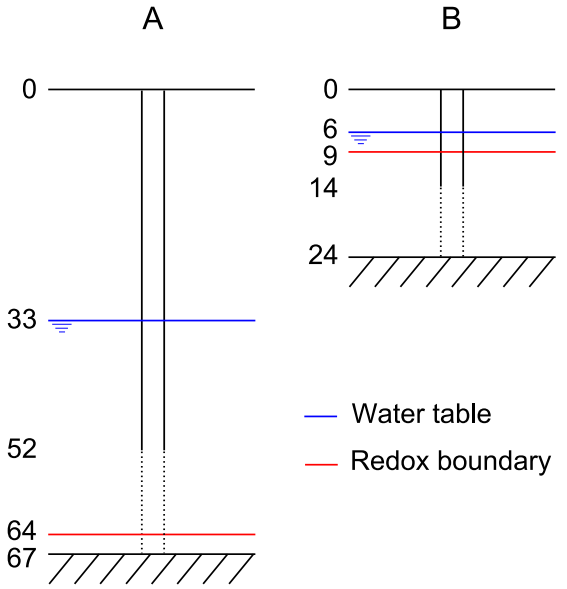

Figure 3.3 Position of the well screen, water table and redox boundary in the Leuven case (A) and the Antwerp case (B).

At both sites, several aquifer tests were performed in the different wells: pumping tests, in-situ multi parameter measurements (Eh, pH, DO) and groundwater sampling. All wells were drilled by direct flush rotary drilling and were airlifted afterwards. For further cleaning of the wells and for removal of the introduced oxygen, the wells were pumped intermittently during several days. The tests in Leuven were carried out with a Grundfos SP pump whereas the tests in Antwerp were carried out with a smaller Grundfos SQ pump because of the wells smaller discharge.

3.2.2 Pumping tests

At the Leuven site, only a pump test at constant rate was performed to determine the transmissivity of the aquifer, since the aquifer properties are well known from the tests performed for the installation of the initial ATES system in 1996. At the site in Antwerp, a variable discharge test as well as a pump test at constant rate were carried out. After the pump test at constant rate, the recovery was also measured for several days. During these tests, the changes in hydraulic head were monitored using automatic pressure sensors in the wells. These measurements were corrected for the atmospheric pressure, in situ monitored by a barometric pressure sensor. Both pumping tests at constant rate had a duration of about 24 hours, the test at variable discharge in Antwerp took four steps of about one hour and the recovery after the constant rate test in Antwerp was monitored during more than four days.

The measurements were processed with analytical as well as numerical methods (Appendix B). The analytical measurements used are the Eden-Hazel method (Eden and Hazel, 1973) for the variable discharge test, the Jacob straight-line method (Cooper and Jacob, 1946) for the pump test at constant rate and the Theis recovery method (Theis, 1935) for the analysis of the residual drawdown (Kruseman and de Ridder, 1991). These three methods all give a good indication of the aquifer transmissivity and hydraulic conductivity. The values obtained with the analytical methods were calibrated using groundwater flow models of the pumping tests. The values for hydraulic conductivity, specific storage, effective porosity and specific yield were obtained and calibrated by trial and error until the model results corresponded well with the drawdown measured during the constant rate and variable discharge tests. The differential equations describing groundwater flow are solved by MODFLOW 2000 (Harbaugh et al., 2000) as supported by the pre- and post-processor Processing Modflow 8 (Chiang, 2010). The calibrated hydraulic parameters are listed in Table 3.4 and are incorporated in the reactive transport models.

3.2.3 Multiparameter measurements

To monitor the dynamics in chemical parameters, a HI9829 Multiparameter Meter of Hanna Instruments was used in a flow cell during pumping. The measured parameters include pH, oxidation-reduction potential (Eh) and dissolved oxygen (DO). At both sites, these parameters were monitored during four days with four flow rate steps of one day. In Antwerp, these parameters were also measured at rest in three monitoring wells with depths of 9 to 10 mbs, 14 to 15 mbs and 19 to 20 mbs.

Dissolved oxygen is measured with a galvanic DO sensor. Basically, this sensor consists of a

cathode, anode, electrolyte solution and a gas permeable membrane. The pH is measured using a glass pH electrode which consists of a pH sensor, a reference electrode and an electrolyte (KCl solution saturated with AgCl). The oxidation-reduction potential (Eh) electrode is packed together with the pH electrode and measures a difference in potential between the platinum electrode and the Ag/AgCl reference electrode (Hanna Instruments, 2012). The pH, Eh and DO sensors were calibrated before each series of measurements.

3.2.4 Sampling and analysis

In Leuven, a mixed sample was taken in the future ATES well. Therefore the sample is made up of water from the whole screened interval of the well, from 52 to 67 mbs. In Antwerp, besides a mixed sample in the test well, groundwater was also sampled in the three monitoring wells with a Grundfos MP1 pump. The mixed ground water samples were analyzed for the main chemical components (Table 3.1). The other samples were analyzed for iron, manganese, nitrate, nitrite, sulfate and sulfide (Table 3.2).

During drilling, aquifer materials were collected each 2.5 m (Leuven) and 1.5 m (Antwerp) and at every clear transition in sediments. For both sites, seven samples were selected for analysis using quantitative X-ray diffractometry (XRD) (Table 3.3). The apparatus used is a Philips PW1830 diffractometer equipped with Bragg-Brentano θ-2θ setup and Cu Kα-radiation. Measurements are recorded from 5-65° 2θ, with 0.02°/step and 2s/step counting time.

3.2.5 Reactive transport models

Based on the hydrological data derived from the pumping tests and the data from the groundwater and soil analyses, a reactive transport model was constructed for each case. The reactive multi-component transport code for saturated porous media PHT3D version 2 (Prommer and Post, 2010) was used for simulation of groundwater flow, solute transport, heat transport and chemical reactions (Figure 3.4). PHT3D is a coupled model of the groundwater flow and solute transport code MODFLOW/MT3DMS (Harbaugh et al., 2000; Zheng and Wang, 1999) and the chemical reactions code PHREEQC-2 (Parkhurst and Appelo, 1999), and enables the simulation of advection, dispersion, diffusion and chemical reactions. Porosity and permeability changes resulting from precipitation reactions are not accounted for. In this study, equilibrium, redox and kinetic reactions of $Fe(OH)_3$ and pyrite were included in the three-dimensional flow field as

Table 3.1 Measured mixed groundwater composition

Aqueous component	Leuven case (mol l^{-1})	Antwerp case (mol l^{-1})
pH	7.00	6.90
pe	7.55	1.77
Al	-	-
C(4)	6.07E-03	-
C(-4)	-	-
Ca	3.75E-03	5.49E-03
Cl	8.47E-04	2.79E-03
F	8.96E-06	2.00E-05
Fe(2) Fe(3)	4.12E-06	4.30E-04
K	4.61E-05	1.18E-04
Mg	9.06E-04	2.18E-04
Mn(2) Mn(3)	6.56E-08	1.08E-05
N(3)	-	1.29E-06
N(5)	8.55E-04	4.57E-05
N(0)	-	-
Na	4.79E-04	1.61E-03
O(0)	1.25E-04	1.25E-05
P	3.23E-07	6.78E-06
S(-2)	-	-
S(6)	8.33E-04	2.29E-03
Si	-	-

- : not measured

Table 3.2 Measured concentrations in the 3 monitoring wells

Parameters	Concentration (mg/l)		
	9 - 10 mbs	14 - 15 mbs	19 - 20 mbs
Iron	4.6	27	4.7
Manganese	0.53	1.5	0.34
Nitrate	<0.90	2.6	<0.90
Nitrite	<0.030	<0.030	<0.030
Sulfate	310	320	130
Sulfide	<0.010	<0.010	<0.010

Table 3.3 Measured mineral concentrations

Leuven case	mbs						
	0 - 37	**37 - 42**	**42 - 47**	**47 - 52**	**52 - 57**	**57 - 64**	**64 - 70**
Minerals (mol l_v^{-1})							
Calcite	2.39E+00	1.52E+00	9.82E-01	5.24E-01	1.96E-01	1.78E-01	5.16E-01
Pyrite				0			8.40E-02
Antwerp case	mbs						
	0 - 7	**7 - 9**	**10 - 13**	**13 - 16**	**16 - 19**	**19 - 22**	**22 - 27**
Minerals (mol l_v^{-1})							
Calcite	3.68E-01	4.80E-01	1.60E-01	3.68E-01	9.91E-01	1.01E+00	2.40E+00
Glauconite	7.22E-01	8.89E-01	7.96E-01	6.85E-01	4.63E-01	2.59E-01	2.22E-01

* l_v: litre bulk volume

well as cation exchange. The effect of temperature on the chemical reactions is considered by defining temperature as a component invoked by PHREEQC-2 to provide the temperature at which the reactions take place, instead of the standard temperature of 25 °C. The heat transport was modeled with the MT3DMS part of PHT3D, which can be used to model heat transport due to the similarity between the solute and heat transport equation (Caljé, 2010; Fossoul et al., 2011; Hecht-Méndez et al., 2010; Sommer et al., 2013; Thorne et al., 2006; Zheng, 2010). Heat transfer in aquifers occurs through heat transport by the fluid phase, conductive transport of heat through the aquifer material and heat exchange between the fluid phase and the aquifer material (De Marsily, 1986). The thermal diffusion coefficient (D_{m_temp}) is calculated as:

$$D_{m\_temp} = \frac{\lambda_e}{n\,\rho_w\,c_w} \tag{3.2}$$

where λ_e is the bulk thermal conductivity of the aquifer, n is the porosity, ρ_w is the density of water and c_w is the specific heat capacity of water. The thermal distribution coefficient (K_{d_temp}) is calculated as:

$$K_{d\_temp} = \frac{c_s}{\rho_w\,c_w} \tag{3.3}$$

where c_s is the specific heat capacity of the solid phase.

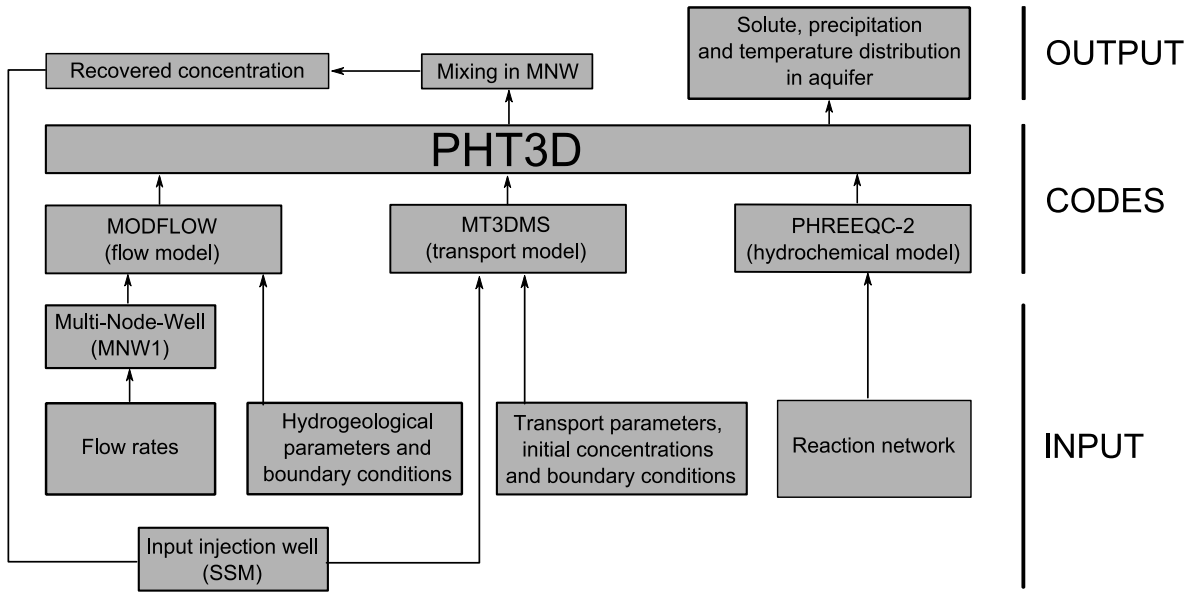

Figure 3.4 Flowchart of PHT3D modeling, with input, codes and output (adapted from Zuurbier, 2011).

In order to realistically simulate the mixing of water qualities in the wells during extraction from several model layers by one well, the multi-node-well version 1 (MNW1) package (Halford and Hanson, 2002) is used. Therefore a modified version of the PHT3D code (Zuurbier, 2011; Zuurbier et al., 2013) was used in order to enable recirculation of the extracted mixed water to the injection well. This modification enables recirculation for the multi-node-well (MNW1) in the same way as for the recirculation for a single-node-well (WEL) (Zheng, 2010). For the creation of the input files and the post-processing the graphical user interface (GUI) Processing Modflow 8 was used (Chiang, 2010).

3.2.6 Conceptual Model and Model Discretization

The Leuven model is a three dimensional local model of 3000 m x 3000 m in the x and y direction and has a thickness of 70 m. The cell sizes range from 250 m at the model boundaries to 1 m at the centre of the model in the x and y direction and the layers at the well screens have a thickness of 1 m. The Antwerp model has the same spatial dimensions and discretization but has a thickness of 27 m. In both models, the two ATES wells are placed 148 m from each other on a transect in the y direction in the centre of the model. Constant hydraulic heads are assigned to the up and downstream vertical boundaries. With a hydraulic conductivity of 10.55 m/day in the Leuven case, a hydraulic gradient of 0.002 m/m will ensure a natural groundwater flow velocity of 7.7 m/year. At the Antwerp site, the aquifer has a hydraulic conductivity of 4.64 m/day and a hydraulic gradient of 0.0012 m/m, ensuring a groundwater flow velocity of 2 m/year. Because of this rather low groundwater flow velocity and to generate a stable initial redox boundary, no hydraulic gradient is applied in the models.

The hydraulic parameters were determined by analytical methods on the drawdown data measured during the performed pumping tests and by calibration of a groundwater flow model using these drawdown data. The thermal parameters were calculated based on literature values of similar lithologies (N.V.O.E., 2006; Zuurbier, 2011) (Table 3.4). The obtained groundwater quality and mineralogical data were equilibrated with PHREEQC-2 and inserted in the model. The Modified Method Of Characteristics (MMOC) advection scheme gave more stable results and faster run times in comparison with the Total Variation Diminishing (TVD) scheme and was therefore used for solving the numerical transport problem. The Courant number was chosen 0.75, so any particle is allowed to move 0.75 x cell size in any direction in one transport step. The maximal Peclet number around the ATES wells is 1.8 for both the Leuven case and the Antwerp case. Thus, a limited numerical dispersion is expected. In the Leuven model, extraction and injection discharges are 720 m^3 day^{-1}. In the Antwerp model, groundwater is extracted and injected at 60 m^3 day^{-1}. Each year is divided in four stress periods, corresponding to the different seasons. Injection in the summer season occurs at a temperature of 16°C, in winter the water is injected at 6°C. In autumn and spring no pumping occurs.

The reaction network includes the equilibrium based speciation and redox reactions of all major ions, mineral equilibrium for calcite and kinetics for $Fe(OH)_3$ in both the Leuven and Antwerp model. According to the measured mineralogy at both cases, in the Leuven model, this reaction network is supplemented with temperature dependent kinetic pyrite oxidation by oxygen and nitrate (Eckert and Appelo, 2002; Prommer and Stuyfzand, 2005; Williamson and Rimstidt, 1994) and cation exchange. In the Antwerp model, the reaction network is supplemented with mineral equilibrium for glauconite ($K_{1.5}Mg_{0.5}Fe(3)_{2.5}Fe(2)_{0.5}AlSi_{7.5}O_{20}(OH)_4$) (Xu et al., 2001).

For the ferrihydrite ($Fe(OH)_3$) kinetics in both models following reactions were included:

$$Fe^{2+} \leftrightarrow Fe^{3+} + e^- \quad (3.4)$$

with equilibrium constant $K = 10^{-13.02}$ and $\Delta H = 40.5$ kJ and

$$Fe(OH)_3 + 3H^+ \leftrightarrow Fe^{3+} + 3H_2O \quad (3.5)$$

with equilibrium constant $K = 10^{-12.56}$ and $\Delta H = -103.8$ kJ. Therefore $K_{16°C} = 10^{-11.99}$ and $K_{6°C} = 10^{-11.32}$. Thus the solubility of $Fe(OH)_3$ increases with decreasing temperature.

Furthermore, a simple rate expression is used:

$$r_{Fe(OH)_3} = \alpha\,(1 - SR_{Fe(OH)3}) \quad (3.6)$$

where α = 1E-14 and SR is the saturation ratio. According to this expression the rate is zero when $Fe(OH)_3$ is in equilibrium with its solution (SR = 1).

Reaction equation 3.5 shows that $Fe(OH)_3$ precipitation will strongly depend on the pH. At higher pH, the equilibrium will shift to the left. The pH will thus play an important role in the precipitation of $Fe(OH)_3$ around the ATES wells. The pH in its turn is determined by the temperature of the groundwater, explained by shifts in equilibria in a number of common reactions in groundwater, e.g.:

$$2H_2O \leftrightarrow O_2 + 4H^+ + 4\,e^- \quad (3.7)$$

with equilibrium constant K = $10^{-86.08}$ and ΔH = 564 kJ and

$$CO_3{}^{2-} + H^+ \leftrightarrow HCO3^- \quad (3.8)$$

with equilibrium constant K = $10^{16.681}$ and ΔH = -24 kJ.

For both reactions a shift to higher temperature will cause more H^+ into solution and thus a lower pH, whereas a shift to lower temperature will ensure a higher pH. Therefore lower temperatures will induce a higher solubility of $Fe(OH)_3$, but also a higher pH, which in its turn will cause more $Fe(OH)_3$ to precipitate (equation 3.5).

Kinetic reactions were defined and included for pyrite oxidation with oxygen:

$$FeS_2 + 3.75\,O_2 + 3.5\,H_2O \leftrightarrow$$

$$Fe(OH)_3 + 2SO_4^{2-} + 4H^+ \quad (3.9)$$

and nitrate:

$$FeS_2 + 3\,NO_3^- + 2\,H_2O \leftrightarrow$$

$$Fe(OH)_3 + 2SO_4^{2-} + 1.5\,N_2 + H^+ \quad (3.10)$$

The rate expression used for this temperature dependent oxidation of pyrite is based on the original rate law of Williamson and Rimstidt (1994) and is adopted from the study of Prommer and Stuyfzand (2005):

$$r_{pyr} = \frac{f_{ar}(T_c)}{f_{ar}(T_{ref})}\left[\left(C_{O_2}^{0.5} + f_2 C_{NO_3^-}^{0.5}\right) C_{H^+}^{-0.11}\left(10^{-10.19}\frac{A_{pyr}}{V}\right)\left(\frac{C}{C_0}\right)_{pyr}^{0.67}\right] \quad (3.11)$$

with

$$f_{ar}(T_c) = -\exp\left(\frac{1}{T_c + 273.15}a_1 + a_2\right) \quad (3.12)$$

and

$$\frac{A_{pyr}}{(V \times C_{pyr})} = k_{pyr} \quad (3.13)$$

where f_{ar} is an Arrhenius equation based temperature factor, T_c is the groundwater temperature (°C), T_{ref} is the reference temperature, C_{O2} is the dissolved oxygen concentration, constant f_2 = 1, C_{NO3-} is the concentration of nitrate, C_{H+} is the proton concentration, A_{pyr}/V is the ratio of pyrite surface area to solution volume, C/C_0 is a factor that accounts for changes in surface area resulting from the progressing reaction, a_1 and a_2 are constants with a_1 = 6758.1, a_2 = 16.1 and k_{pyr} = 115 dm^{-1} mol^{-1} l.

The equilibrium reaction used for glauconite is:

$$K_{1.5}Mg_{0.5}Fe_{2.5}Fe_{0.5}AlSi_{7.5}O_{20}(OH)_4 + 14H^+ + 6H_2O$$

$$\leftrightarrow \quad 1.5K^+ + 2.5Fe^{3+} + 0.5Fe^{2+} + 0.5Mg^{2+} + Al^{3+} + 7.5H_4SiO_4 \quad (3.14)$$

with equilibrium constant K = $10^{-6.2001}$.

From reactions 3.4 to 3.14, it is clear that pH, temperature, Eh and the electron donors oxygen and nitrate are very important for the processes regarding pyrite oxidation and solubility and precipitation of $Fe(OH)_3$.

The described models are based on real-world data and measurements but do not tend to incorporate all possible geochemical processes as the aim of this study is to understand the processes around ATES wells on the boundary between oxidized and reduced conditions and their impact on $Fe(OH)_3$ precipitation. The concentration changes in the groundwater and the hydrochemistry should therefore be analyzed relative to each other rather than as absolute values. As the field data were gathered

in the context of the construction of a new well for an existing ATES installation (Leuven) and in the context of a feasibility study for ATES (Antwerp), no data were available during and after ATES operation. Therefore, the model predictions cannot be verified and the results should be handled with care.

3.3 Results and Discussion

The hydraulic data derived from the pumping tests in Leuven and Antwerp can be found in Table 3.4 and were incorporated in the reactive transport models of both sites.

Table 3.4 Parameters used in the models.

Parameter	Leuven	Antwerp	Unit
Model dimensions	3000 x 3000 x 70	3000 x 3000 x 27	m
Discretisation Δx	1 to 250	1 to 250	m
Discretisation Δy	1 to 250	1 to 250	m
Discretisation Δz	1 to 33	1 to 6	m
Time step length	1	1	day
Horizontal hydraulic conductivity K_h (sand / clay)	10.55 / 1E-4	4.64 / 1E-4	$m\ d^{-1}$
Vertical hydraulic conductivity K_v (sand / clay)	3.52 / 3.33E-5	2 / 3.33E-5	$m\ d^{-1}$
Effective porosity	0.2	0.05	
Specific yield	0.2	0.05	
Specific storage	3.00E-04	1.00E-03	m^{-1}
Longitudinal dispersivity	1	1	m
Horizontal transversal dispersivity	0.1	0.1	m
Vertical transversal dispersivity	0.1	0.1	m
Molecular diffusion coefficient D_m	0	0	$m^2\ d^{-1}$
Equilibrium constants K	PHREEQC database	PHREEQC database	
Thermal distribution coefficient K_{d_temp} (sand / clay)	2.13e-4 / 2.61e-4	2.17e-4 / 2.61e-4	$m^3\ kg^{-1}$
Thermal diffusion coefficient D_{m_temp} (sand / clay	0.104 / 0.077	0.093 / 0.077	$m^2\ d^{-1}$
Bulk density ρ	2000	2000	$kg\ m^{-3}$

The results from the multiparameter measurements (DO, pe and pH) and the data from the groundwater and mineralogical analyses (Table 3.1 and 3.3) were equilibrated and used as the initial groundwater composition in the reactive transport models (Tables 3.5 - 3.7). Comparing the measured groundwater composition with the equilibrated groundwater composition shows major differences in oxygen concentrations. The equilibrated oxygen concentrations for both cases are extremely low and are explained by iron and pyrite oxidation. This is demonstrated by comparison of the measured and equilibrated iron concentrations and mineralogy. In the upper part of the Leuven model (0 – 64 mbs) the oxygen is depleted by oxidation of the dissolved iron resulting in $Fe(OH)_3$ precipitation. In the lower part of the Leuven model (64 – 70 mbs) the oxygen is depleted by pyrite oxidation, resulting in a higher sulfate concentration in the groundwater. In the Antwerp case the oxygen is depleted by oxidation of the dissolved iron which resulted in $Fe(OH)_3$ precipitation. The difference between the measured and equilibrated concentrations is explained by the fact that in a natural system, the groundwater is never in equilibrium with the aquifer material. However, to create a stable initial groundwater composition in the models, equilibration of the groundwater chemistry and the mineralogy is necessary. Though, future modeling work should implement more realistic oxygen concentrations. This can be done by setting the dissolved iron concentration to zero in the zone above the redox boundary. In this way no precipitation of $Fe(OH)_3$ will occur in the equilibration phase and the oxygen concentrations will remain higher.

Table 3.5 Equilibrated initial groundwater composition.

Aqueous component	Leuven model		Antwerp model	
	0 - 64 mbs (mol l_w^{-1})	64 - 70 mbs (mol l_w^{-1})	0 - 9 mbs (mol l_w^{-1})	9 - 27 mbs (mol l_w^{-1})
pH	7.06	7.08	7.72	8.00
pe	13.33	-2.45	12.03	-1.72
Al	-	-	7.59E-07	1.10E-07
C(4)	6.19E-03	5.97E-03	8.13E-04	4.58E-04
C(-4)	0	1.92E-14	0	1.43E-29
Ca	3.84E-03	3.92E-03	6.28E-03	5.90E-03
Cl	2.43E-03	2.43E-03	9.37E-03	9.37E-03
F	8.96E-06	8.96E-06	2.00E-05	2.00E-05
Fe(2)	1.19E-16	1.44E-05	2.26E-17	1.89E-04
Fe(3)	6.66E-09	1.45E-13	3.67E-09	3.33E-09
K	4.69E-05	4.68E-05	1.19E-04	1.18E-04
Mg	9.29E-04	9.46E-04	2.18E-04	2.18E-04
Mn(2)	6.88E-08	6.91E-08	1.08E-05	1.08E-05
Mn(3)	7.09E-21	1.17E-36	7.18E-20	1.29E-33
N(3)	1.95E-14	0	4.44E-15	0
N(5)	8.53E-04	0	9.96E-06	0
N(0)	2.10E-06	8.55E-04	3.70E-05	4.70E-05
Na	4.84E-04	4.84E-04	1.61E-03	1.61E-03
O(0)	8.64E-10	0	2.26E-12	0
P	3.23E-07	3.23E-07	6.78E-06	6.78E-06
S(-2)	0	7.86E-12	0	5.36E-26
S(6)	8.33E-04	1.44E-03	2.29E-03	2.29E-03
Si	-	-	5.69E-06	8.25E-07

* l_w: litre pore water

Table 3.6 Equilibrated initial mineral concentrations and exchanger compositions for the Leuven case.

	mbs						
	0 - 37	37 - 42	42 - 47	47 - 52	52 - 57	57 - 64	64 - 70
Minerals (mol l_v^{-1})							
Calcite	2.39E+00	1.52E+00	9.82E-01	5.24E-01	1.96E-01	1.78E-01	5.16E-01
$Fe(OH)_3$(a)				1.13E-06			0
Pyrite				0			8.39E-02
Initial exchanger composition (mol l_v^{-1})							
CaX2				4.32E-02			4.31E-02
FeX2				5.26E-16			6.31E-05
KX				1.70E-04			1.70E-04
MgX2				6.55E-03			6.54E-03
MnX2				3.57E-07			3.57E-07
NaX				3.21E-04			3.21E-04

* l_v: litre bulk volume

Table 3.7 Equilibrated initial mineral concentrations for the Antwerp case.

	mbs							
	0 - 7	**7 - 9**	**9 - 10**	**10 - 13**	**13 - 16**	**16 - 19**	**19 - 22**	**22 - 27**
Minerals (mol l_v^{-1})								
Calcite	3.68E-01	4.80E-01	4.80E-01	1.60E-01	3.68E-01	9.91E-01	1.01E+00	2.40E+00
$Fe(OH)_3(a)$	2.16E-05				1.21E-05			
Glauconite	7.22E-01	8.89E-01	8.89E-01	7.96E-01	6.85E-01	4.63E-01	2.59E-01	2.22E-01

* l_v: litre bulk volume

As the oxygen concentrations implemented in the models are lower than the actual measured values, the modeled $Fe(OH)_3$ precipitation around the ATES wells will probably be significantly lower than the actual $Fe(OH)_3$ precipitation around the ATES wells. This modeling study should therefore rather be interpreted qualitatively, than quantitatively. The study contributes to the understanding of redox processes around ATES wells but does not tend to do quantitative statements on the risk of clogging at the studied cases. The results of the reactive transport modeling show that for both the Leuven and Antwerp case precipitation of $Fe(OH)_3$ occurs around the ATES wells.

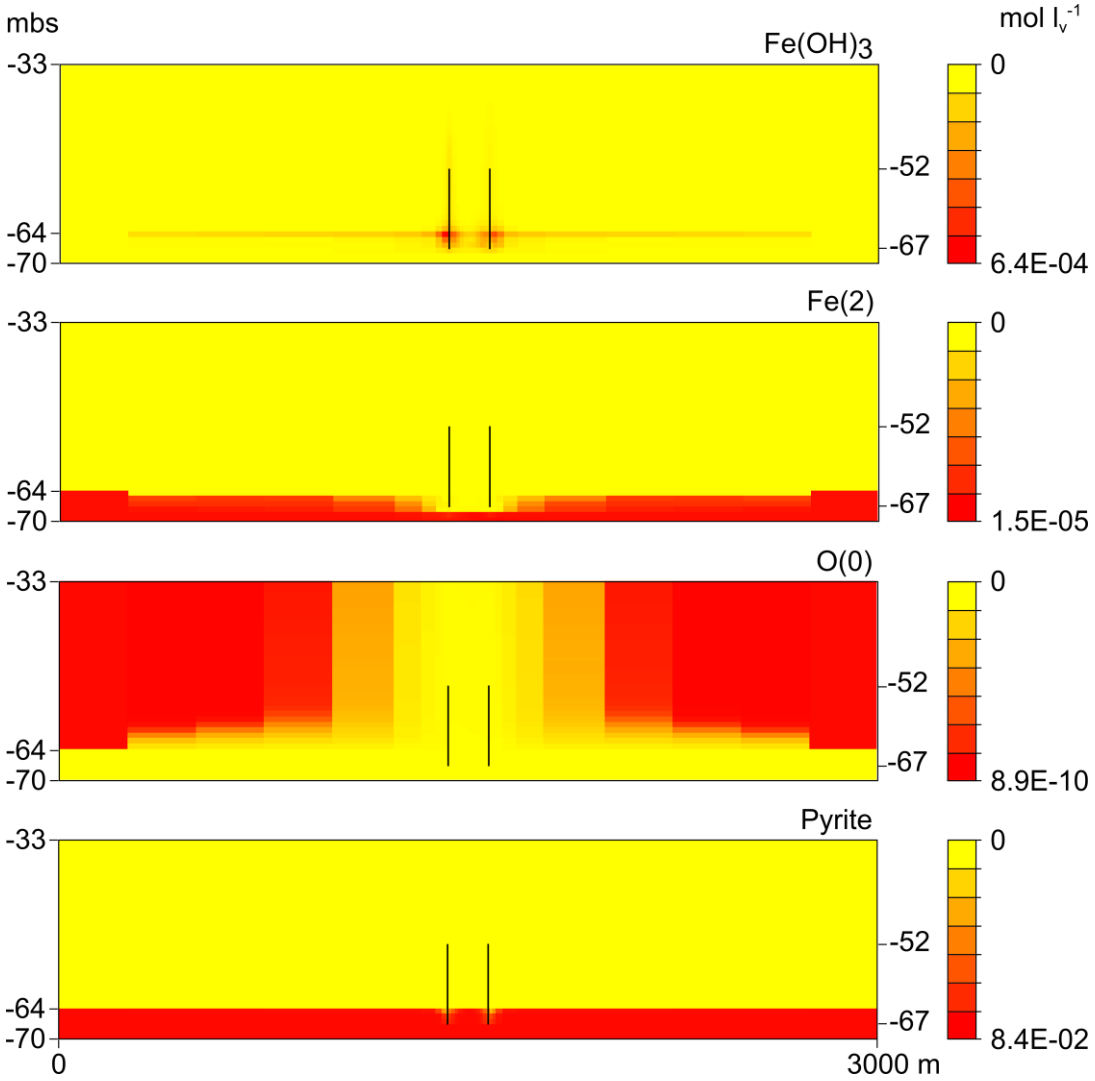

Figure 3.5 Leuven case. Modeled $Fe(OH)_3$, Fe(2), O(0) and pyrite concentration around the ATES wells after 20 years of operation. The black lines on the plots show the position of the ATES well screens

3.3.1 Leuven case

Model results after 20 years of ATES operation are presented in Figure 3.5. Most $Fe(OH)_3$ precipitation seems to occur around the well screens, especially in the reduced part. By this process, Fe(2) and O(0) are consumed whereby the Fe(2) concentration around the reduced part of the well screen strongly decreases as well as the O(0) concentration around the wells in the formerly oxidized part of the aquifer. By the introduction of oxygen and nitrate, pyrite turns out to be oxidized resulting in $Fe(OH)_3$ precipitation (reaction equations 3.9 and 3.10). As was already mentioned, most $Fe(OH)_3$ precipitation occurs in and around the reduced part of the well screens, with highest precipitation just below the redox boundary (Figure 3.6). Concentration of $Fe(OH)_3$ in the part of the well screen above the redox boundary decreases with increasing distance above the redox boundary. Figure 3.6 also shows that $Fe(OH)_3$ precipitation still occurs after 20 years of operation. However after 2 to 3 years already half of the total precipitation (over 20 years) has occurred, determined by an initially higher Fe(2) and O(0) availability.

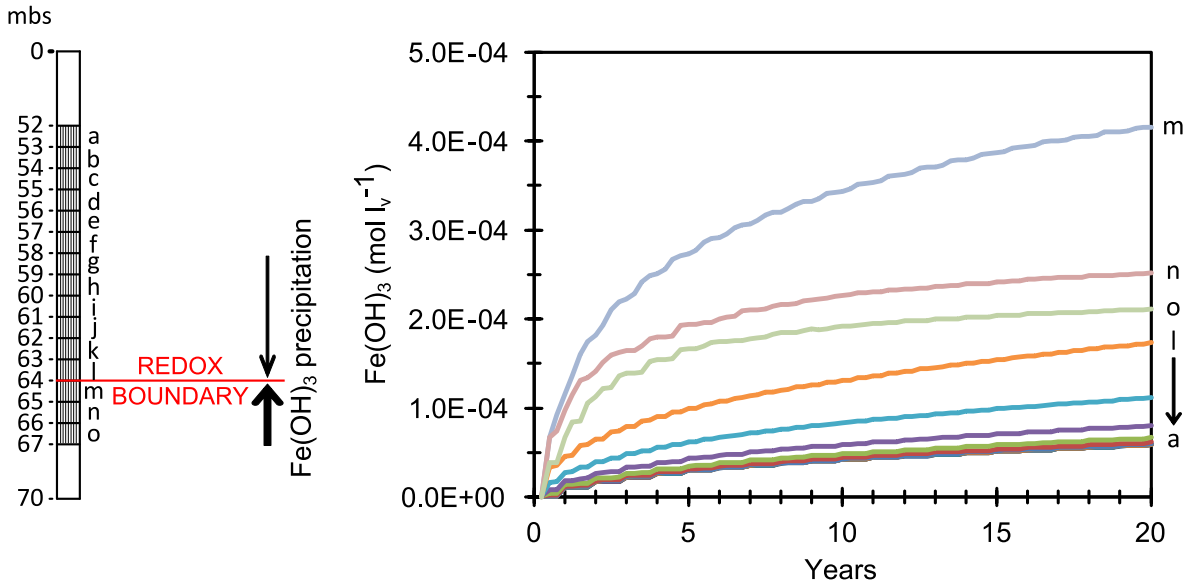

Figure 3.6 Leuven case. Modeled evolution of $Fe(OH)_3$ concentration in the well screen cells of the cold well.

Temperature also seems to affect $Fe(OH)_3$ precipitation (Figure 3.7). To separate the mixing effect from the temperature effect, three simulations with different temperature conditions were performed. For all three simulations, extraction started in well A and injection started in well B. For simulation 1, the injection temperature for both wells is the same as the initial ambient groundwater temperature (11°C). Therefore, the difference between the $Fe(OH)_3$ concentration in well A and B can be fully attributed to mixing processes. Highest $Fe(OH)_3$ concentration occurs at the well where the injection was started in the first operation season (well B). This effect can be explained by a strong drop in Fe(2) concentrations around both wells in this first season by precipitation of $Fe(OH)_3$ around both the injection and extraction well. The strongest precipitation in the wells always occurs during injection (steeper parts of the curves), but when the injection phase starts in well A in the next operation season, less Fe(2) is available around the wells, in comparison with the first operating season, so that the precipitation rate of $Fe(OH)_3$ in the injection well is lower than it was in operating season 1. The concentration of $Fe(OH)_3$ in each of the ATES wells will therefore be strongly determined by this initial mixing effect. Simulation 2 shows that when the injection is started in the warm well, highest $Fe(OH)_3$ concentration no longer occurs in the well where the injection was started (well B), but in the cold well (well A). This cannot be explained as a direct effect of temperature, as at lower temperatures the solubility of $Fe(OH)_3$ is higher (Equation 3.5). It can be explained however by an indirect effect of temperature, as a lower

temperature causes a higher pH (Equations 3.7 - 3.8, Figure 3.8), which in its turn will cause more $Fe(OH)_3$ to precipitate. So temperature has a higher influence on $Fe(OH)_3$ precipitation than the initial mixing effect. The highest concentration as well as the lowest concentration are modeled in simulation 3, where the highest $Fe(OH)_3$ concentration occurs at the cold well, where the injection was started (well B) and the lowest concentration occurs in the warm well (well A). Around well B the initial mixing effect is enhanced by the temperature effect.

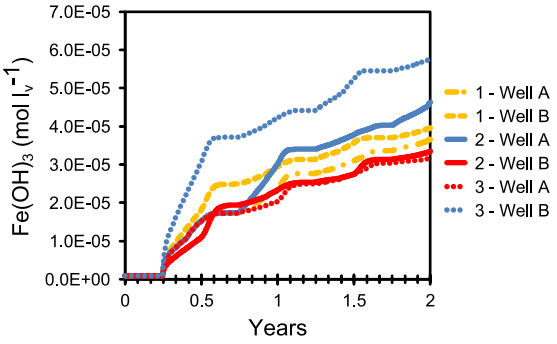

Figure 3.7 Leuven case. Temperature effect. Extraction starts in well A, injection starts in well B. 1: same injection temperature in both wells; 2: injection started in warm well; 3: injection started in cold well.

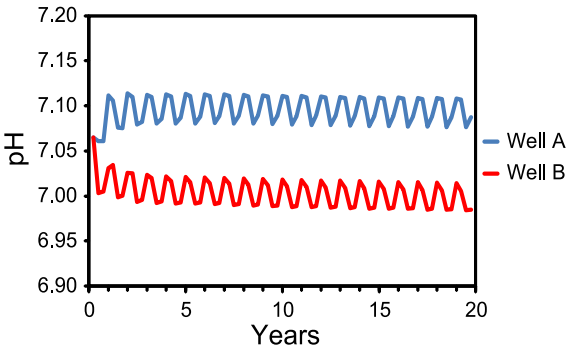

Figure 3.8 Leuven case. Effect of temperature on pH. Well A (blue) is the cold well, well B (red) is the warm well.

Beginning the injection in the cold well will cause this well to have the highest precipitation in $Fe(OH)_3$, whereas meanwhile the warm well will have the lowest concentration. Beginning the injection in the warm well will cause the temperature effect and initial mixing effect to counteract each other, still with the highest concentration of $Fe(OH)_3$ in the cold well, but with a concentration closer to the one in the warm well. So even at these low injection temperatures of 6°C for the cold well and 16°C for the warm well, the models predict a significant temperature influence.

To determine possible measures to decrease the $Fe(OH)_3$ precipitation in and around the wells, and therefore the risk of well clogging, different model scenarios were developed (Figure 3.9). As starting point for the five scenarios the reference case was used. In variant 1 the flow rate of the reference case was divided by two (360 m^3 day^{-1}). For variant 2 shorter well screens (10 m) were implemented, from 52 to 62 mbs, so that the redox boundary is 2 m below the bottom of the wells screens. For variant 3 the well screen positions are the same as in variant 2, but the flow rate is divided by two (360 m^3 day^{-1}). Variant 4 also has well screens of 10 m, but now the wells are screened from 49 to 59 mbs, with the well screen bottoms 5 m above the redox boundary. Variant 5 has the same well screen positions as variant 4, but a two times smaller flow rate (360 m^3 day^{-1}). The results show that with decreasing flow rate and with well screens further from the redox boundary, the $Fe(OH)_3$ precipitation in the wells becomes smaller. The position of the redox boundary is hereby more important than reducing the flow rate of the wells (Table 3.8). Lowering the flow rate of the reference case with factor 2, will only ensure a reduction in $Fe(OH)_3$ precipitation with factor 1.2, both in the warm and the cold well. Installing the well screen two meters above the redox boundary, however, provides a reduction in $Fe(OH)_3$ precipitation with factor 3.2 for the cold well and factor 4.2 for the warm well, where installing the well screen five meters above the redox boundary will even ensure a reduction with factor 7.9 for the cold well and factor 8.9 for the warm well. It should be noted however that the precipitated concentration in the well cells is rather low, e.g. maximum 5.19 g m^{-3} for the cold well in the reference case (Table 3.8). These calculated concentrations are average concentrations for the cells wherein the ATES wells are positioned, 15 cells of 1m x 1m x 1m for the reference case and variant 1, 10 cells of 1m x 1m x 1m for the other cases.

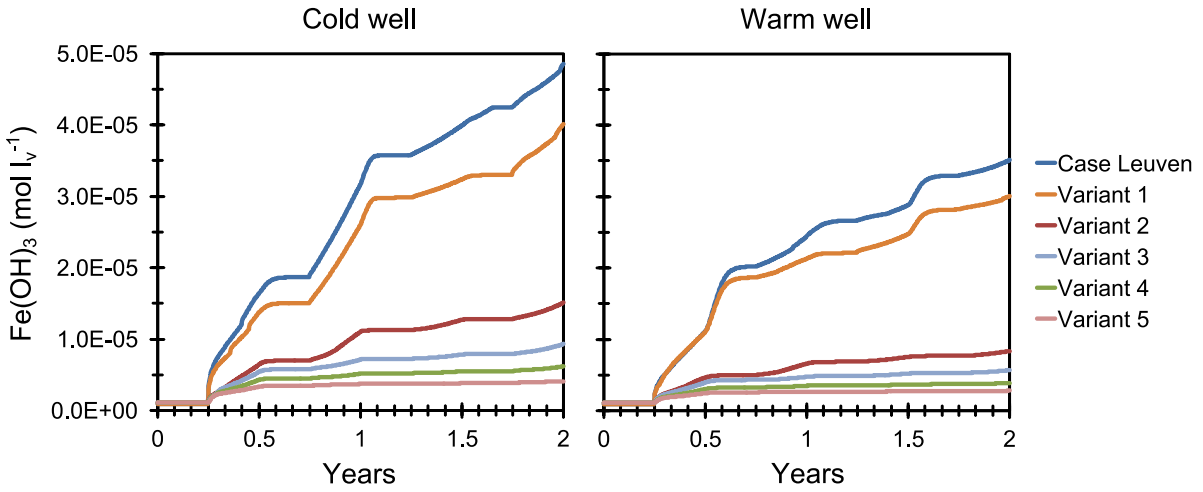

Figure 3.9 Leuven case. Modeled evolution of $Fe(OH)_3$ concentration in the cold and warm well for the reference case and 5 variants (Table 3.8). For the reference case, well screen positions (Figure 3.6) and flow rate are as described above. Variant 1: the flow rate of the reference case is divided by two; Variant 2: shorter well screens (10 m) so that the redox boundary is 2m below the well screens bottoms; Variant 3: same well screen positions as in variant 2, but flow rate is divided by two; Variant 4: shorter well screens (10 m) and positioned 3 m higher, so that the redox boundary is 5 m below the well screen bottoms; Variant 5: same well screen positions as in variant 4, but flow rate is divided by two.

Table 3.8 Flow rate, well screen length, position of the well screen bottom with respect to the redox boundary and average cumulative concentration of $Fe(OH)_3$ precipitated in the well cells after 2 years for the different model scenarios of the Leuven case.

Scenario	Flow rate	Well screen		$Fe(OH)_3$ concentration	
		Length	Bottom above redox boundary	Cold well (A)	Warm well (B)
	$m^3\ day^{-1}$	m	m	$g\ m^{-3}$	$g\ m^{-3}$
Reference case	720	15	-3	5.19	3.75
Variant 1	360	15	-3	4.29	3.21
Variant 2	720	10	2	1.61	0.90
Variant 3	360	10	2	0.99	0.61
Variant 4	720	10	5	0.66	0.42
Variant 5	360	10	5	0.44	0.30

3.3.2 Antwerp case

Model results after 20 years of ATES operation are shown in Figure 3.10. $Fe(OH)_3$ precipitation causes the Fe(2) concentration in the ATES wells to drop and oxidizing agents O(0) and N(5) to be consumed. This is reflected by the fact that when Fe(2) is totally depleted, the O(0) and N(5) concentration as well as the redox potential (pe) in the wells show a slight increase and the $Fe(OH)_3$ precipitation is slowed down. Notable however is that in this case the highest $Fe(OH)_3$ concentrations are found in the well where the extraction was started. At extraction the oxygen rich water above is attracted and most $Fe(OH)_3$ is precipitated around the extraction well, consuming most of the attracted oxygen. Figure 3.10 also shows that $Fe(OH)_3$ concentration in the ATES wells still gradually increases after 20 years of operation, but in the first 5 years, already half of the total precipitation (over 20 years) has occurred, also here determined by an initially higher Fe(2) and O(0) availability. The evolution of glauconite concentration is characterized by dissolution in the warm well and precipitation in the cold well.

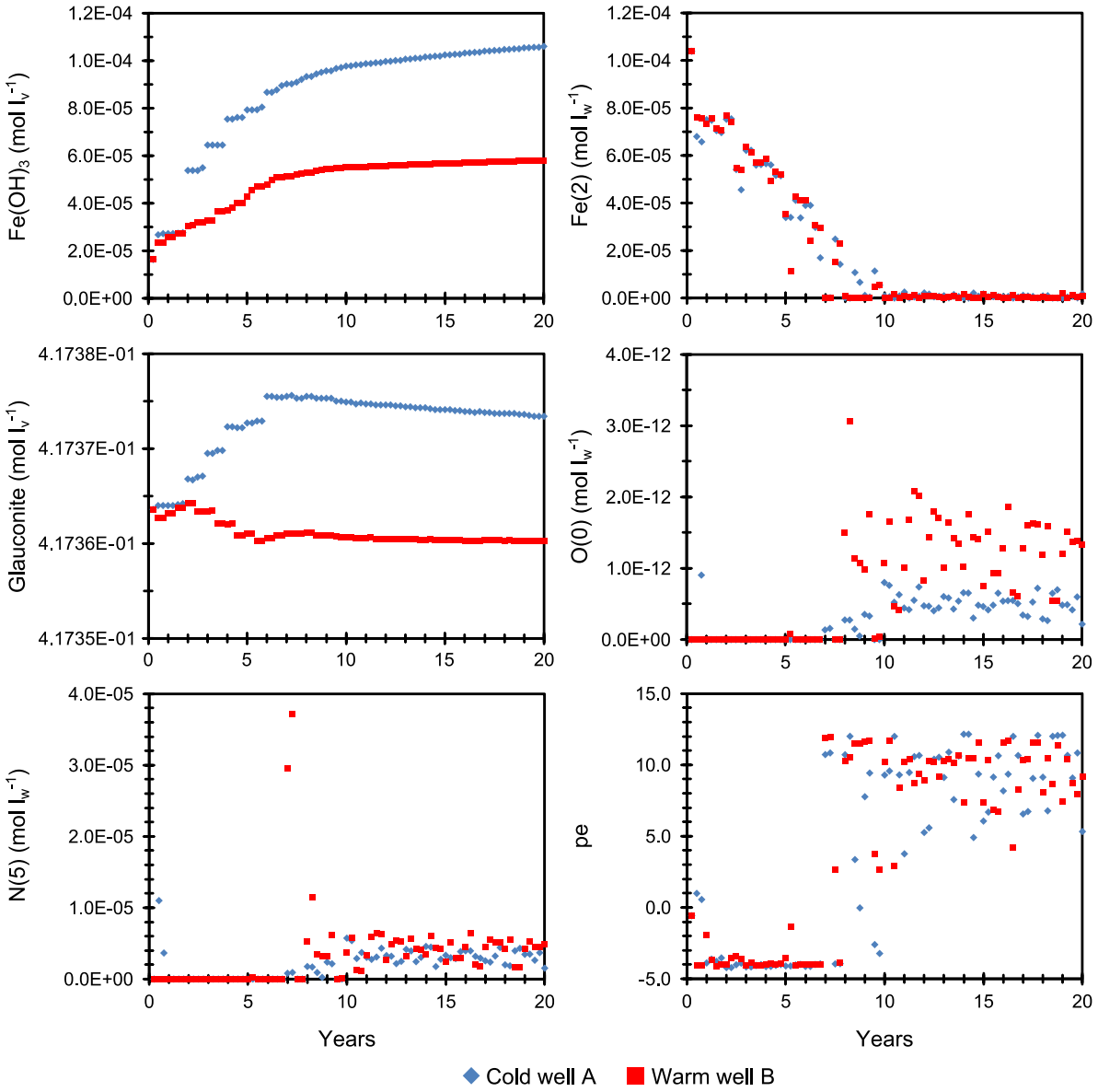

Figure 3.10 Antwerp case. Modeled evolution of $Fe(OH)_3$, Fe(2), glauconite, O(0), N(5) concentration and pe in the ATES wells. Extraction started in the cold well, injection started in the warm well.

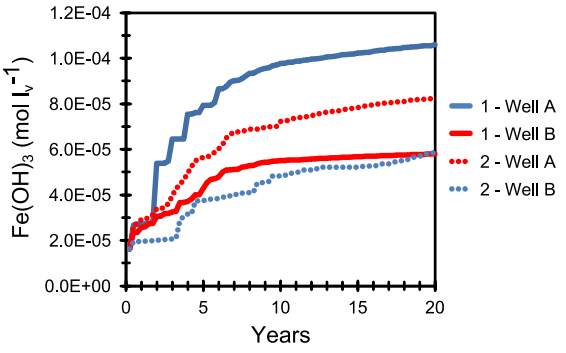

Figure 3.11 Antwerp case. Temperature effect. Extraction starts in well A, injection starts in well B. 1: extraction started in cold well, injection started in warm well; 2: extraction started in warm well, injection started in cold well.

Figure 3.11 shows that temperature also plays a role in the $Fe(OH)_3$ precipitation in the Antwerp case, but less pronounced than in the Leuven case. Both in the case where the extraction was started in the cold well as in the case where the extraction was started in the warm well, the $Fe(OH)_3$ concentration is highest in and around well A, where the extraction was started. The $Fe(OH)_3$ concentration in the extraction well however is highest when the operation started in the summer season, with extraction in the cold well and injection in the warm well. After two years the models predict an average cumulative $Fe(OH)_3$ concentration in the well cells of 5.75 g m^{-3} and 3.26 g m^{-3} for the cold and warm well respectively.

In both the Leuven and Antwerp models the $Fe(OH)_3$ precipitation was highest in the beginning of ATES operation, explained by the initial mixing effect. It should be noted however that no hydraulic gradient was applied in the models to obtain a stable initial redox boundary. Though, in almost all natural systems a hydraulic gradient will be present. A part of the mixed bubble will therefore be drifted away by natural groundwater flow before it is recovered by the ATES system. This will ensure an influx of O(0) and Fe(2) that will continue to react and which will result in a higher $Fe(OH)_3$ precipitation than predicted by the models without natural groundwater flow (Bustos Medina et al., 2013). With a natural groundwater flow velocity of 7.7 m/year in the Leuven case and a groundwater flow velocity of 2 m/year in the Antwerp case, the groundwater flow velocity is rather small. Therefore the bubble drift will not be large at both discussed sites. At other sites with higher hydraulic conductivity and larger hydraulic gradient this effect can be important and small bubble radii should be avoided. Hence, it is better to have a limited screen length to create thin but wide ATES bubbles. Over-dimensioning of ATES systems in groundwater systems with different groundwater qualities should thus be avoided.

In both modeling cases, the concentration of $Fe(OH)_3$ is highest in the cold wells. This is explained by an indirect effect of temperature, as a lower temperature induces a higher pH, which in its turn will cause more $Fe(OH)_3$ to precipitate. The cold wells will therefore be more prone to clogging by iron (hydr)oxides than the warm wells. Furthermore, modeling results show that highest $Fe(OH)_3$ precipitation does not always have to occur at the injection well, but that it depends on the position of the well screens in relation with the redox boundary. When the well screens are largely in the oxidized zone, the extracted water is oxygen rich and at injection over the whole filter length, most $Fe(OH)_3$ will precipitate around the well screen in the reduced, Fe(2) rich part of the aquifer. When the well screens are in the reduced part of the aquifer, at extraction the oxygen rich water above will be attracted and most $Fe(OH)_3$ will precipitate around the extraction well consuming most of the attracted oxygen, resulting in less oxygen available to react in the injection well.

3.4 Conclusions

This study focused on identifying the extent and location of $Fe(OH)_3$ precipitation around ATES wells and the effect of temperature and mixing of different water types. It is shown via both case studies that the initial mixing effect plays an important role in the $Fe(OH)_3$ precipitation process. If the well screens are largely in the oxidized zone, such as in the Leuven case, the largest concentration of $Fe(OH)_3$ will develop at the well where the injection started. When the well screens are in the reduced zone, such as in the Antwerp case, however, most $Fe(OH)_3$ precipitation will develop at the well where the extraction started. Notable also is that the models predict that even at small temperature differences (ΔT = 10°C), there is a significant temperature influence, with highest precipitation of $Fe(OH)_3$ in and around the cold wells. In the future, this model result has to be confirmed with field evidence.

The best way to avoid $Fe(OH)_3$ precipitation is positioning the ATES well screens far enough from the redox boundary to prevent mixing oxygen/nitrate rich with reduced, iron rich groundwater. However as the results show that most $Fe(OH)_3$ precipitation occurs in the first years of operation, controlled by Fe(2) availability, in-situ iron removal as also used in drinking water production could be a solution (Appelo and de Vet, 2003; Appelo et al., 1999; van Halem et al., 2012, 2011, 2010). This should, however, be further investigated in the context of ATES.

Both models predict very low concentrations of $Fe(OH)_3$, e.g. 5.19 g m^{-3} and 5.75 g m^{-3} in the first meter around the cold well for the Leuven and Antwerp case respectively. With a density of 3.8 g cm^{-3}, the effect of this precipitation will be negligible. However, the modeled initial oxygen concentrations are much lower than the measured concentrations. Therefore the expected $Fe(OH)_3$ concentration around the ATES wells is expected to be higher than that predicted by the models. Although very

important in the formation of iron (hydr)oxides (Lerm et al., 2013, 2011; Vetter et al., 2012), microbial iron oxidation was not incorporated in the reactive transport models for simplification reasons. Furthermore, the non-lineair effect of precipitation on the permeability of the aquifer, was not investigated. Future modeling work should therefore focus on incorporating more realistic oxygen concentrations in the models, biogenic reactions in the reaction network and link the modeled $Fe(OH)_3$ precipitation to permeability changes around ATES wells to assess the impact of well clogging on ATES performance. Finally, this study only focused on $Fe(OH)_3$ precipitation around the ATES wells, in the aquifer. The $Fe(OH)_3$ precipitation in the facility piping, in the wells and on the well screens was not accounted for. Precipitation at these locations however can also largely reduce the capacity of an ATES system.

Chapter 4

Modeling the effect of clay drapes on the efficiency of Aquifer Thermal Energy Storage

Modified from: Possemiers, M., Huysmans, M., Batelaan, O. (in review) Modeling the effect of clay drapes on the efficiency of Aquifer Thermal Energy Storage (ATES).

4.1 Introduction

In Aquifer Thermal Energy Storage, warm and cold zones arise around the ATES wells in the subsurface. In efficient ATES systems, loosing this stored heat and cold by high natural groundwater flow or by interference between the warm and cool zones in the aquifer should be avoided. As there is an increasing demand for ATES, the subsurface planning of such systems should be optimized to use the available space as efficient as possible. Groundwater flow and heat transport models are therefore indispensable to determine the most optimal location of ATES wells within a particular system but also to determine the optimal location for ATES systems relatively to each other. In this way negative interference between ATES systems and between different wells within an ATES system can be avoided.

Heat transport in ATES systems is already well established, but most studies consider homogeneous aquifers (e.g. Andrews, 1978; Gringarten and Sauty, 1975). More recent studies (Bridger and Allen, 2013, 2010; Caljé, 2010; Ferguson, 2007; Rodrigo-Ilarri et al., 2014, 2010; Sommer et al., 2013) indicate that heterogeneity in the permeability field of an aquifer introduces considerable uncertainty in the distribution of heat associated with injection of warm and cold water into an aquifer. Furthermore heterogeneity in the permeability field was found to reduce the ability to recover the introduced heat and cold at a later time. In their modeling study, Bridger and Allen (2013, 2010) compared the results from both a non-layered and layered model and found that heat was transported preferentially along high hydraulic conductivity layers, resulting in a distorted and elongated plume. They found further that at instantaneous recovery (no storage), the efficiency is higher for the layered model, which is likely related to the presence of lower conductivity layers at the well screens, retaining the thermal energy closer to the wells. After 120 days of storage, the storage efficiency is found to be lower for both the layered and non-layered models compared to the storage efficiency at instantaneous recovery. The layered model shows a lower storage efficiency (62 %) compared to the non-layered model (72 %) reflecting a more dominant role of the high conductivity layers at larger storage times. Caljé (2010) modeled heterogeneity in two ways, by simulation of a gravel layer and by geostatistically generating heterogeneities in the horizontal plane. With a gravel layer present, the recovered energy is found to be 10% lower in comparison with the homogeneous model, caused by a larger thermal interference between the warm and cold well. The generated random hydraulic conductivity fields have a significant effect on the shape of the warm and cold bubbles, but the recovered temperatures seem to be independent of these heterogeneities. Only for variogram ranges in the order of the distance between the warm and cold well, a decline of 3 % in ATES efficiency is found. With the variogram range being the distance between data pairs from which an increase of this distance does not result anymore in a larger average squared difference between the data pairs. At this point the variogram reaches a plateau. Ferguson (2007) used the geostatistical properties from two aquifers, the Borden aquifer, Ontario, Canada (Woodbury and Sudicky, 1991) and the Carbonate Rock Aquifer, Manitoba, Canada (Kennedy and Woodbury, 2002) to determine the influence of heterogeneity on the recoverability of thermal energy. For the Borden aquifer, which is a rather homogeneous sand body, a reduction of 5.5% in energy recovered with respect to the homogeneous model is found while for the more heterogeneous, paleokarstic Carbonate Rock Aquifer, a reduction of 8.2% is reported. Further the simulated heterogeneity results in a larger spreading of heat in the aquifer. Also Rodrigo-Ilarri et al. (2014, 2010) and Sommer et al. (2013) generated several heterogeneous hydraulic conductivity fields. The first study confirms the major impact of heterogeneity on the shape and development of a thermal plume, the latter study additionally shows that the median thermal recovery in heterogeneous media with a log conductivity standard deviation of 1 to 2 is 6 to 15 % lower than in a homogeneous medium.

However, all these studies introduce heterogeneity either with a variogram-based stochastic approach (Ferguson, 2007; Rodrigo-Ilarri et al., 2010; Sommer et al., 2013) or on a large scale, e.g. as a gravel layer in a sandy aquifer (Caljé, 2010) or as lenses and interlayers of distinct permeability (Bridger and

Allen, 2013, 2010). The influence of small scale sedimentary features, such as clay drapes, on the distribution of heat and cold around ATES wells, however, has not been investigated so far. Despite the limited thickness of clay drapes of often only a few centimeters (Houthuys, 1990; Stright, 2006), several studies point out that they have an influence on groundwater flow and solute transport at different scales (Huysmans and Dassargues, 2012, 2009; Koltermann and Gorelick, 1996; Li and Caers, 2011; Mikes, 2006; Morton et al., 2002; Ringrose et al., 1993; Stright, 2006; Willis and White, 2000; Zheng and Gorelick, 2003). The aim of the present study is therefore to assess the influence of small-scale clay drapes on the distribution of the warm and cold plume around an ATES system and to determine the effect of this fine-scale heterogeneity on the recoverability of the stored heat and cold.

4.2 Materials and Methods

The models used for the present study are based on the MODFLOW (Harbaugh et al., 2000) models constructed by Huysmans and Dassargues (2012). These flow models were adapted to allow simulation of heat transport by MT3DMS (Zheng and Wang, 1999).

4.2.1 Geological setting

As typical example of an aquifer characterized by complex geological heterogeneity, the Brussels Formation is chosen for this modeling study. The Brussels Formation is an early Middle Eocene shallow marine sand deposit in central Belgium. The aquifer constitutes a major groundwater resource in the region. The Brussels Sands are a tidal sandbar deposit which filled two central major SSW-NNE troughs and several smaller troughs with the same orientation. The sandbar deposits are characterized by sedimentary features such as cross bedding, clay drapes and reactivation surfaces (Houthuys, 2011, 1990). Huysmans et al. (2008) and Possemiers et al. (2012) found that there is a direct relation between these small scale geological heterogeneities and the spatial variability of permeability. The site chosen for the model is situated in Bierbeek (Belgium) (Figure 4.1). The geology at this site consists of a 4 m thick Pleistocene sandy loam cover, 35 m of Brussels Sands and 12 m of Ieper Clay (Huysmans and Dassargues, 2012).

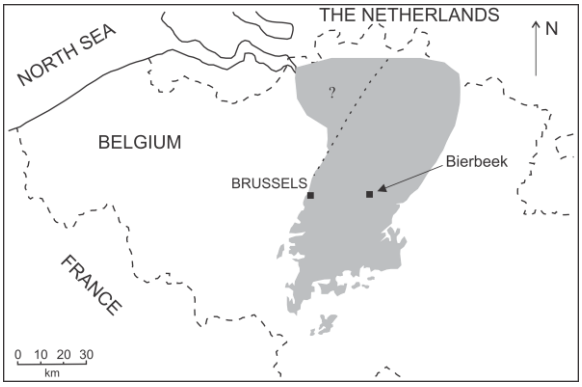

Figure 4.1 Map of Belgium showing the outcrop and subcrop area of the Brussels Sands (grey part) (adapted from Houthuys, 1990).

4.2.2 Incorporation of clay drapes

To incorporate the complex pattern of the clay drape distribution (Figure 4.2) in the models, multiple-point geostatistics is used. This technique has proven to be very suitable for the simulation of complex heterogeneity structures (Comunian et al., 2011; dell'Arciprete et al., 2011; Hu and Chugunova, 2008; Huysmans and Dassargues, 2009; Strebelle, 2002). Multiple-point geostatistics uses training images to characterize the geological heterogeneity. Training images are explicitly grid-based representations of the expected patterns of geological heterogeneity. During model construction, these patterns are reproduced in the model domain (Caers and Zhang, 2004; Huysmans and Dassargues, 2012; Strebelle, 2002). As multiple-point geostatistics infers the multivariate distributions directly from training images, it allows to incorporate a conceptual geological model in a stochastic simulation framework (Caers and Zhang, 2004; Comunian et al., 2011; Hu and Chugunova, 2008; Huysmans and Dassargues, 2012; Strebelle, 2002). However, the drawback of implementing multiple-point geostatistics in large-scale three-dimensional grids is that they are computationally very intensive. Therefore the method of direct multiple-point geostatistical simulation of edge properties (Huysmans and Dassargues, 2011) was used in the current

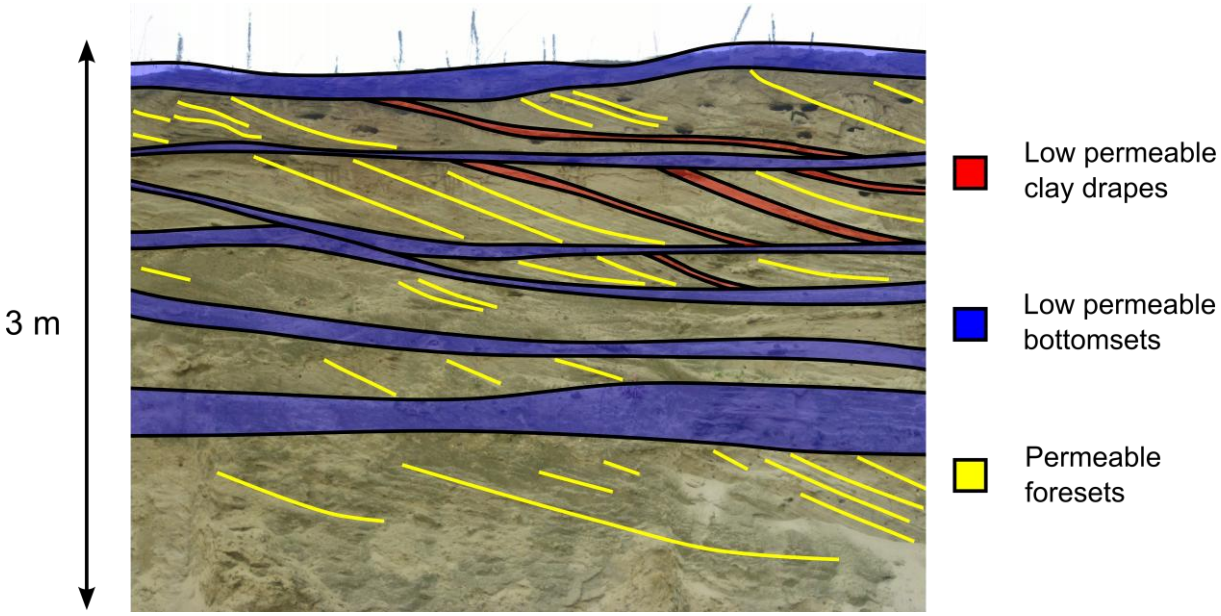

Figure 4.2 Interpreted field picture showing clay drapes, bottomsets and foresets.

models. This method enables simulation of thin irregularly shaped surfaces with a smaller CPU and RAM demand in comparison with the more conventional multiple-point geostatistical techniques. Instead of representing the clay drapes as objects consisting of several cells, the clay drapes are incorporated as edge properties between cells. These edge properties are assigned to the cell faces (Huysmans and Dassargues, 2011; Stright, 2006).

The 2D training image used for this study was constructed based on detailed in situ mapping (Huysmans and Dassargues, 2009; Huysmans et al., 2008). In the third dimension perpendicular to the 2D training image, clay drapes show a continuous horizontal layering. All layers and sedimentary features are therefore assumed continuous in that direction. The constructed 2D training image shows a sand facies intercalated with clay drapes. In the simulation step, these patterns are adopted from the training image and represented in the simulation domain (Figure 4.3). For more details about the incorporation of the clay drapes in the models we refer to Huysmans and Dassargues (2012).

4.2.3 Heat transport

Heat transfer in aquifers occurs through heat transport by the fluid phase, conductive transport of heat through the aquifer material and heat exchange between the fluid phase and the aquifer material (De Marsily, 1986). Due to the similarity between the solute and heat transport equation, MT3DMS can be used to model heat transport (Caljé, 2010; Fossoul et al., 2011; Hecht-Méndez et al., 2010; Sommer et al., 2013; Thorne et al., 2006; Zheng, 2010). The thermal parameters were calculated based on literature values of similar lithologies (N.V.O.E., 2006; Zuurbier, 2011). Different thermal parameters were calculated for the Brussels Sands and Ieper Clay. However, no difference is made between the foresets and clay drapes within the Brussels Sands, as the effect is expected to be negligible (Ferguson, 2007). The thermal diffusion coefficient (D_{m_temp}) is calculated as:

$$D_{m\_temp} = \frac{\lambda_e}{n\,\rho_w\,c_w} \quad (4.1)$$

where λ_e is the bulk thermal conductivity of the aquifer, n is the porosity, ρ_w is the density of water and c_w is the specific heat capacity of water. The thermal distribution coefficient (K_{d_temp}) is calculated as:

$$K_{d\_temp} = \frac{c_s}{\rho_w\,c_w} \quad (4.2)$$

where c_s is the specific heat capacity of the solid phase.

4.2.4 Model setup

To assess the impact of clay drapes on heat transport, several model variants with the following characteristics were built: heterogeneous versus homogeneous, with a hydraulic gradient versus without a hydraulic gradient, and the ATES wells parallel to the clay drape strike versus the ATES wells perpendicular to the clay drape strike. Combining these features gives eight combinations and heat transport models (Table 4.1). In the heterogeneous models a random clay drape realization was incorporated. The homogeneous models are horizontally isotropic models without clay drapes (Huysmans and Dassargues, 2012).

Each model is a three dimensional local model of 600 m x 600 m in the x and y direction and has a thickness of 39.7 m (Figure 4.3). The top of each model corresponds to an elevation of 49.8 m, corresponding to the initial groundwater level at the well site before pumping. In the model variants with a regional groundwater flow,

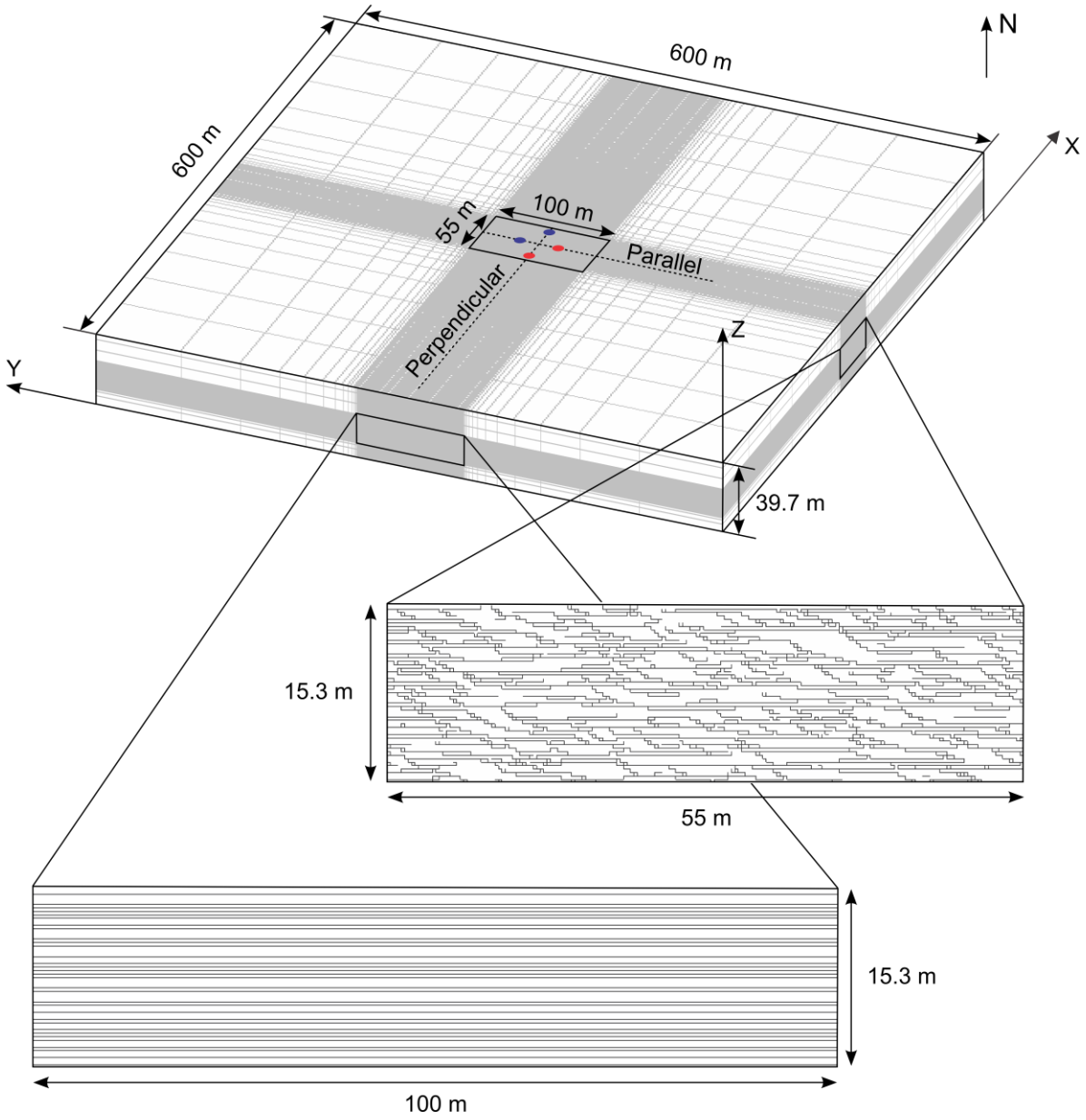

Figure 4.3 Model grid and edge realization. On the model grid, the two modeled layouts of the ATES doublets are indicated with an ATES doublet parallel to the clay drape strike and one doublet perpendicular to the clay drape strike. The red dots represent the warm wells, the blue dots represent the cold wells (adapted from Huysmans and Dassargues, 2012).

Table 4.1 Model variants.

	Model variant							
	1	2	3	4	5	6	7	8
Heterogeneous	x		x		x		x	
Homogeneous		x		x		x		x
Gradient			x	x			x	x
No gradient	x	x			x	x		
Parallel	x	x	x	x				
Perpendicular					x	x	x	x

a hydraulic gradient of 0.002 m/m was imposed by applying constant head boundaries at the up and downstream end. With an average hydraulic conductivity of 22.2 m/day, this hydraulic gradient results in a natural groundwater flow velocity of 16.2 m/year. Two geological layers are present in the model, the Brussels Sands from 49.8 m to 19.4 m and the Ieper Clay from 19.4 m to 10.1 m. In order to account for the thermal conduction, the Ieper Clay is discretized by 5 layers with thicknesses increasing by a factor 2 starting from 0.3 m at the bottom of the Brussels Sands. Each model has a central inner zone of 55 m x 100 m x 15.3 m with very small cell sizes (0.3 m x 0.3 m x 0.3 m), which allows individual clay drapes to be assigned as edge properties to the cell faces. The cell sizes in the outer zone are larger, between 0.45 and 82 m in the x and y direction, and with layer thicknesses between 3 m and 6 m. Each model is run in transient conditions with a total period of 5 years (1826.25 days) subdivided in 20 stress periods of 91.3125 days each representing one season. In each model two ATES wells, one cold and one warm well, are incorporated with a distance of 49.8 m from each other. This well-to-well distance corresponds to two thermal radii. The thermal radius (R_{th}) is the maximal distance of the thermal front from the injection well in a homogeneous environment. Vertical flow, advection by regional flow, thermal conduction and dispersion are neglected in this calculation (Sommer et al., 2013).

$$R_{th} = \sqrt{\frac{c_w \cdot V}{c_a \cdot \pi \cdot H}} \qquad (4.3)$$

where c_w is the volumetric heat capacity of water, V is the volume of water that is injected in one storage phase, c_a is the volumetric heat capacity of the aquifer (matrix and water) and H is the well screen length.

Each model run is started in summer, with extraction of water with an ambient temperature (11°C) and injection of water with a temperature of 16 °C. In autumn, both wells are turned off. In winter, the stored warm water is extracted and water with a temperature of 6°C is injected. In spring, the system is turned off again. This seasonal cycle is repeated for 5 years. The temperature differences are sufficiently small to neglect the temperature dependency of density and viscosity (Bridger and Allen, 2010; Fossoul et al., 2011; Sommer et al., 2014; Ward et al., 2007; Zuurbier et al., 2013). The screens of the ATES wells have a length of 15 m and are positioned between 34.4 and 19.4 m depth. A pumping rate of 100 m³/day is applied in both the injection and the extraction well. The ATES wells are oriented perpendicular to the hydraulic gradient, so that both wells are affected equally by advective heat loss. The wells are incorporated with the Multi-Node Well Version 1 Package (MNW1) (Halford and Hanson, 2002). The Multi-Node Well distributes the imposed flow rate of the well over different nodes by the calculated pressure and calculates a flux weighted extraction temperature. This makes the package very suitable for extraction and injection in heterogeneous aquifers. Dispersivity was chosen zero in all models so that the effects of hydrodynamic dispersion were simulated directly by including heterogeneity in the hydraulic conductivity (Ferguson, 2007; Sommer et al., 2013). In the heterogeneous models, the clay drapes are incorporated in layers 4 to 54 using the Horizontal-Flow Barrier Package (HFB6) (Hsieh and Freckleton, 1993) and vertical leakance (VCONT). With the Horizontal-Flow Barrier the vertical parts of the clay drapes are simulated, while with the vertical leakance the horizontal parts of the clay drapes are incorporated (Huysmans and Dassargues, 2012). In layers 1 to 3, no clay drapes are incorporated as these layers belong to the outer zone of the model. Layers 55 to 59 represent the top of the Ieper Clay.

The hydraulic and thermal parameters used in the models are presented in Table 4.2. The Modified Method Of Characteristics (MMOC) advection scheme generated less oscillations and had smaller computation times in comparison with the Total Variation Diminishing (TVD) scheme and was therefore used for

solving the numerical transport problem. The Courant number was chosen 0.75, allowing particles to move 0.75 x cell size in one transport step. The maximal Peclet number around the ATES wells is 0.9 for the heterogeneous models and 0.8 for the homogeneous models. Therefore, limited numerical dispersion is expected. The differential equations describing groundwater flow and heat transport are solved by MODFLOW 2000 (Harbaugh et al., 2000) and MT3DMS (Zheng and Wang, 1999) as supported by the pre- and post-processor Processing Modflow 8 (Chiang, 2010).

Table 4.2 Model parameter values.

	Heterogeneous	Homogeneous
Total model		
Dimensions (m)	600 x 600 x 39.7	
Grid cells (columns x rows x layers)	213 x 361 x 59	
Cell size	0.45-82 x 0.45-82 x 3-6	
Inner zone		
Dimensions (m)	55 x 100 x 15.3	
Grid cells (columns x rows x layers)	51 x 183 x 51	
Cell size (m)	0.3 x 0.3 x 0.3	
Horizontal hydraulic conductivity (K_h) (m/day) - Brussels Sands / Ieper Clay	23 / 1.00E-4	22.2 / 1.00E-4
Vertical hydraulic conductivity (K_v) (m/day) - Brussels Sands / Ieper Clay	4 / 3.33E-5	4.8 / 3.33E-5
Specific storage (m^{-1})	3.00E-05	3.00E-05
Clay drape parameter[1] (m/day)	0.175-9.905	-
Effective porosity	0.13	
Dispersivity (m)	0	
Water density (kg/m^3)	1000	
Water heat capacity (J/kg/K)	4193	
Water thermal conductivity (W/m/K)	0.58	
Solid density (kg/m^3) - Brussels Sands / Ieper Clay	2640 / 2200	
Solid heat capacity (J/kg/K) - Brussels Sands / Ieper Clay	890 / 1090	
Solid thermal conductivity (W/m/K) - Brussels Sands / Ieper Clay	2.4 / 1.7	
Thermal distribution coefficient (m^3/kg) - Brussels Sands / Ieper Clay	2.12E-04 / 2.6E-04	
Thermal diffusion coefficient m^2/day) - Brussels Sands / Ieper Clay	3.43E-01 / 2.46E-01	

[1] Hydraulic conductivity of clay drapes divided by clay drape thickness

4.2.5 ΔT and Energy output

To quantify the impact of the clay drapes on the efficiency of the modeled ATES system, the ΔT (°C) and the energy output (kWh) of the ATES system are calculated. The ΔT is calculated as the difference in temperature between the water in the cold well and the water in the warm well. It is the difference in temperature between the extracted and the injected water. The energy output is derived from this temperature difference (ΔT):

$$\text{Energy Output (kWh)} = \frac{\text{Power (W)}}{1000}\,\partial t(\text{h}) \qquad (4.4)$$

where

$$\text{Power (W)} = c_w \,.\, \rho_w \,.\, Q \,.\, \Delta T \qquad (4.5)$$

and c_w = 4193 J/kg°C, ρ_w = 1000 kg/m^3, Q = 4.17 m^3/h.

4.3 Results and Discussion

4.3.1 Thermal distribution

Figures 4.4 and 4.5 show the thermal distribution around the ATES wells for the different heterogeneous (a) and homogeneous (b) model variants after 5 years of operation. The third part (c) of each figure presents the difference in temperature distribution between the heterogeneous and homogeneous model. The cold storage is clearly more developed as the results present the situation at the end of spring, a passive storage phase after cold storage in winter, just before the injection in the warm well starts in summer. The thermal distribution around the ATES wells in the heterogeneous and the homogeneous model with the wells parallel to the clay drape strike and without a hydraulic gradient is shown in the upper part of Figure 4.4.

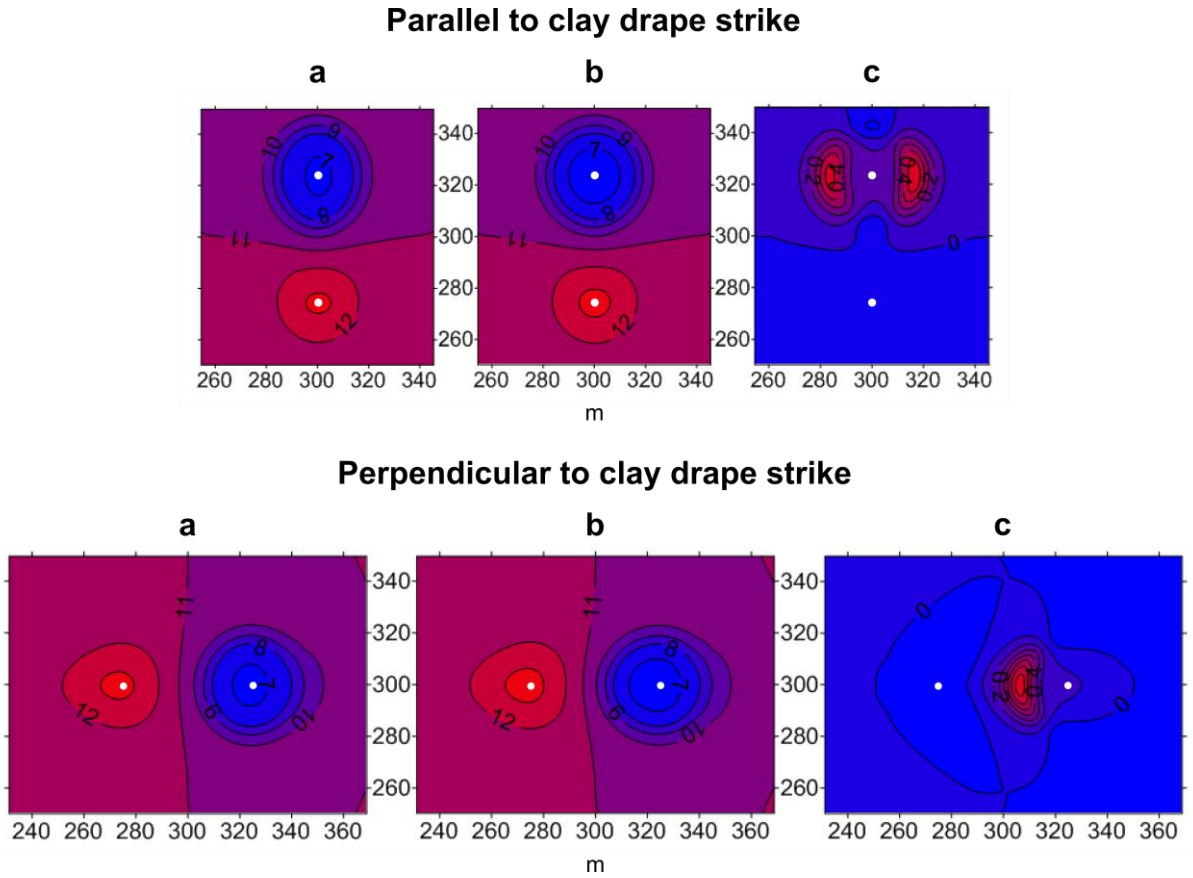

Figure 4.4 Temperature distribution (°C) around the ATES wells after 5 years of operation, without a hydraulic gradient: **a**: heterogeneous model; **b**: homogeneous model; **c**: difference between heterogeneous and homogeneous model.

In the heterogeneous model the cold bubble has a clear elliptical shape with the major axis of the ellipse parallel with the strike of the clay drapes. Whereas the cold bubble in the homogeneous model has a radial shape. The anisotropy in the thermal distribution around the wells in the heterogeneous model also becomes apparent when the temperature distribution of the homogeneous model is subtracted from the temperature distribution of the heterogeneous model. In the models with the wells parallel to the clay drape strike but with a hydraulic gradient of 0.002 m/m (Figure 4.5, upper part), the heat and cold obviously moves down gradient. Comparing the heterogeneous with the homogeneous model, however, still reveals the anisotropy direction parallel to the clay drape strike, e.g. the elliptical 8°C contour for the heterogeneous case and the temperature residuals. The same observations can be made for the model variants with the ATES wells perpendicular to the clay drape strike. In the bottom part of Figure 4.4 the 7°C contour has an elliptical shape in the heterogeneous model and

a radial shape in the homogeneous model and in the model with a hydraulic gradient (Figure 4.5, bottom part) the 8°C contour has a more pronounced elliptical shape in the heterogeneous model than in the homogeneous model. The temperature residuals are clearly aligned according to the clay drape strike. The models predict that the presence of small scale clay drapes creates anisotropy in the distribution of thermal energy in the subsurface. The major anisotropy axis is parallel to the strike of the clay drapes.

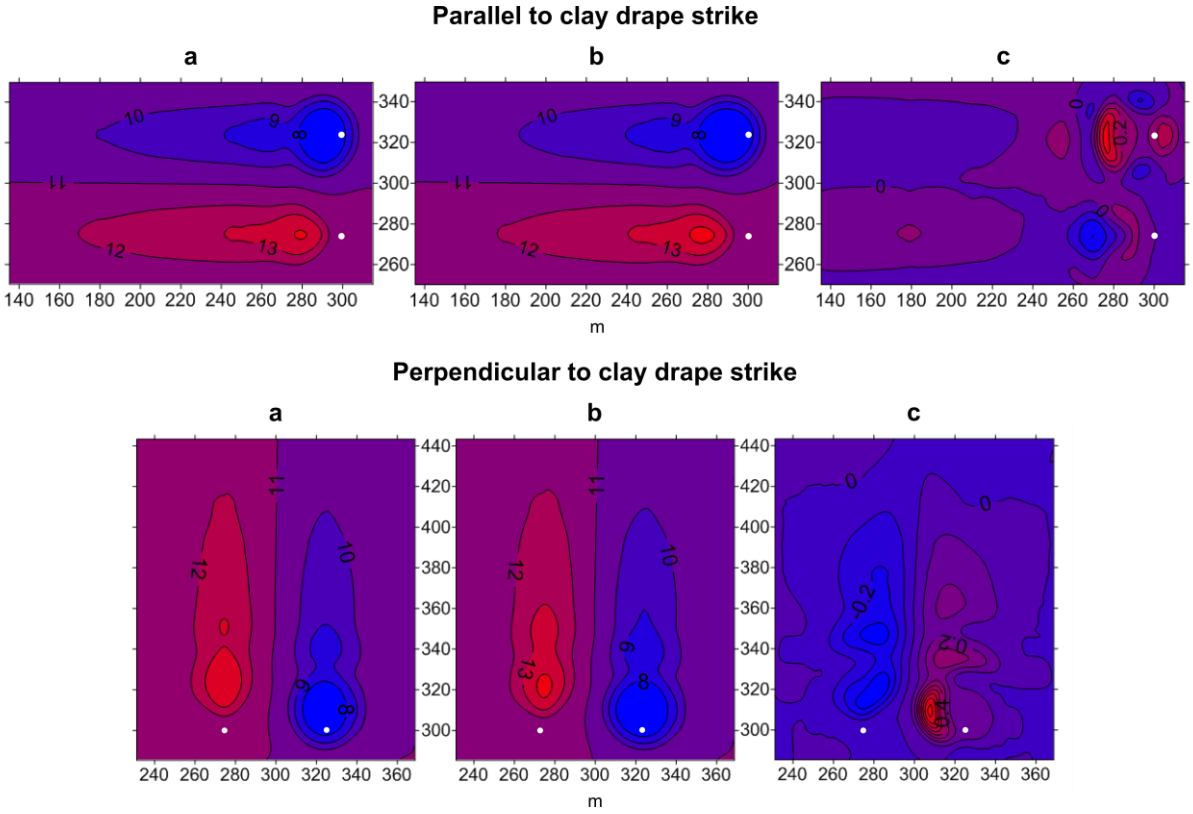

Figure 4.5 Temperature distribution (°C) around the ATES wells after 5 years of operation, with a hydraulic gradient of 0.002 m/m: **a**: heterogeneous model; **b**: homogeneous model; **c**: difference between heterogeneous and homogeneous model.

These results demonstrate that in addition to large scale heterogeneities (Bridger and Allen, 2013, 2010; Caljé, 2010; Rodrigo-Ilarri et al., 2014, 2010), also small scale sedimentary features have an influence on the distribution of thermal energy around an ATES system.

4.3.2 ATES efficiency

Figure 4.6 shows the injected and recovered temperatures in the ATES wells. In the models without a hydraulic gradient (Figure 4.6a,c), the recovered temperatures in the warm well are higher and in the cold well are lower compared to the temperatures recovered in the models with a hydraulic gradient (Figure 4.6b,d). This results in higher ΔT values for the models without a hydraulic gradient. This is explained by the advective heat loss in case of a hydraulic gradient.

Without a hydraulic gradient the clay drapes have a negative impact on the recovered temperatures. In the warm well the recovered temperatures are higher in case of the homogeneous models, whereas in the cold well the recovered temperatures are lower in the case of the homogeneous models, resulting in higher ΔT values for the homogeneous models compared with the heterogeneous models. This is explained by the clay drapes causing more dispersion of the thermal energy. For the models with a hydraulic gradient, however, the clay drapes have a positive impact on the recovered thermal energy. For the heterogeneous models the recovered temperatures in the warm well are

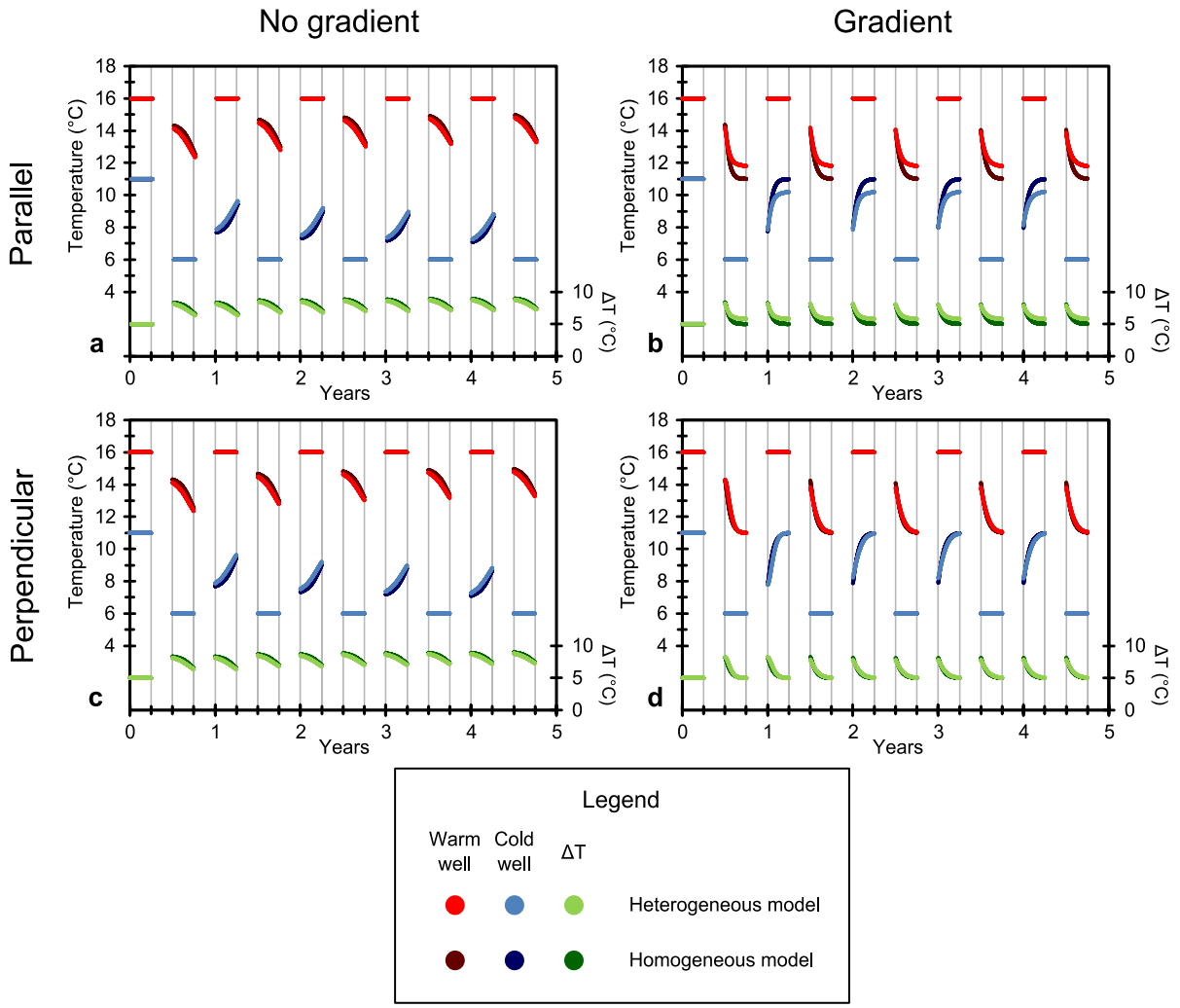

Figure 4.6 Injected and recovered temperatures. Water was injected at 16°C in the warm well (red) and 6°C in the cold well (blue), with an ambient groundwater temperature of 11°C. The green lines represent the temperature difference between the warm and cold well (ΔT). The light colors represent the temperatures simulated with the heterogeneous model, the darker colors represent the temperatures simulated with the homogeneous model. **a**: ATES wells parallel to the clay drape strike, without a hydraulic gradient; **b**: ATES wells parallel to the clay drape strike, with a hydraulic gradient of 0.002 m/m; **c**: ATES wells perpendicular to the clay drape strike, without a hydraulic gradient; **d**: ATES wells perpendicular to the clay drape strike, with a hydraulic gradient of 0.002 m/m.

higher and in the cold well are lower compared to the homogeneous models. Especially with the ATES wells parallel to the clay drape strike (Figure 4.6b) the model with a hydraulic gradient predicts a positive influence of the clay drapes on the recovered temperatures. In this case the recovered temperature at the end of summer is 0.8°C lower and at the end of winter is 0.8°C higher in the heterogeneous model compared to the homogeneous model. In the homogeneous models with a hydraulic gradient, the recovered temperatures at the end of an operating season approximate the ambient groundwater temperature (11°C). In case of a hydraulic gradient, the clay drapes ensure the thermal energy being retained closer to the wells, reducing the advective heat loss. This effect is largest in the model with the ATES wells parallel to the clay drape strike, because here the groundwater flow is perpendicular to the strike of the clay drapes.

The average ΔT and the total energy output after 5 years are shown in Table 4.3. The models without a hydraulic gradient predict a 3.3 to 3.6% lower energy output for the heterogeneous clay drape model compared with the homogeneous model, the models with a hydraulic gradient predict a 1.6% higher energy output for the heterogeneous model when the ATES doublet is positioned perpendicular to the clay drape strike to even a 10.2% higher energy

Table 4.3 Average ΔT and total energy output after 5 years of operation

	No gradient		Gradient	
	ΔT	**Energy output**	**ΔT**	**Energy output**
	°C	**kWh**	**°C**	**kWh**
Heterogeneous parallel model	7.56	803879	6.15	653583
Homogeneous parallel model	7.82	831292	5.58	593060
Difference	-0.26	-27413	0.57	60523
		-3.30%		10.21%
Heterogeneous perpendicular model	7.54	801477	5.76	612067
Homogeneous perpendicular model	7.81	831113	5.66	602260
Difference	-0.27	-29636	0.1	9807
		-3.57%		1.63%

output with the ATES wells parallel to the clay drape strike. Therefore it is clear that the different subsurface distributions of thermal energy between the heterogeneous and homogeneous models also have an impact on the recovered temperatures and the energy output of an ATES system.

Comparing these results with the modeling studies in literature (Caljé, 2010; Ferguson, 2007; Sommer et al., 2013), the orders of magnitude of the effects of heterogeneity on the recovered temperatures and on the efficiency of an ATES system are similar. Depending on the type of incorporated heterogeneity or the conductivity standard deviation, literature reports a reduction of 3 to 15 % in energy recovered for the heterogeneous models in comparison with the homogeneous models. So, small scale sedimentary features can have a similar impact on ATES efficiency compared with larger scale heterogeneity. Another interesting result of the current study is that optimizing the position of the ATES wells in relation with the anisotropy in the subsurface can give a positive impact on the ATES efficiency.

4.4 Conclusions

This study has investigated the effect of clay drapes on the distribution of thermal energy around ATES wells and the impact that these small scale clay drapes have on the efficiency of an ATES system. Therefore a heterogeneous clay drape model and homogeneous model constructed by Huysmans and Dassargues (2012) were adapted to allow heat transport modeling. Eight different model variants, either with or without hydraulic gradient, either heterogeneous or homogeneous and either with the ATES wells parallel or perpendicular to the clay drape strike, were build for this modeling study.

The models show that small scale clay drapes have their influence both on the distribution of thermal energy in the subsurface and on the efficiency of an ATES system. The distribution of the thermal energy in the subsurface is determined by the strike of the clay drapes, with the major anisotropy axis of the thermal storage volume parallel to the clay drape strike. The clay drapes have a negative impact on the ATES efficiency when there is no hydraulic gradient present. The models however predict that clay drapes can also have a positive impact on the efficiency when there is a hydraulic gradient present. In this case the clay drapes ensure that the thermal energy is retained, whereby the negative influence of the hydraulic gradient is smaller. This retention effect is largest when the hydraulic gradient is perpendicular to the clay drape strike.

This modeling study demonstrates that implementing small scale heterogeneities using multiple-point geostatistics can be a valuable tool to build more accurate heat transport models in aquifers with a complex geological heterogeneity. This allows a better dimensioning of particular ATES systems, but can also be used for optimizing well-to-well distances within

an ATES system and between different systems. Future research should therefore focus on incorporating other types of complex geological heterogeneities (e.g. alluvial sediments) using multiple-point geostatistics in heat transport models for ATES simulation.

Chapter 5

Conclusions

5.1 Introduction

In this chapter, the outcomes of this PhD project are summarized and discussed on the basis of the research questions and the sub-questions defined in Chapter 1. Finally, some recommendations and perspectives for future research are given.

5.2 Answers to research questions

1. What is the impact of existing ATES systems on groundwater quality on the long term?

- *What does the international literature report on the effects of ATES on groundwater quality?*

The reviewed literature reports that ATES can have an impact on groundwater quality in two different ways, by changing temperature and by mixing different water qualities. The small temperature changes (<15°C) caused by ATES systems, seem to have hardly any effect on the chemistry of the main chemical constituents in the groundwater. Redox reactions on the other hand are sensitive to small changes in temperature (Prommer and Stuyfzand, 2005). Especially the increased mobility of arsenic observed in laboratory experiments at temperatures of 25°C (Bonte et al., 2013b) shows that further research and monitoring are necessary. Mixing of shallow groundwater with deeper groundwater over a large well screen length can have an important influence on groundwater quality. Trace elements and organic carbon can be mobilized by changing the natural redox conditions in aquifers and contaminants can be introduced deeper in the aquifer.

- *Do the small temperature differences (<10°C) at which the ATES systems in Flanders operate have an influence on groundwater quality?*

Comparing the quality of the water extracted from the cold bubble with the quality of the water extracted from the warm bubble shows no larger differences than between the samples from the same bubble over time. So, it can be concluded that the small temperature differences induced by the studied ATES systems seem to have no significant influence on the concentrations of the main chemical constituents in the groundwater.

- *Does mixing of shallow with deeper groundwater have an influence on groundwater quality?*

For some of the investigated ATES systems, upward trends in sulfate, chloride and sodium concentrations are reported. For one of the ATES systems, an increased concentration of nitrate was reported. In the majority of these cases this can be attributed to the injection of shallow groundwater, which is more influenced by human activity. The largest risk exists for phreatic aquifers, which are less protected against contamination. This can lead to a deterioration of water quality of pumped water if a public drinking water supply well field is nearby.

Both the design of the ATES system (depth and length of well screens) and the site specific conditions (groundwater quality, land-use and possible input of contaminants) will determine the impact of the ATES system on groundwater quality. Therefore an integrated design of the ATES system taking into account the local conditions is indispensable, especially for future ATES systems built in the vicinity of public drinking water supply well fields.

2. What is the effect of alternating pumping by ATES systems near the redox boundary on the precipitation of iron (hydr)oxides?

- *What is the extent and location of the precipitation?*

Modeling results for both case studies in Leuven and Antwerp show that the location of highest $Fe(OH)_3$ precipitation depends on the position of the well screens in relation with the redox boundary. When the well screens are largely in the oxidized zone, the extracted water is oxygen rich and most $Fe(OH)_3$ will precipitate around the well screen of the injection well in the reduced, Fe(2) rich part of the aquifer. When the well screens are in the reduced part of the

aquifer, during extraction oxygen rich water from above will be captured and most $Fe(OH)_3$ will precipitate around the extraction well consuming most of the available oxygen, resulting in less oxygen available to react in the injection well. Both case studies show that with a small natural groundwater flow velocity, the initial mixing effect plays an important role in the $Fe(OH)_3$ precipitation process, as most $Fe(OH)_3$ precipitation occurs in the first years of operation, controlled by ferrous iron and oxygen availability.

- *What is the impact of temperature, well screen setting and flow rate on the precipitation?*

The models predict that even at small temperature differences ($\Delta T = 10°C$), there is a significant temperature influence, with highest precipitation of $Fe(OH)_3$ in and around the cold wells. This is explained by the effect of temperature on the pH. Lower temperatures cause a higher pH, which in its turn will cause more $Fe(OH)_3$ to precipitate. Cold wells will therefore be more sensitive to clogging by iron (hydr)oxides than warm wells. In addition, the results show that with well screens further from the redox boundary and with decreasing flow rate, the $Fe(OH)_3$ precipitation in the wells becomes smaller. Model variants of the Leuven case show that installing the well screens two meters above the redox boundary provides a reduction in $Fe(OH)_3$ precipitation with a factor of 3.2 for the cold well and a factor of 4.2 for the warm well, whereas installing the well screen five meters above the redox boundary will even ensure a reduction with a factor of 7.9 for the cold well and a factor of 8.9 for the warm well. Lowering the flow rate of the reference case with a factor of 2, will only ensure a reduction in $Fe(OH)_3$ precipitation with a factor of 1.2, both in the warm and the cold well. So, optimizing the well screen setting has a larger impact than reducing the flow rate of the wells.

- *Can reactive transport modeling help in determining the effects?*

The performed modeling study shows that reactive transport modeling is a valuable tool to develop a better understanding of the processes around ATES wells and in particular to assess iron hydroxide precipitation and the risk of well clogging, as it allows simulating the interactions between the occurring physical and geochemical processes in aquifers. However, a careful geochemical characterization of the aquifer and groundwater is indispensable in order to incorporate the relevant and correct set of reactions in the models.

3. **Do centimeter-scale clay drapes have an effect on heat transport around ATES wells?**

   - *What is the effect of clay drapes on the distribution of thermal energy around the wells?*

The distribution of the thermal energy in the subsurface is determined by the strike of the centimeter-scale clay drapes, with the major anisotropy axis of the cold and warm bubble aligned according to the clay drape strike. This shows that also small scale sedimentary features can have an influence on the distribution of thermal energy around an ATES system.

- *What is the effect of clay drapes on the recovered temperatures and the efficiency of an ATES system?*

The clay drapes have a negative impact on the recovered temperatures and ATES efficiency when there is no hydraulic gradient present, which is explained by the clay drapes causing more dispersion of the thermal energy. Clay drapes, however, can also have a positive impact on the recovered temperatures and ATES efficiency when there is a hydraulic gradient present. In this case the clay drapes ensure the thermal energy being retained closer to the wells, reducing the advective heat loss induced by the hydraulic gradient. This retention effect is largest when the hydraulic gradient is perpendicular to the clay drape strike.

5.3 Recommendations and perspectives

At the end of each chapter suggestions for further research were made. These suggestions will be summarized in this section supplemented

with more general recommendations and perspectives.

5.3.1 Recommendations on groundwater quality monitoring at ATES sites

It is important that groundwater is monitored in each phase of ATES operation, minimally one sample should be taken from the cold well during summer and from the warm well during winter. Furthermore, the moment and location of sampling is important. To investigate the effect of temperature, the groundwater should be sampled approximately halfway the heating/cooling season. At this time the water around the wells had the longest residence time in the centre of the warm and cold bubble and was influenced the most. To study the impact of mixing of different groundwater compositions, the groundwater should be sampled near the end of each season as capturing shallower groundwater is most likely in this phase of ATES operation. It is recommended to sample in nearby piezometers downstream the groundwater flow direction, taking into account bubble size and bubble drift. In this way groundwater can be sampled from different parts of the ATES bubble. To make a proper assessment of the effect of mixing groundwater by ATES, it is necessary to have information on the groundwater composition at several depths at the site. It is therefore recommended to install several monitoring wells at different depths at each ATES site. It is clear that each monitoring campaign should be adapted to the local conditions.

Future monitoring and research on the impact of ATES on the groundwater quality should focus on trace elements and microbiology. Both were not included in this study (Chapter 2) as no trace element and microbiological monitoring data are available from the beginning of the different ATES installations. However these parameters are of high importance for the impact assessment of ATES on the groundwater quality as they pose a major risk for human health and environment when present in elevated concentrations.

5.3.2 Recommendations on reactive transport modeling of redox processes at ATES sites

The models described in Chapter 3 give a good impression on the extent and location of iron hydroxide precipitation around ATES wells as well as on the influence of temperature, well screen location and flow rate. The implemented reaction network, however, was simplified, incorporating equilibrium reactions, kinetic reactions and cation exchange. Only homogeneous iron hydroxide precipitation was modeled in this way. Heterogeneous iron hydroxide precipitation on reactive surfaces and the influence of microbial iron oxidation were not accounted for. Therefore, future research should focus on incorporating these reactions in the models. In this way, a more accurate assessment can be made on the precipitation of iron hydroxides around ATES wells. Furthermore, future modeling work should incorporate more realistic oxygen concentrations and link the modeled $Fe(OH)_3$ precipitation to permeability changes in order to assess the impact of well and aquifer clogging on ATES performance.

At the two considered sites, the hydraulic gradient is rather small. Therefore the assumption of no hydraulic gradient is likely. At other sites with a higher hydraulic gradient, it is necessary to incorporate the natural advective flow in the reactive transport models. In these cases there will be a constant influx of ferrous iron and oxygen that continue to react resulting in a higher iron hydroxide precipitation than predicted by a model without hydraulic gradient.

Before installing ATES wells in aquifers with varying redox conditions, it is recommended to do a thorough assessment of the redox chemistry at the potential ATES location. This assessment should exist of installing several piezometers at different depths. In this way a proper analysis can be made of the groundwater chemistry at these different depths. With this information the ATES design can be optimized and possible $Fe(OH)_3$ precipitation can be avoided or at least minimized.

Finally, the applicability of in-situ iron removal, as also used in potable water production

(Appelo and de Vet, 2003; Appelo et al., 1999; van Halem et al., 2012, 2011, 2010), could be investigated for ATES.

5.3.3 Recommendations on incorporating heterogeneity in heat transport models for ATES

The models discussed in Chapter 4 demonstrate that implementing small scale heterogeneities using multiple-point geostatistics is a valuable tool to build more accurate models in aquifers with complex geological heterogeneities. Accurate models allow a better dimensioning of particular ATES systems and optimization of well-to-well distances. In this study small scale clay drapes were incorporated in heat transport models for ATES simulation. Future research can focus on incorporating other types of complex geological heterogeneities (e.g. in alluvial sediments) using multiple-point geostatistics or other geostatistical techniques in heat transport models for ATES simulation.

5.3.4 General recommendations and perspectives

In addition to the suggestions made in the context of the three main topics of this PhD research, some general recommendations and perspectives for the development of Aquifer Thermal Energy Storage are covered briefly.

Since there are more and more users of the subsurface, a 3D subsurface planning is urgently needed, especially in dense urban areas. Poorly positioned ATES and other UTES systems can negatively interfere with each other, significantly lowering the efficiency of such systems. This possible interference in the subsurface is not only limited to thermal energy storage. Interactions exist between all shallow underground resources: space, groundwater, geomaterials and thermal energy storage. Traditionally, subsurface works are planned on a single-project basis, not taking into account other potential uses. This first-come, first-served approach leads to an inefficient use of the subsurface, often making other uses impossible at this location or producing interference between uses, e.g. tunnels interfering with thermal energy storage, thermal energy storage interfering with drinking water production (Bonte et al., 2011a; Maire et al., 2006). Mutual benefits on the other hand are also possible, e.g. in the Vienna metro, heat exchangers are installed in the tunnel lining and foundations of the stations (Unterberger et al., 2005). Another possible combination is to make use of the thermal energy in the water pumped for potable water supply, irrigation or industrial processes. This water is already extracted for these purposes, so no extra energy is needed for the extraction and injection of the water, making this combination very cost effective. It is clear that the development of 3D subsurface plans indicating all possible subsurface uses will facilitate a more efficient use of the subsurface, with large environmental and economical benefits.

A specific challenge for Flanders, and one of the reasons that there are much less UTES systems operational in comparison with e.g. The Netherlands, is that these thermal energy storage techniques are not sufficiently known by developers, architects and contractors. Therefore it is important that the knowledge about these techniques is transferred to the market. This is currently dealt with in the Smart Geotherm project (2011-2017), where guidelines, codes of good practice and demonstration projects are developed and disseminated to the market.

Appendix A

Time series of monitoring data from seven ATES systems and ambient concentrations

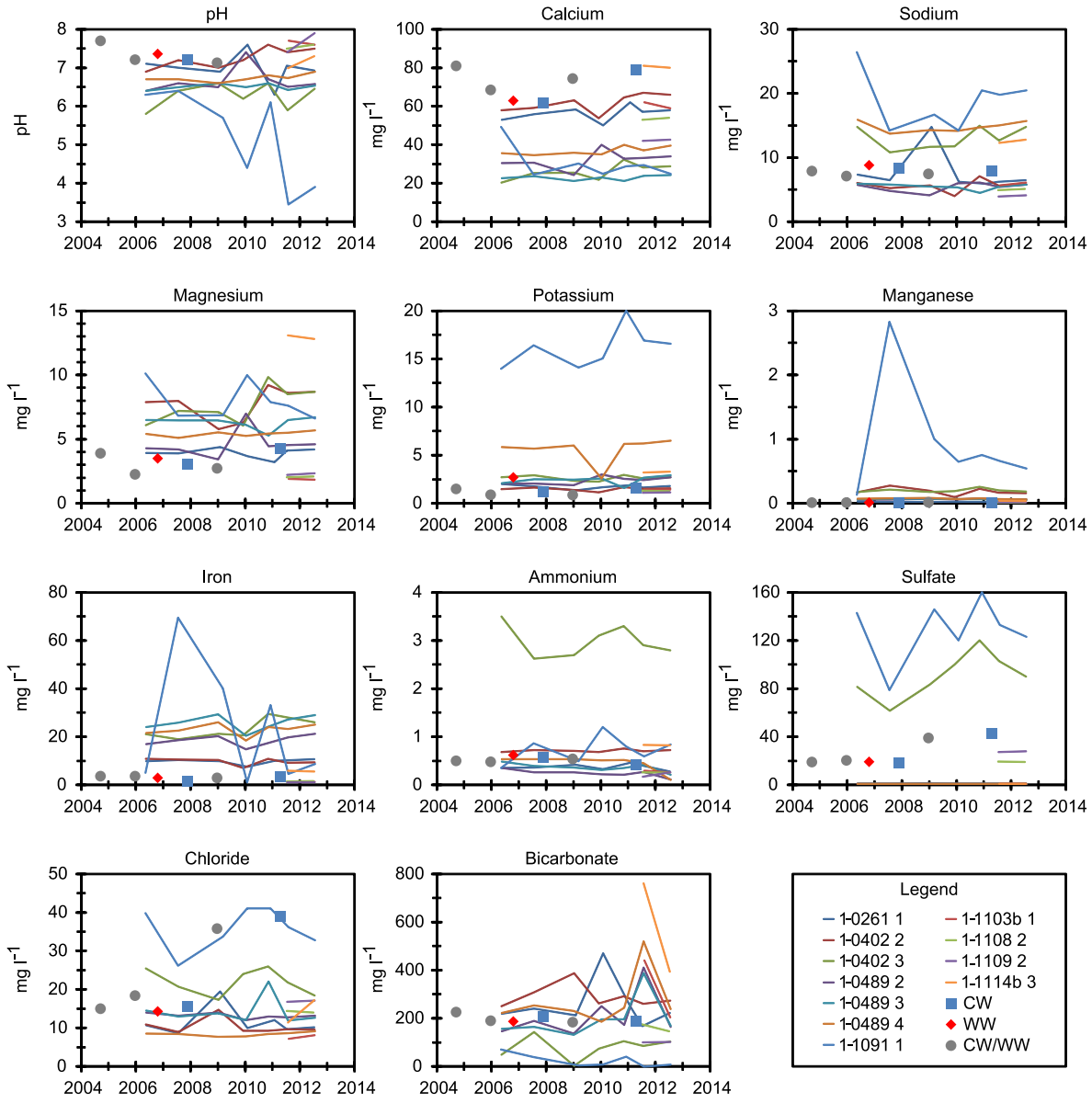

Figure A.1 Time series of monitoring data from ATES system A with time series of ambient concentrations measured in monitoring wells in the used aquifer in a 10 km radius around the ATES system. CW: cold well, WW: warm well.

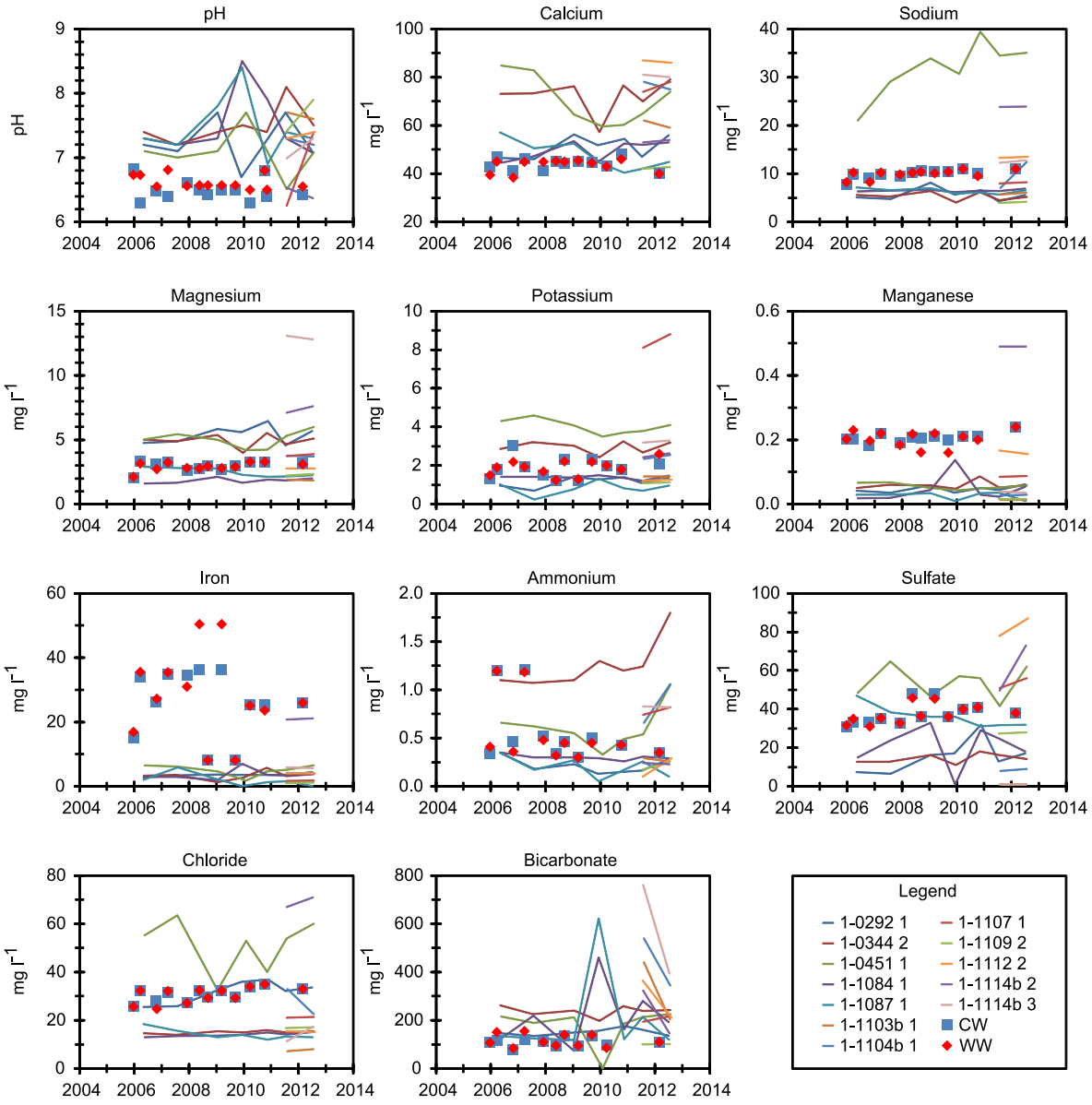

Figure A.2 Time series of monitoring data from ATES system B with time series of ambient concentrations measured in monitoring wells in the used aquifer in a 10 km radius around the ATES system. CW: cold well, WW: warm well.

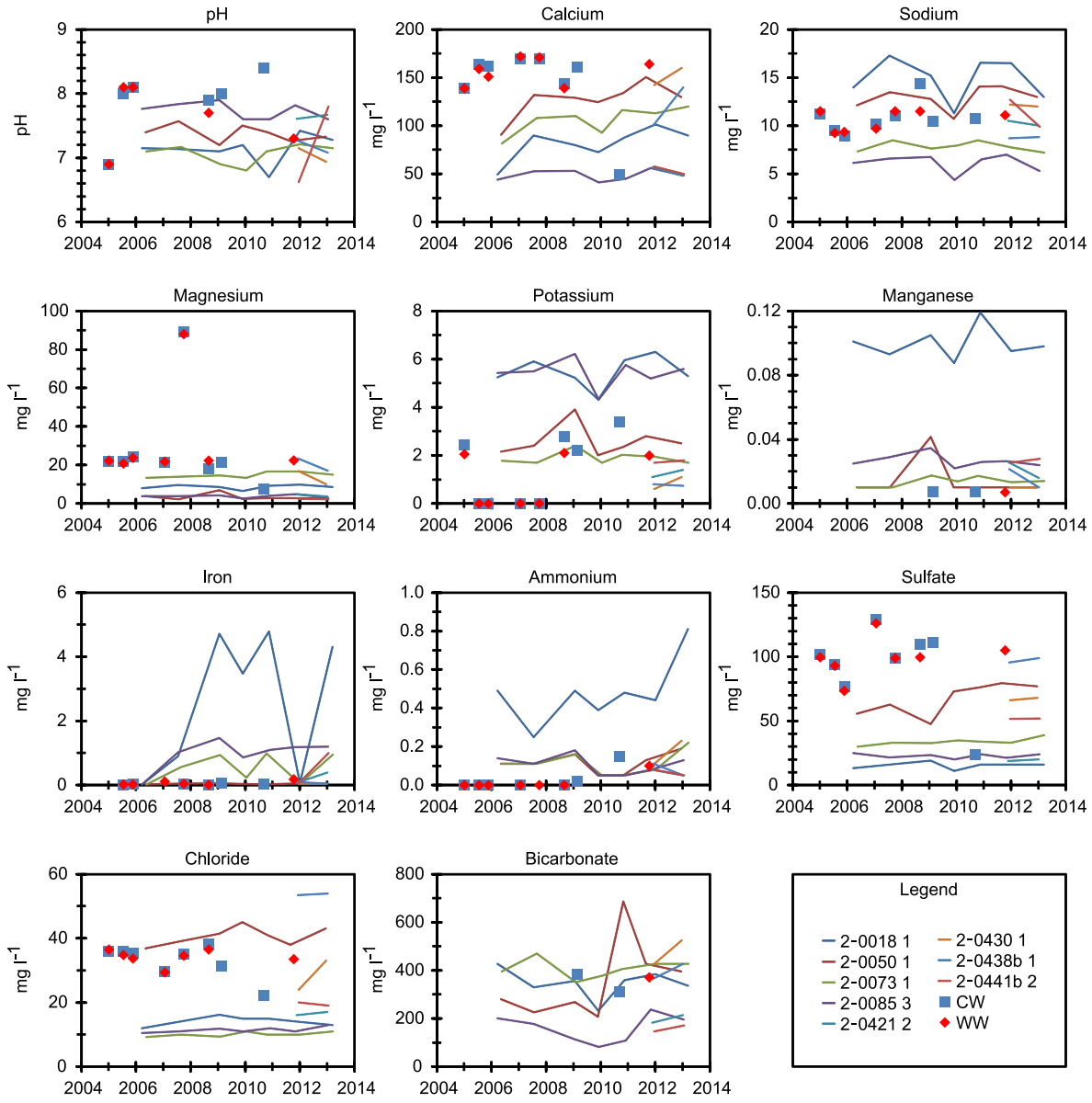

Figure A.3 Time series of monitoring data from ATES system C with time series of ambient concentrations measured in monitoring wells in the used aquifer in a 10 km radius around the ATES system. CW: cold well, WW: warm well.

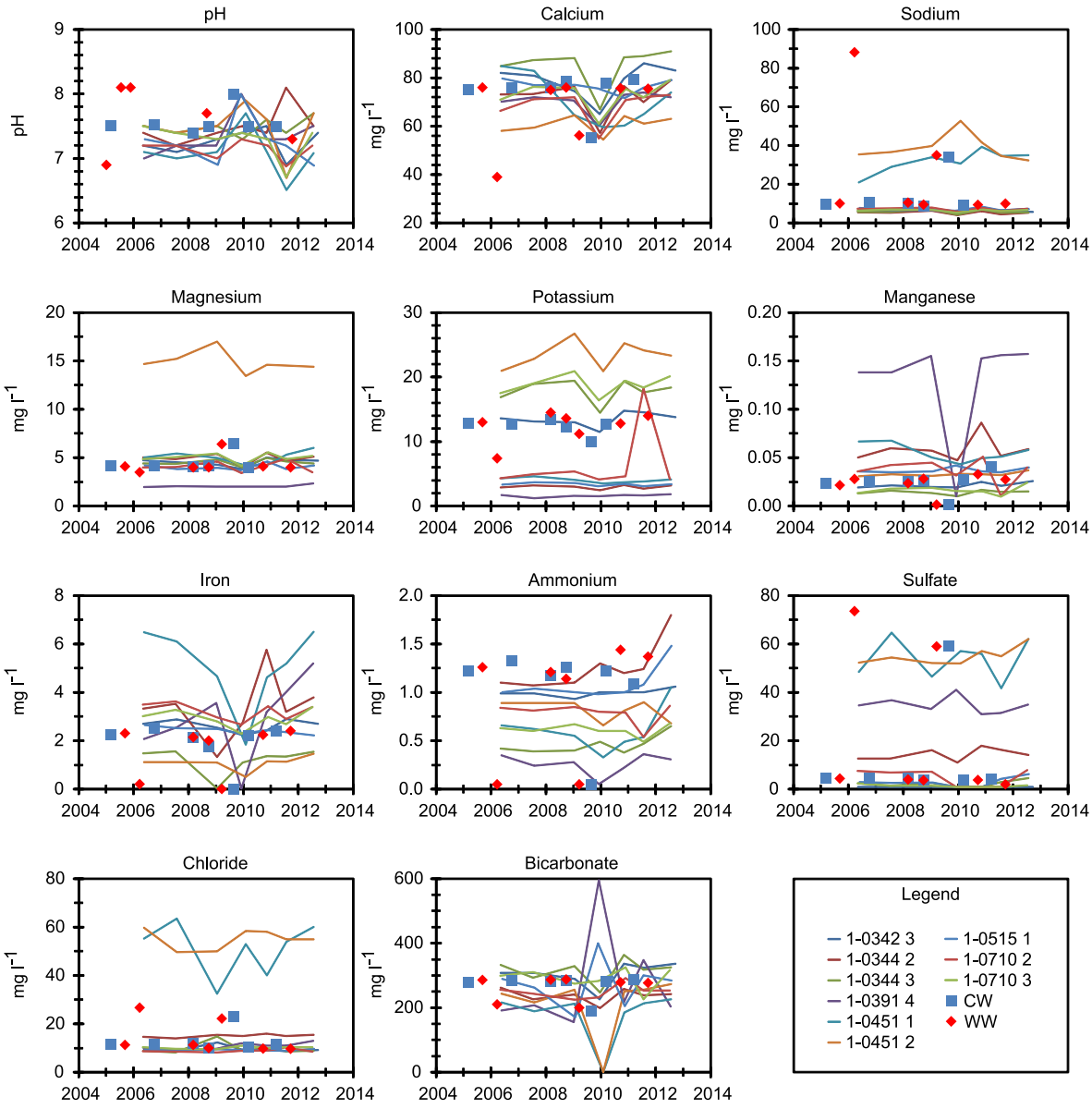

Figure A.4 Time series of monitoring data from ATES system D with time series of ambient concentrations measured in monitoring wells in the used aquifer in a 10 km radius around the ATES system. CW: cold well, WW: warm well.

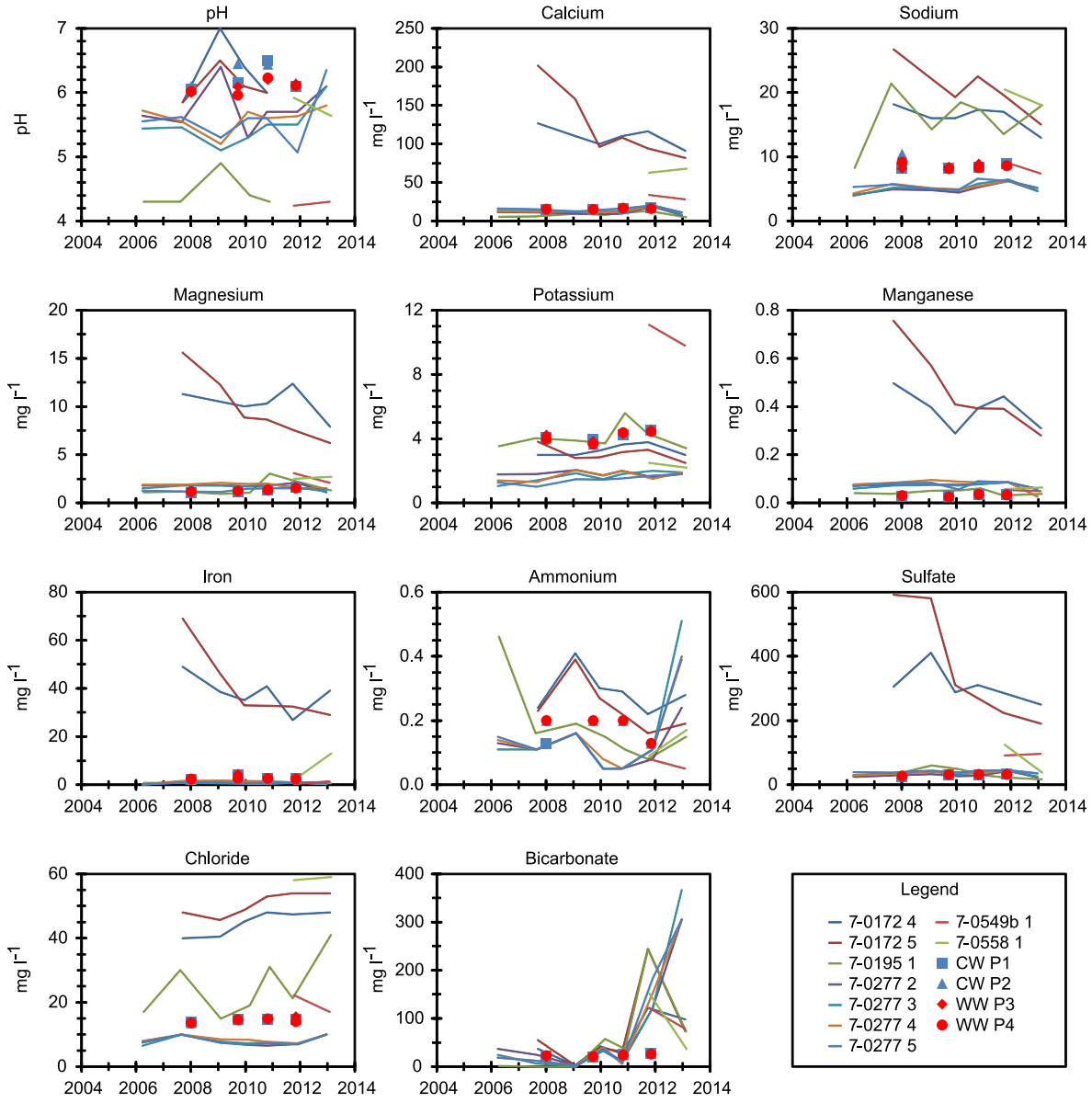

Figure A.5 Time series of monitoring data from ATES system E with time series of ambient concentrations measured in monitoring wells in the used aquifer in a 10 km radius around the ATES system. CW: cold well, WW: warm well.

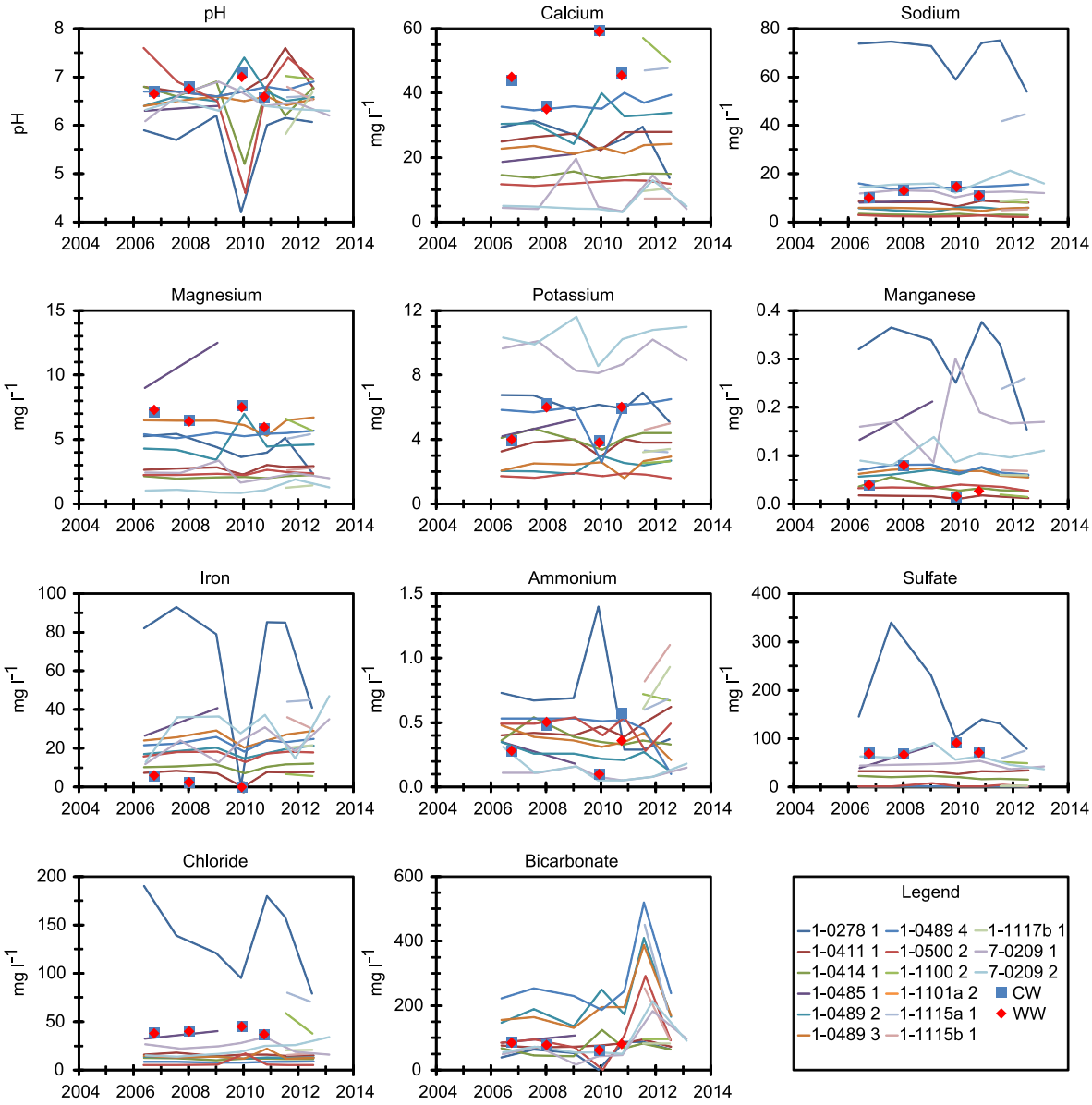

Figure A.6 Time series of monitoring data from ATES system F with time series of ambient concentrations measured in monitoring wells in the used aquifer in a 10 km radius around the ATES system. CW: cold well, WW: warm well.

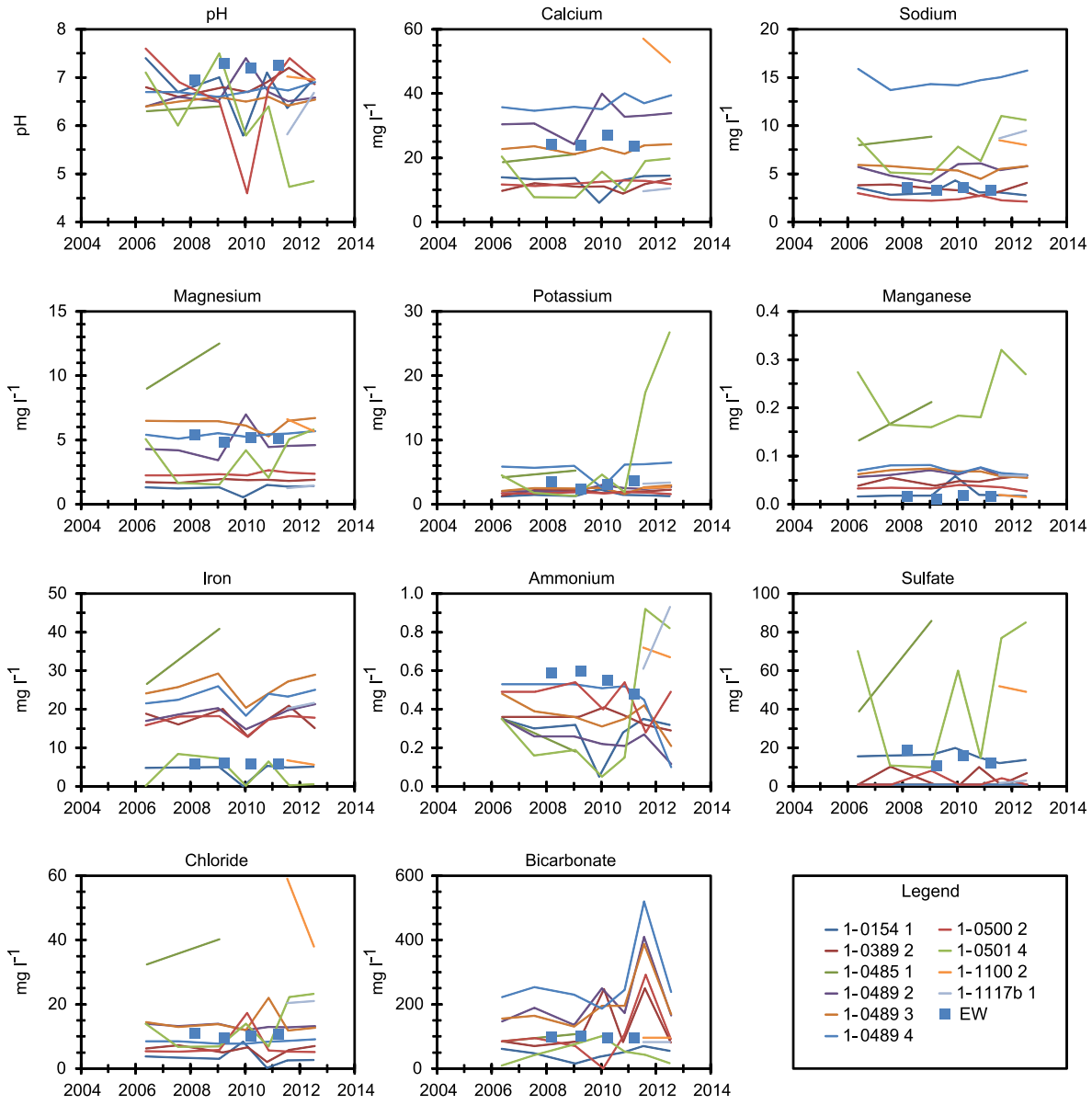

Figure A.7 Time series of monitoring data from ATES system G with time series of ambient concentrations measured in monitoring wells in the used aquifer in a 10 km radius around the ATES system. EW: extraction well.

Table A.1 Resulting p-values from testing the null hypothesis: the slope of the regression line is zero.

System	Well	pH	Ca	Na	Mg	K	Mn	Fe	NH_4	SO_4	Cl	HCO_3
A		0.085	0.793	0.991	0.566	0.898	0.193	0.817	0.517	0.029	0.031	0.249
B	CW	0.928	0.062	0.001	0.512	0.992	0.543	0.469	0.051	0.054	0.056	0.162
	WW	0.053	0.222	0.009	0.561	0.482	0.685	0.649	0.049	0.040	0.100	0.808
C	CW	0.181	0.114	0.372	0.812	0.129	*	0.520	0.062	0.300	0.079	*
	WW	0.745	0.530	0.355	0.876	0.336	*	0.098	0.020	0.507	0.788	*
D	CW	0.649	0.876	0.468	0.504	0.409	0.724	0.595	0.477	0.634	0.693	0.673
	WW	0.785	0.376	0.307	0.667	0.306	0.821	0.529	0.417	0.435	0.343	0.702
E	CW P1	0.645	0.086	0.184	0.056	0.191	0.041	0.858	0.290	0.038	0.259	0.239
	CW P2	0.781	0.075	0.310	0.058	0.389	0.346	0.892	0.290	0.092	0.109	0.312
	WW P3	0.180	0.037	0.145	0.040	0.497	0.186	0.903	0.290	0.032	0.042	0.106
	WW P4	0.428	0.392	0.433	0.073	0.304	0.591	0.980	0.290	0.125	0.564	0.345
F	CW	0.920	0.485	0.670	0.683	0.721	0.670	0.198	0.835	0.521	0.809	0.057
	WW	0.820	0.548	0.650	0.609	0.712	0.448	0.194	0.744	0.518	0.809	0.522
G		0.322	0.833	0.407	0.777	0.764	0.735	0.413	0.107	0.436	1.000	0.538

* To little data for regression analysis

Appendix B

Pumping test analyses

B.1 Introduction

In this Appendix B, the pumping test analyses for Chapter 3 are elaborated. The pumping test analyses were carried out to determine the hydraulic aquifer properties to be used in the reactive transport model.

At the Leuven site, a pumping test with a constant flow rate of 48.5 m³/h was carried out to determine the hydraulic properties in the Brussels Sands Aquifer at this location. During a constant flow rate test, the well is pumped at a constant discharge rate until the drawdown within the well is fully stabilized. The pumping test was carried out and monitored in the new ATES well and had a duration of 24 hours.

To determine the hydraulic properties of the Kattendijk Sands and Berchem Sands Aquifer at the Antwerp site, two pumping tests are performed, a step drawdown test and a constant rate test. A step-drawdown test is a single-well test in which the well is pumped at a constant discharge rate until the drawdown within the well stabilizes. The pumping rate is then increased to a higher constant-discharge rate and the well is pumped until the drawdown stabilizes once more. This process is repeated through several steps, which are all of about equal duration. At the Antwerp site, the step drawdown test was carried out by means of four steps of one hour with increasing flow rate (Q_1 = 1.07 m^3/h, Q_2 = 1.90 m^3/h, Q_3 = 3.75 m^3/h and Q_4 = 4.84 m^3/h). During the test, the heads were monitored in the test well. The pumping test at constant flow rate (3.53 m^3/h) had a duration of 24 hours and was monitored in the test well (P1) as well as in 3 monitoring wells (P2, P3a, P4). The monitoring wells P2, P3 and P4 are located respectively at 20 m, 10 m and 3 m from the test well (P1). When the pump is shut down after a pumping test, the water levels in the well and the piezometers will start to rise. This rise in water levels is known as residual drawdown, s'. It is expressed as the difference between the original water level before the start of pumping and the water level measured at a time t' after the cessation of pumping. After the pumping test at constant rate this recovery was measured during four days.

B.2 Methods

B.2.1 Analytical Methods

Although both the Brussels Sands Aquifer at the Leuven site and the Kattendijk Sands and Berchem Sands Aquifer at the Antwerp site are unconfined aquifers, the drawdown data do not show the typical delayed water table response, rather both aquifers behave as confined aquifers. This could be explained by the fine loam and clay layers present.

Therefore analytical methods for confined aquifers are used in the analysis, the Eden-Hazel method for the step drawdown test, the Jacob's method for the pumping test at constant rate and the Theis recovery method for the analysis of the residual drawdown.

Eden-Hazel method

From step-drawdown tests in a fully penetrating well in a confined aquifer, the Eden-Hazel method (Eden and Hazel, 1973; Kruseman and de Ridder, 1991) can determine the well losses, and also the transmissivity of the aquifer. The method is based on Jacob's approximation of the Theis equation. The drawdown in the well is given by the Jacob equation, written as

$$s = (a + b\ log\ t)Q \quad \text{(B.1)}$$

where $$a = \frac{2.30}{4\pi\ KD} log \frac{2.25\ KD}{r_{ew}^2\ S} \quad \text{(B.2)}$$

$$b = \frac{2.30}{4\pi\ KD} \quad \text{(B.3)}$$

and K hydraulic conductivity

D aquifer thickness

r_{ew} effective radius of the well

S storativity

Using the principle of superposition at the different stages of the variable discharge test and the addition of a term for the non-linear well losses, the previous formula is rewritten as

$$s_{(n)} = aQ_n + bH_n + CQ_n^2 \quad \text{(B.4)}$$

where $$H_n = \sum_{i=1}^{n} \Delta Q_i \log (t - t_i) \quad \text{(B.5)}$$

Q_n constant discharge during timestep n

ΔQ_i flow increase between timestep i and i-1

t_i starting time at timestep i

The measured drawdown $s_{(n)}$ is plotted against the calculated H_n values. Parallel straight lines of best fit are drawn through the plotted points. The slope of the parallel straight lines through these points gives the value of b, from which the transmissivity can be calculated.

The intersection points of the straight lines with the Y-axis, for $H_n = 0$, yields A_n values:

$$A_n = aQ_n + CQ_n^2 \quad \text{(B.6)}$$

or

$$\frac{A_n}{Q_n} = a + CQ_n \quad \text{(B.7)}$$

The ratio A_n/Q_n can be calculated for each time step and plotted against Q_n. The slope of this line gives C and the intersection point with the Y-axis gives a, the specific non-linear well losses and the specific linear well losses respectively.

Jacob's method

Jacob's method (Cooper and Jacob, 1946; Kruseman and de Ridder, 1991) is based on the Theis formula, where for sufficiently large pumping times and at short distance from the pumping well the Theis equation can be simplified to

$$s = \frac{2.30\,Q}{4\pi\,KD} log \frac{2.25\,KD\,t}{r^2 S} \quad \text{(B.8)}$$

where s drawdown

KD transmissivity

r distance to the pumping well

S storativity of the aquifer

t time

Q well discharge

One of the assumptions made for the use of this method is a constant thickness of the aquifer. As the effective thickness of the saturated zone decreases by drawdown, following correction has to be made:

$$s" = s - \frac{s^2}{2D} \quad \text{(B.9)}$$

where s" corrected drawdown

D saturated thickness of the aquifer

Since KD, Q, S and r are constants, a straight line is obtained when the corrected drawdown (s") is fitted against the logarithm of time (t). The slope of this straight line, or the difference in drawdown Δs over one log-cycle is given by:

$$\Delta s" = \frac{2.30\,Q}{4\pi\,KD} \quad \text{(B.10)}$$

From which the transmissivity can be calculated:

$$KD = \frac{2.30\,Q}{4\pi\,\Delta s"} \quad \text{(B.11)}$$

Similarly to the above method (procedure 1), t can be held constant with r the variable (procedure 2).

Since KD, Q, S and t are constants, a straight line is obtained when the drawdown (s) in the monitoring wells is fitted against the logarithm of the distance to the pumping well (r). The slope of this straight line, or the difference in drawdown Δs over one log-cycle is given by:

$$\Delta s = \frac{2.30\,Q}{2\pi\,KD} \quad \text{(B.12)}$$

From which the transmissivity can be calculated:

$$KD = \frac{2.30\,Q}{2\pi\,\Delta s} \quad \text{(B.13)}$$

Since the drawdown with respect to the fully saturated zone at the monitoring wells is small, the measured drawdown is not corrected in this method.

A third procedure of Jacob's method is plotting the drawdown (s) against t/r^2. When this is plotted on a semi-logarithmic scale, a straight line can be drawn through these points. The slope of this line again generates Δs over one log-cycle:

$$\Delta s = \frac{2.30\,Q}{4\pi\,KD} \quad \text{(B.14)}$$

From which again the transmissivity can be calculated:

$$KD = \frac{2.30\ Q}{4\pi\ \Delta s} \quad \text{(B.15)}$$

Theis recovery method

This method is based on the formula of Theis (Kruseman and de Ridder, 1991; Theis, 1935), where for sufficiently large times and at short distance from the pumping well the Theis equation for the recovery phase can be simplified to:

$$s' = \frac{Q}{4\pi\ KD}\left(\ln\left(\frac{4\ KD\ t}{r^2\ S}\right) - ln\left(\frac{4\ KD\ t'}{r^2\ S'}\right)\right) \quad \text{(B.16)}$$

where s' drawdown

KD transmissivity

r distance to the well

S storativity during the pumping phase

S' storativity during the recovery phase

t time since the start of pumping

t' time since the cessation of pumping

Q discharge rate

If we assume that S, S' and KD are constant and we assume that S = S':

$$s' = \frac{2.30\ Q}{4\pi\ KD}\ log\left(\frac{t}{t'}\right) \quad \text{(B.17)}$$

The slope of this straight line (s' versus t/t' in logarithmic scale) or the difference in drawdown Δs' over a log-cycle is given by:

$$\Delta s' = \frac{2.30\ Q}{4\pi\ KD} \quad \text{(B.18)}$$

From which the transmissivity can be calculated:

$$KD = \frac{2.30\ Q}{4\pi\ \Delta s'} \quad \text{(B.19)}$$

B.2.2 Numerical model calibration

The values obtained with these analytical methods were verified and calibrated using a groundwater flow model. The values for hydraulic conductivity, specific storage, effective porosity and specific yield were obtained and calibrated by trial and error until the model results corresponded well with the drawdown measured during the constant rate tests. The differential equations describing groundwater flow are solved by Processing Modflow 8 (Chiang, 2010), a pre- and post-processor for, among other MODFLOW 2000 (Harbaugh et al., 2000), MT3DMS (Zheng and Wang, 1999) and PHT3D (Prommer and Post, 2010).

Leuven case

The groundwater flow model is a three dimensional local model of 5000 m x 5000 m x 70 m including the test well in the middle of the model (Figure B.1a). Constant hydraulic heads are assigned to the up and downstream vertical boundaries according to the measured hydraulic gradient of 0.2%. The grid cell sizes change from 100 m at the model boundaries to 0.25 m at the centre of the model, where the test well is situated. The model consists of 101 cells in the x and y-direction and 4 layers (0 to 1 mbs, 1 to 52 mbs, 52 to 67 mbs and 67 to 70 mbs). The well is installed in layer 3, from 52 to 67 mbs. The total number of cells in the model is 40804 cells.

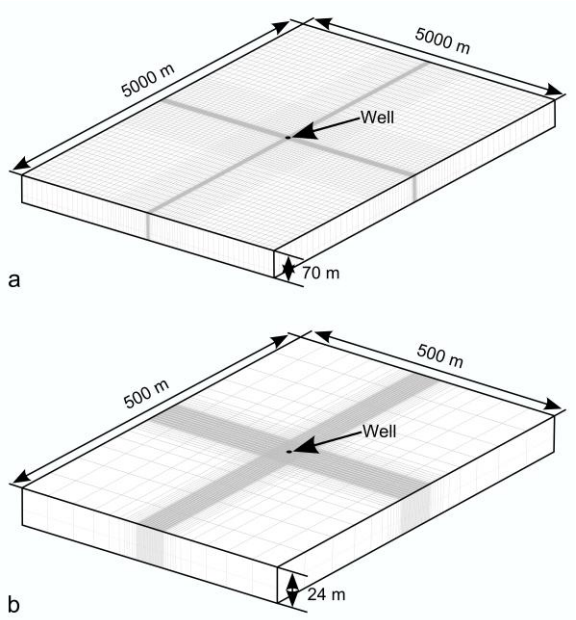

Figure B.1 Model geometry. **a**: Leuven case; **b**: Antwerp case.

Antwerp case

The groundwater flow model is a three dimensional local model of 500 m x 500 m x 24 m including the test well in the middle of the model (Figure B.1b). Constant hydraulic heads are assigned to the model boundaries. The grid cell sizes change from 50 m at the model boundaries to 1 m at the centre of the model, where the test well and monitoring wells are situated. The model consists of 76 cells in the x- and y-direction and 2 layers, layer 1 reaching from 0 mbs to 14 mbs and layer 2 reaching from 14 mbs to 24 mbs containing the well. The Boom Clay acts as the basis of the model. The total number of cells in the model is 11552 cells.

B.3 Results

B.3.1 Leuven case

The drawdown curve of the pumping test at constant flow rate is shown in Figure B.2a. These data were used to determine the transmissivity (T) and hydraulic conductivity (K) of the aquifer using the Jacob's method (procedure 1). Figure B.2b shows the drawdown (s) plotted versus the logarithm of the time. The slope of the straight line through the data points is read as the difference in drawdown on a log-time interval (Δs). The results of the analysis are shown in Table B.1.

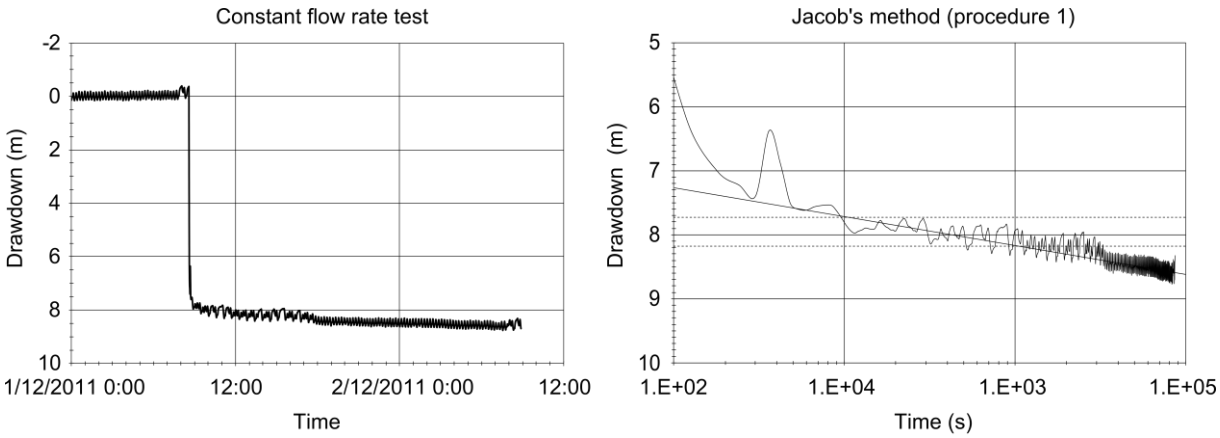

Figure B.2 Pumping test at constant rate (Leuven case). **a**: drawdown curve; **b**: Jacob's method analysis (procedure 1).

Table B.1 Flowrate (Q) and aquifer properties for the Leuven case derived by the Jacob's method.

	Δs	Q	Q	KD	D	K	K
	m	m^3/h	m^3/day	m^2/day	m	m/day	m/s
Jacob's method (procedure 1)	0.45	48.50	1164.0	478.75	33.5	14.29	1.65E-04

Figure B.3 shows both the measured drawdown curve and the modeled drawdown curve. As the measured drawdown curve shows a shift to a higher drawdown after 9 hours of pumping, two simulations with the same hydraulic parameters but with different flow rates were made. The shift in the data can be explained by a small increase of the flow rate from 47 m^3/h to 48.5 m^3/h. The model calibrated aquifer properties can be found in Table B.2.

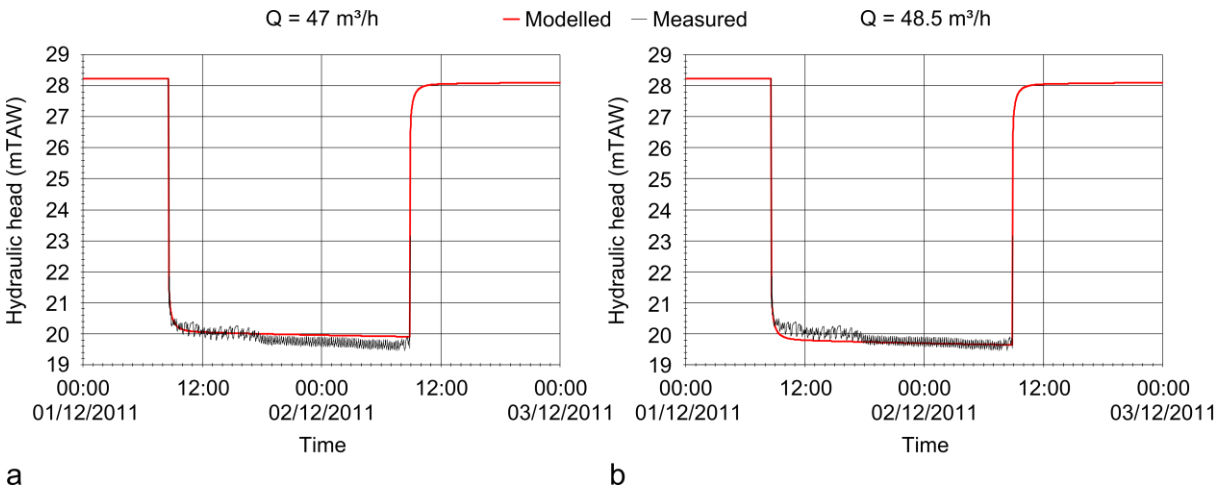

Figure B.3 Measured and modeled drawdown curve (Leuven case). **a**: modeled flowrate of 47 m^3; **b**: modeled flow rate of 48.5 m^3.

Table B.2 Model calibrated aquifer properties for the Leuven case.

Layer	Top	Bottom	K_h	K_v	Specific storage	Effective porosity	Specific yield
	mbs	mbs	$m\,d^{-1}$	$m\,d^{-1}$	m^{-1}		
1	0	1	10.6	3.52	3.0E-04	0.20	0.20
2	1	52	10.6	3.52	3.0E-04	0.20	0.20
3	52	67	10.6	3.52	3.0E-04	0.20	0.20
4	67	70	1.0E-04	3.33E-05	3.0E-04	0.20	0.20

B.3.2 Antwerp case

The drawdown curve of the variable discharge test is shown in Figure B.4, the drawdown curve shows aberrations due to difficulties with flow rate setting and maintenance. To determine the transmissivity (KD) and hydraulic conductivity (K) of the aquifer, as well as the well losses the Eden-Hazel Method was used (Figure B.5). Using the starting time t_i and the flow rate increases ΔQ_i, the $H_i(t)$ is calculated to which the drawdown (s) is plotted. The slope of the parallel straight lines through these points gives the value of b, through which the transmissivity can be calculated. The results of the Eden-Hazel analysis are shown in Table B.3. The well losses can be derived from Figure B.5b with a = 0.077d/m^2 and C = -3E-06, e.g. giving a linear well loss of 6.5 meter at a pumping rate of 84.72 m^3/d (3.53 m^3/h).

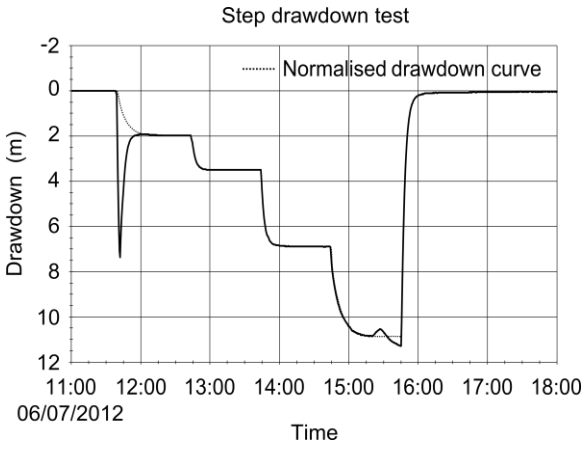

Figure B.4 Step drawdown test (Antwerp case) with 4 flow rate steps, Q_1 = 1.07 m³/h, Q_2 = 1.90 m³/h, Q_3 = 3.75 m³/h, Q_4 = 4.84 m³/h.

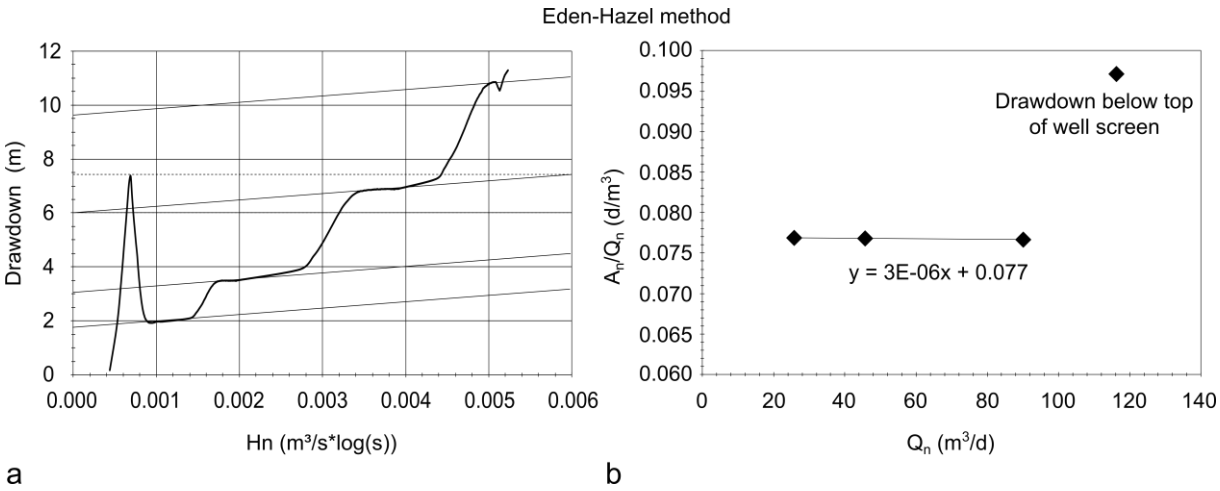

Figure B.5 Step drawdown test (Antwerp case) with 4 flow rate steps, Q_1 = 1.07 m³/h, Q_2 = 1.90 m³/h, Q_3 = 3.75 m³/h, Q_4 = 4.84 m³/h. **a**: Eden-Hazel plot; **b**: Eden-Hazel well losses calculation.

Table B.3 Flowrate (Q) and aquifer properties for the Antwerp case derived by the Eden-Hazel method.

	Δs	ΔHn	b	KD	D	K	K
	m	m^3/s	m^2s	m^2/day	m	m/day	m/s
Eden-Hazel method	1.43	0.006	238.33	66.35	17.8	3.73	4.31E-05

The drawdown in wells P1, P2, P3a and P4 of the pump test at constant rate and the recovery is shown in Figure B.6. To determine the hydraulic parameters of the aquifer the Jacob's method (procedures 1, 2 and 3) and the Theis recovery method were used. Figure B.7 shows the Jacob's method (procedure 1) analyses for the 4 wells. The drawdown (s) is plotted to the logarithm of the time and the slope of the straight line through the data points is read as the difference in drawdown on a log-time interval (Δs). The Jacob's method (procedure 2) analysis is given in Figure B.8, the drawdown is plotted against the logarithm of the distance to the pumping well. The slope of the straight lines is read as the difference in drawdown over one log-distance interval (Δs). In Figure B.9, the Jacob's method (procedure 3) analysis is shown. Here the drawdown is plotted in function of t/r^2. Again straight lines can be drawn that fit the data, the slope of the lines gives the difference in drawdown over one log-cycle (Δs). The results of the Jacob's method analyses are summarized in Table B.4.

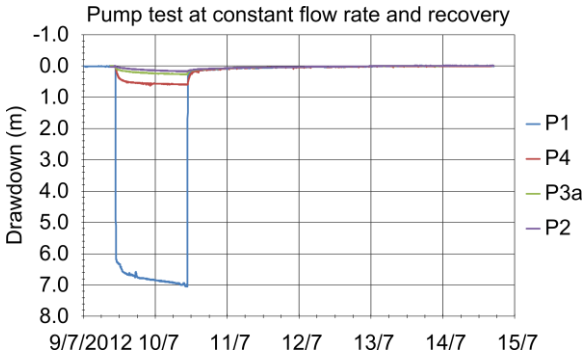

Figure B.6 Pumping test at constant rate (Leuven case).

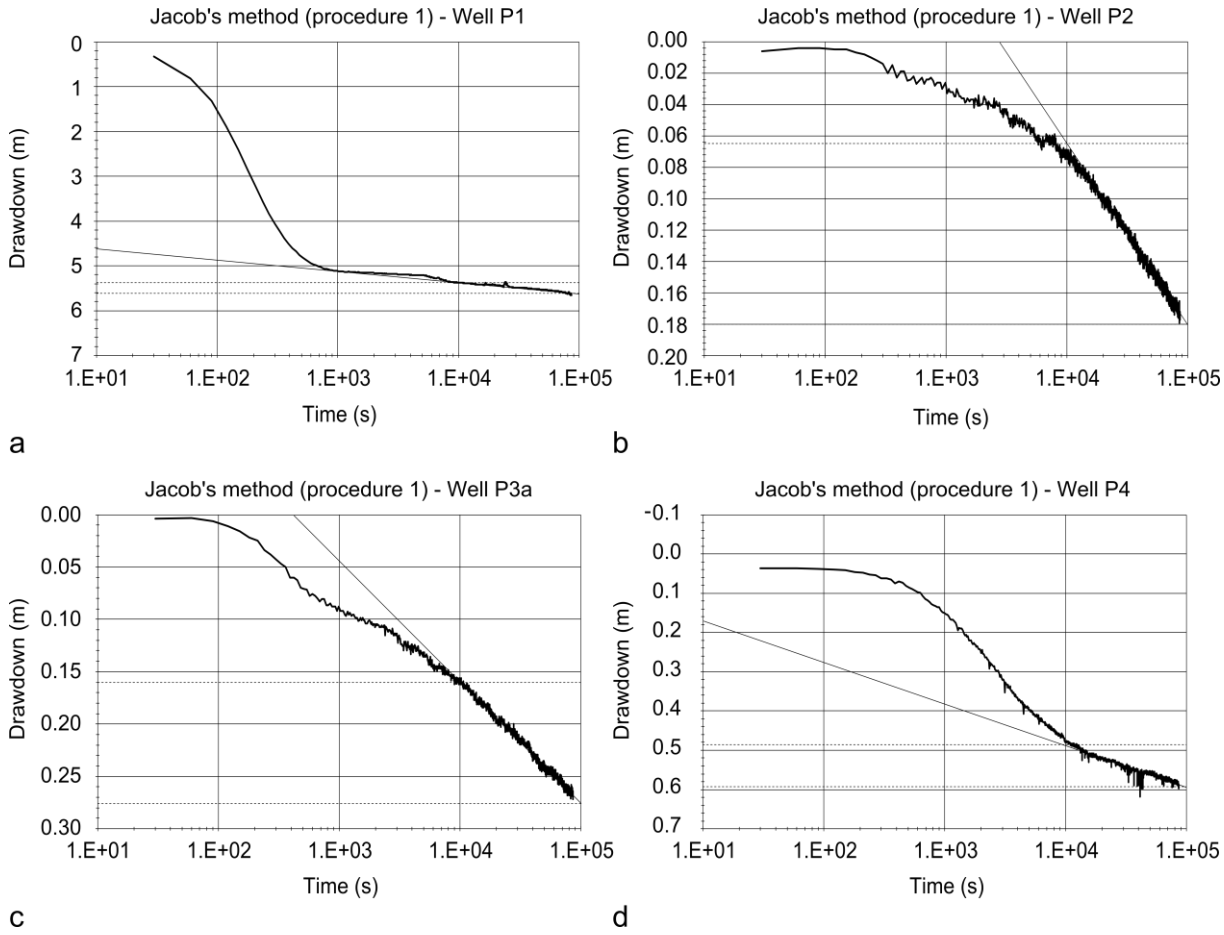

Figure B.7 Pump test at constant rate (Leuven case), Jacob's method (procedure 1). **a**: well P1; **b**: well P2; **c**: well P3a; **d**: well P4.

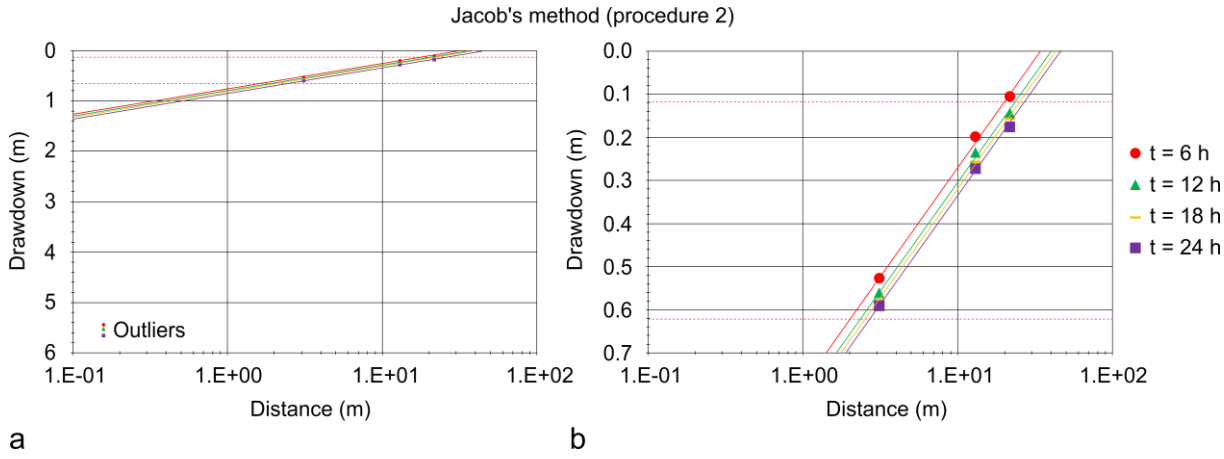

Figure B.8 Pump test at constant rate (Leuven case), Jacob's method (procedure 2). **a**: with heads measured in pumping well (outliers); **b**: detail without the heads measured in the pumping well.

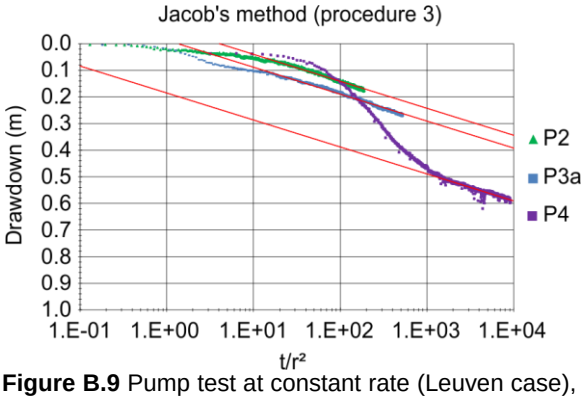

Figure B.9 Pump test at constant rate (Leuven case), Jacob's method (procedure 3).

The analysis with the Theis recovery method is shown in Figure B.10, here the drawdown s' was plotted against the logarithm of t/t'. The slope is read as the difference in drawdown over a log-time interval (Δs'). The Theis recovery method analysis was repeated for all 4 wells. The results of the analyses are given in Table B.4.

Figure B.11 shows both the measured drawdown curves and modeled drawdown curves for the 4 wells. The hydraulic parameters in the model were primarily calibrated on the drawdown curves of well P2, P3a and P4. The drawdown curve of P1 is not used for model calibration because of the significant well losses (see Eden-Hazel method analysis). These well losses are now also confirmed by the numerical model which predicts a well loss of about 6 meter. This corresponds well with the result obtained with the Eden-Hazel method, namely 6.5 meter well loss at a flow rate of 3.53 m^3/h. The model calibrated aquifer properties can be found in Table B.5.

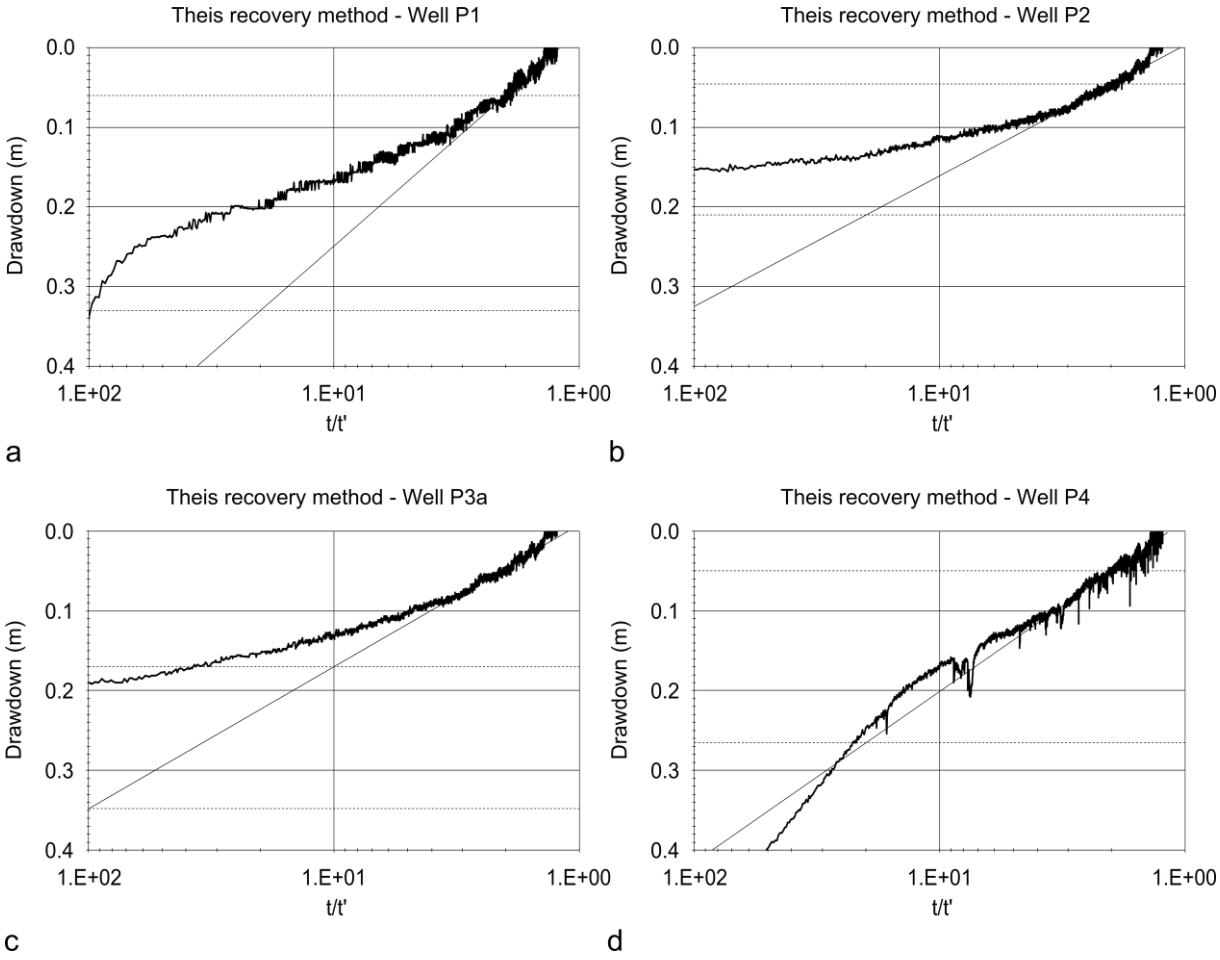

Figure B.10 Pump test at constant rate (Leuven case), Theis recovery method. **a**: well P1; **b**: well P2; **c**: well P3a; **d**: well P4.

Table B.4 Flowrate (Q) and aquifer properties for the Antwerp case derived by the Jacob's method and Theis recovery method.

	Δs	Q	Q	KD	D	K	K
	m	m^3/h	m^3/day	m^2/day	m	m/day	m/s
Jacob's method (procedure 1) - P1	0.25	3.53	84.6	63.20	17.8	3.55	4.11E-05
Jacob's method (procedure 1) - P2	0.12	3.53	84.6	134.65	17.8	7.56	8.76E-05
Jacob's method (procedure 1) - P3a	0.12	3.53	84.6	133.48	17.8	7.50	8.68E-05
Jacob's method (procedure 1) - P4	0.11	3.53	84.6	144.71	17.8	8.13	9.41E-05
Jacob's method (procedure 2)	0.50	3.53	84.6	61.45	17.8	3.45	4.00E-05
Jacob's method (procedure 3)	0.10	3.53	84.6	153.31	17.8	8.61	9.97E-05
Theis Recovery method - P1	0.27	3.53	84.6	57.35	17.8	3.22	3.73E-05
Theis Recovery method - P2	0.16	3.53	84.6	94.42	17.8	5.30	6.14E-05
Theis Recovery method - P3a	0.18	3.53	84.6	86.99	17.8	4.89	5.66E-05
Theis Recovery method - P4	0.22	3.53	84.6	72.02	17.8	4.05	4.68E-05

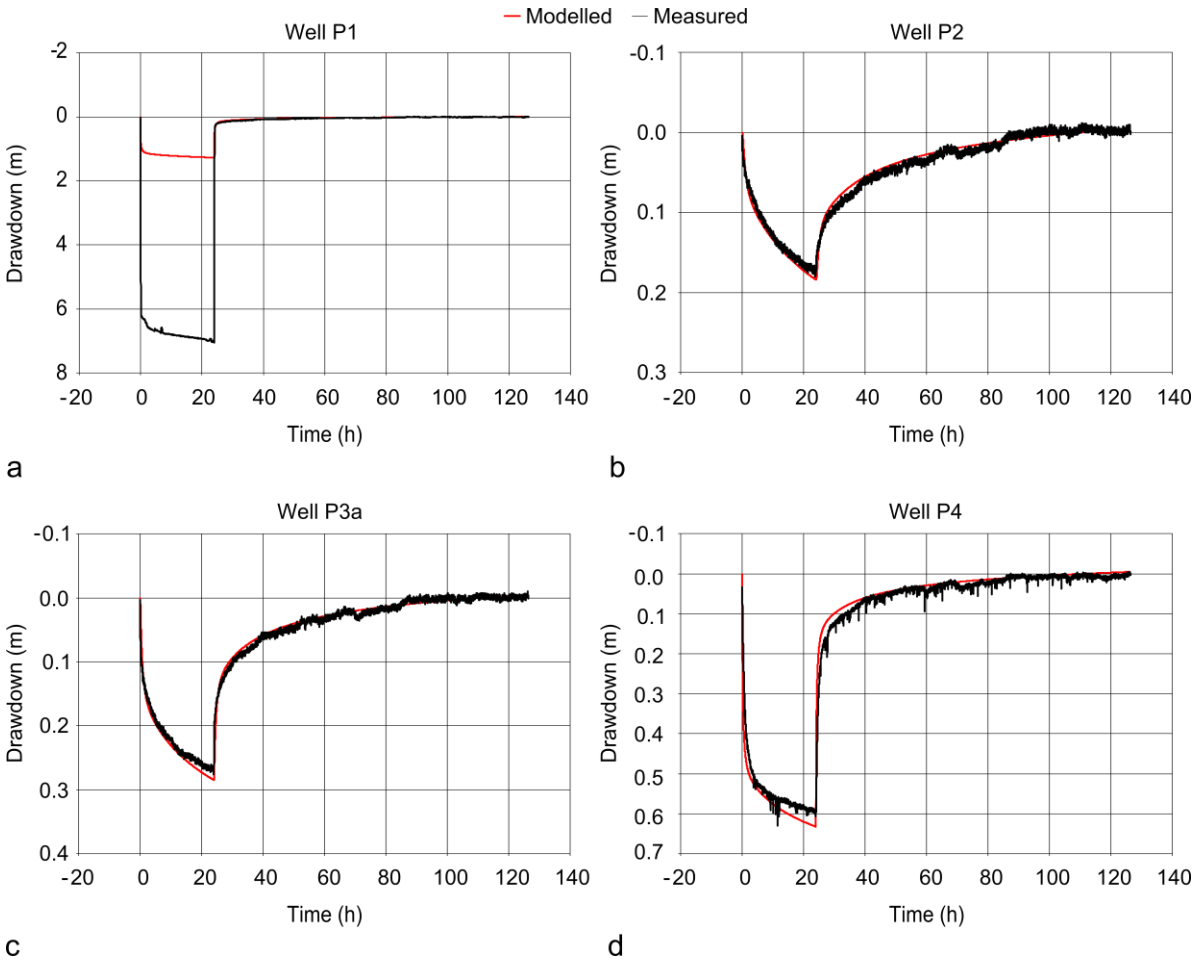

Figure B.11 Measured and modeled drawdown curve (Antwerp case). **a**: well P1; **b**: well P2; **c**: well P3a; **d**: well P4.

Table B.5 Model calibrated aquifer properties for the Antwerp case.

Layer	Top	Bottom	K_h	K_v	Specific storage	Effective porosity	Specific yield
	mbs	mbs	m d^{-1}	m d^{-1}	m^{-1}		
1	0	14	4.64	2.00	1.0E-03	0.05	0.05
2	14	24	4.64	2.00	1.0E-03	0.05	0.05

The values obtained with the Eden-Hazel method, Jacob's method and Theis recovery method give an indication of the hydraulic properties of the studied aquifers. These values were used as initial input in the numerical models in which they were optimized on the basis of model calibration. Model calibration was carried out by searching the best fit between the measured drawdown curves and the modeled drawdown curves by trial and error. The hydraulic properties obtained by this calibration are displayed in Tables B.2 and B.5 and are adopted in the reactive transport models.

Bibliography

Andrews, C.B., 1978. The impact of the use of heat pumps on ground-water temperatures. Ground Water 16, 437–443.

Appelo, C.A.J., de Vet, W.W.J.M., 2003. Modeling in situ iron removal from groundwater with trace elements such as As, in: Welch, A.H., Stollenwerk, K.G. (Eds.), Arsenic in Groundwater. Kluwer Academ., pp. 381–401.

Appelo, C.A.J., Drijver, B.C., Hekkenberg, R., de Jonge, M., 1999. Modeling in situ iron removal from ground water. Ground Water 37, 811–817.

Appelo, C.A.J., Griffioen, J., van der Weiden, M.J.J., 1990. IEA Annex VI: Environmental and chemical aspects of thermal energy storage in aquifers and research and development of water treatment methods; Subtask B: Geochemical reactions - Subtask Report.

Appelo, C.A.J., Postma, D., 2005. Geochemistry, groundwater and pollution, 2nd ed. CRC Press, 649p.

Arning, E., Kölling, M., Panteleit, B., Reichling, J., Schulz, H.D., 2006. Einfluss oberflächennaher wärmegewinnung auf geo-chemische prozesse im grundwasserleiter. Grundwasser 1, 27–39.

Bayer, P., Saner, D., Bolay, S., Rybach, L., Blum, P., 2012. Greenhouse gas emission savings of ground source heat pump systems in Europe: A review. Renew. Sustain. Energy Rev. 16, 1256–1267. doi:10.1016/j.rser.2011.09.027

Bonte, M., 2013. Impacts of shallow geothermal energy on groundwater quality - A hydrochemical and geomicrobial study of the effects of ground source heat pumps and aquifer thermal energy storage. PhD Thesis, Department of Earth Sciences, VU Amsterdam, 175p.

Bonte, M., Röling, W.F.M., Zaura, E., van der Wielen, P.W.J.J., Stuyfzand, P.J., van Breukelen, B.M., 2013a. Impacts of shallow geothermal energy production on redox processes and microbial communities. Environ. Sci. Technol. 47, 14476–84. doi:10.1021/es4030244

Bonte, M., Stuyfzand, P.J., Hulsmann, A., Van Beelen, P., 2011a. Underground Thermal Energy Storage : environmental risks and policy developments in the Netherlands and European Union. Ecol. Soc. 16, 22.

Bonte, M., Stuyfzand, P.J., Van Den Berg, G.A., Hijnen, W.A.M., 2011b. Effects of aquifer thermal energy storage on groundwater quality and the consequences for drinking water production: a case study from The Netherlands. Water Sci. Technol. 63, 1922–1931.

Bonte, M., van Breukelen, B.M., Stuyfzand, P.J., 2013b. Temperature-induced impacts on groundwater quality and arsenic mobility in anoxic aquifer sediments used for both drinking water and shallow geothermal energy production. Water Res. 47, 5088–5100. doi:10.1016/j.watres.2013.05.049

Bonte, M., Van Breukelen, B.M., Stuyfzand, P.J., 2013c. Environmental impacts of aquifer thermal energy storage investigated by field and laboratory experiments. J. Water Clim. Chang. 4, 77–89. doi:10.2166/wcc.2013.061

Bridger, D.W., Allen, D.M., 2010. Heat transport simulations in a heterogeneous aquifer used for aquifer thermal energy storage (ATES). Can. Geotech. J. 47, 96–115. doi:10.1139/T09-078

Bridger, D.W., Allen, D.M., 2013. Influence of geologic layering on heat transport and storage in an aquifer thermal energy storage system. Hydrogeol. J. 22, 233–250. doi:10.1007/s10040-013-1049-1

Brielmann, H., Griebler, C., Schmidt, S.I., Michel, R., Lueders, T., 2009. Effects of thermal energy discharge on shallow groundwater ecosystems. FEMS Microbiol. Ecol. 68, 273–86. doi:10.1111/j.1574-6941.2009.00674.x

Brielmann, H., Lueders, T., Schreglmann, K., Ferraro, F., Avramov, M., Hammerl, V., Blum, P., Bayer, P., Griebler, C., 2011. Oberflächennahe geothermie und ihre potenziellen auswirkungen auf grundwasserökosysteme. Grundwasser 16, 77–91. doi:10.1007/s00767-011-0166-9

Brons, H.J., Griffioen, J., Appelo, C.A.J., Zehnder, A.J.B., 1991. (Bio)geochemical reactions in aquifer material from a thermal energy storage site. Water Res. 25, 729–736. doi:10.1016/0043-1354(91)90048-U

Brown, C.J., Misut, P.E., 2010. Aquifer geochemistry at potential aquifer storage and recovery sites in coastal plain aquifers in the New York city area, USA. Appl. Geochemistry 25, 1431–1452. doi:10.1016/j.apgeochem.2010.07.001

Bustos Medina, D. a., Berg, G. a., Breukelen, B.M., Juhasz-Holterman, M., Stuyfzand, P.J., 2013. Iron-hydroxide clogging of public supply wells receiving artificial recharge: near-well and in-well hydrological and hydrochemical observations. Hydrogeol. J. 21, 1393–1412. doi:10.1007/s10040-013-1005-0

Caers, J., Zhang, T., 2004. Multiple-point geostatistics : a quantitative vehicle for integrating geologic analogs into Stanford University , Stanford Center for Reservoir Forecasting, in: Intergration of Outcrop and Modern Analog Data in Reservoir Models. AAPG Memoire 80. pp. 383–394.

Caljé, R.J., 2010. Future use of Aquifer Thermal Energy Storage below the historic centre of Amsterdam. Master Thesis, Department of Watermanagement, TU Delft, 79p.

Chiang, W.-H., 2010. Processing Modflow: an integrated modeling environment for the simulation of groundwater flow, transport and reactive processes. Simcore Software.

Chiang, Y.-C., Chiang, P.-C., Huang, C.-P., 2001. Effects of pore structure and temperature on VOC adsorption on activated carbon. Carbon N. Y. 39, 523–534. doi:10.1016/S0008-6223(00)00161-5

Coetsiers, M., Van Camp, M., Walraevens, K., 2004. Influence of the former marine conditions on groundwater quality in the Neogene phreatic aquifer, Flanders, in: Proceedings 18th Sea Water Intrusion Meeting (SWIM), Cartagena (Spain). pp. 499–509.

Coetsiers, M., Van Camp, M., Walraevens, K., 2014. Neogeen pakket van watervoerende lagen (Mioceen, Plio-Pleistoceen, Complex van de Kempen), in: Dassargues, A., Walraevens, K. (Eds.), Watervoerende Lagen en Grondwater in België - Aquifères et Eaux Souterraines en Belgique. Academia Press, Ghent, p. XXIV + 455 p.

Comunian, A., Renard, P., Straubhaar, J., Bayer, P., 2011. Three-dimensional high resolution fluvio-glacial aquifer analog – Part 2: Geostatistical modeling. J. Hydrol. 405, 10–23. doi:10.1016/j.jhydrol.2011.03.037

Cooper, H.H., Jacob, C.E., 1946. A generalized graphical method for evaluating formation constants and summarizing well field history. Am. Geophys. Union Trans. 27, 526–534.

De Marsily, G., 1986. Quantitative hydrogeology. Academic Press, Orlando, USA, 440p.

dell'Arciprete, D., Bersezio, R., Felletti, F., Giudici, M., Comunian, A., Renard, P., 2011. Comparison of three geostatistical methods for hydrofacies simulation: a test on alluvial sediments. Hydrogeol. J. 20, 299–311. doi:10.1007/s10040-011-0808-0

Descourvières, C., Hartog, N., Patterson, B.M., Oldham, C., Prommer, H., 2010. Geochemical controls on sediment reactivity and buffering processes in a heterogeneous aquifer. Appl. Geochemistry 25, 261–275. doi:10.1016/j.apgeochem.2009.11.012

Dinkla, I., Lieten, S., Drijver, B., Hartog, N., 2012. Meer Met Bodemenergie, Effecten op de ondergrond - Effecten van bodemenergiesystemen op de geochemie en biologie in praktijk. Resultaat metingen op pilotstudies en labtesten. Bioclear, IF Technology, Deltares and Wageningen University.

DOV, 2014. Databank Ondergrond Vlaanderen [WWW Document]. URL http://dov.vlaanderen.be (accessed 3.19.14).

Drijver, B.C., 2011. High Temperature Aquifer Thermal Energy Storage (HT-ATES): water treatment in practice, in: 1e Nationaal Congres Bodemenergie - Utrecht, Nederland, 13 - 14 Oktober 2011. p. 5.

Drijver, B.C., Willemsen, A., 2004. Temperatuureffecten op grondwaterkwaliteit. IFTechnology, Arnhem.

Eckert, P., Appelo, C.A.J., 2002. Hydrogeochemical modeling of enhanced benzene, toluene, ethylbenzene, xylene (BTEX) remediation with nitrate. Water Resour. Res. 38, 5–1 – 5–11. doi:10.1029/2001WR000692

Eden, R.N., Hazel, C.P., 1973. Computer and graphical analysis of variable discharge pumping test of wells. Civ. Eng. Trans. Inst. Eng. Aust. 5–10.

Engesgaard, P., Kipp, K.L., 1992. A geochemical transport model for redox-controlled movement of mineral fronts in groundwater flow systems: A case of nitrate removal by oxidation of pyrite. Water Resour. Res. doi:10.1029/92WR01264

EU-WFD, 2000. European Water Framework Directive, 2000/60/EC. European Parliament.

Ferguson, G., 2007. Heterogeneity and thermal modeling of ground water. Ground Water 45, 485–90. doi:10.1111/j.1745-6584.2007.00323.x

Fossoul, F., Orban, P., Dassargues, A., 2011. Numerical simulation of heat transfer associated with low enthalpy geothermal pumping in an alluvial aquifer. Geol. Belgica 14, 45–54.

Gao, Q., Li, M., Yu, M., Spitler, J.D., Yan, Y.Y., 2009. Review of development from GSHP to UTES in China and other countries. Renew. Sustain. Energy Rev. 13, 1383–1394. doi:10.1016/j.rser.2008.09.012

Griffioen, J., Appelo, C.A.J., 1993. Nature and extent of carbonate precipitation during aquifer thermal energy storage. Appl. Geochemistry 8, 161–176. doi:10.1016/0883-2927(93)90032-C

Gringarten, A.C., Sauty, J.P., 1975. A theoretical study of heat extraction from aquifers with uniform regional flow. J. Geophys. Res. doi:10.1029/JB080i035p04956

Gulinck, M., Hacquaert, A., 1954. L'Eocène, in: Prodrôme D'une Description Géologique de La Belgique. pp. 451–493.

Gullentops, F., Bogemans, F., Moor, G. De, Paulissen, E., Pissart, A., 2001. Quaternary lithostratigraphic units (Belgium). Geol. Belgica 4, 153–164.

Hähnlein, S., Bayer, P., Ferguson, G., Blum, P., 2013. Sustainability and policy for the thermal use of shallow geothermal energy. Energy Policy 59, 914–925. doi:10.1016/j.enpol.2013.04.040

Halford, K.J., Hanson, R.T., 2002. User Guide for the drawdown-limited , multi-node well (MNW) package for the U.S. Geological Survey's modular three-dimensional finite-difference ground-water flow model,

Versions MODFLOW-96 and MODFLOW-2000. U.S. Geological Survey, 33p.

Hall, E.K., Neuhauser, C., Cotner, J.B., 2008. Toward a mechanistic understanding of how natural bacterial communities respond to changes in temperature in aquatic ecosystems. ISME J. 2, 471–81. doi:10.1038/ismej.2008.9

Hanna Instruments, 2012. Ph and ORP electrodes. 44p.

Harbaugh, A.W., Banta, E.R., Hill, M.C., Mcdonald, M.G., 2000. MODFLOW-2000, The U.S. Geological Survey modular ground-water Model — User guide to modularization concepts and the ground-water flow process. U.S. Geological Survey, 121p.

Hartog, N., 2011. Anticipated temperature effects on biogeochemical reaction rates in seasonal Aquifer Thermal Energy Storage (ATES) systems: an evaluation using the Arrhenius equation, in: 1e Nationaal Congres Bodemenergie - Utrecht, Nederland, 13 - 14 Oktober 2011. p. 5.

Hartog, N., Drijver, B., Dinkla, I., Bonte, M., 2013. Field assessment of the impacts of Aquifer Thermal Energy Storage (ATES) systems on chemical and microbial groundwater composition, in: European Geothermal Congress. p. 8.

Hartog, N., Griffioen, J., van der Weijden, C.H., 2002. Distribution and reactivity of O2-reducing components in sediments from a layered aquifer. Environ. Sci. Technol. 36, 2338–44.

Hecht-Méndez, J., Molina-Giraldo, N., Blum, P., Bayer, P., 2010. Evaluating MT3DMS for heat transport simulation of closed geothermal systems. Ground Water 48, 741–56. doi:10.1111/j.1745-6584.2010.00678.x

Heidemij, 1987. Well clogging at heat storage in shallow aquifers (in Dutch). Beop cooperation agreement nr. 54202-20.13-I.4.18.

Hidalgo, J.J., Carrera, J., Dentz, M., 2009. Steady state heat transport in 3D heterogeneous porous media. Adv. Water Resour. 32, 1206–1212. doi:10.1016/j.advwatres.2009.04.003

Holm, T.R., Eisenreich, S.J., Rosenberg, H.L., Holm, N.P., 1987. Groundwater geochemistry of short-term aquifer thermal energy storage test cycles. Water Resour. Res. 23, 1005. doi:10.1029/WR023i006p01005

Houben, G., 2001. Well ageing and its implications for well and piezometer performance, in: Impact of Human Activity on Groundwater Dynamics (Proceedings of a Symposium Held during the Sixth IAHS Scientific Assemby at Maastricht, The Netherlands. pp. 297–300.

Houben, G.J., 2003. Iron oxide incrustations in wells. Part 1: genesis, mineralogy and geochemistry. Appl. Geochemistry 18, 927–939. doi:10.1016/S0883-2927(02)00242-1

Houben, G.J., 2004. Modeling the buildup of iron oxide encrustations in wells. Ground Water 42, 78–82.

Houben, G.J., 2006. The influence of well hydraulics on the spatial distribution of well incrustations. Ground Water 44, 668–75. doi:10.1111/j.1745-6584.2006.00216.x

Houben, G.J., Weihe, U., 2010. Spatial distribution of incrustations around a water well after 38 years of use. Ground Water 48, 53–58. doi:10.1111/j.1745-6584.2009.00641.x

Houthuys, R., 1990. Afzettingstructuur van de zanden van Brussel. Aardkundige Mededelingen, vol. 5. Leuven University Press, 137p.

Houthuys, R., 2011. A sedimentary model of the Brussels Sands , Eocene , Belgium. Geol. Belgica 14, 55–74.

Hoyer, M., Hallgren, J., Eisenreich, S., Sterling, R., 1994. Field-test results of Aquifer Thermal Energy Storage at St. Paul, Minnesota. J. Energy Eng. 120, 67–85.

Hsieh, P.A., Freckleton, J.R., 1993. Documentation of a computer program to simulate horizontal-flow barriers using the U.S. Geological Survey's modular three-dimensional finite-difference ground-water flow model. U.S. Geological Survey Open File, Report 92-477, 32p.

Hu, L.Y., Chugunova, T., 2008. Multiple-point geostatistics for modeling subsurface heterogeneity: A comprehensive review. Water Resour. Res. doi:10.1029/2008WR006993

Huysmans, M., Dassargues, A., 2009. Application of multiple-point geostatistics on modelling groundwater flow and transport in a cross-bedded aquifer (Belgium). Hydrogeol. J. 17, 1901–1911. doi:10.1007/s10040-009-0495-2

Huysmans, M., Dassargues, A., 2011. Direct multiple-point geostatistical simulation of edge properties for modeling thin irregularly shaped surfaces. Math. Geosci. 43, 521–536. doi:10.1007/s11004-011-9336-7

Huysmans, M., Dassargues, A., 2012. Modeling the effect of clay drapes on pumping test response in a cross-bedded aquifer using multiple-point geostatistics. J. Hydrol. 450-451, 159–167. doi:10.1016/j.jhydrol.2012.05.014

Huysmans, M., Peeters, L., Moermans, G., Dassargues, A., 2008. Relating small-scale sedimentary structures and permeability in a cross-bedded aquifer. J. Hydrol. 361, 41–51. doi:10.1016/j.jhydrol.2008.07.047

IEA, 2014. International Energy Agency [WWW Document]. URL http://www.iea.org (accessed 8.13.14).

IFTechnology, 2006. Kansenkaart ondergrondse energieopslag. Gemeente Nijmegen. Arnhem, 50p.

Jenne, E.A., Andersson, O., Willemsen, A., 1992. Well, hydrology, and geochemistry problems encountered in ATES systems and their solutions, in: Intersociety Energy Conversion Engineering Conference, San Diego, CA (United States). Pacific Northwest Laboratory, Richland, Washington, p. 21.

Jesußek, A., Grandel, S., Dahmke, A., 2012. Impacts of subsurface heat storage on aquifer hydrogeochemistry. Environ. Earth Sci. 69, 1999–2012. doi:10.1007/s12665-012-2037-9

Kennedy, P.L., Woodbury, A.D., 2002. Geostatistics and Bayesian updating for transmissivity estimation in a multiaquifer system in Manitoba, Canada. Ground Water 40, 273–283. doi:10.1111/j.1745-6584.2002.tb02655.x

Knoche, G., Koch, M., Metzger, J.W., 2003. Scaling-tests on groundwater for use in high-temperature-ATES in respect to calcite precipitates in heat exchangers, in: Proceedings Futurestock 2003, Warsaw, Poland.

Kohfahl, C., Massmann, G., Pekdeger, A., 2008. Sources of oxygen flux in groundwater during induced bank filtration at a site in Berlin, Germany. Hydrogeol. J. 17, 571–578. doi:10.1007/s10040-008-0389-8

Koltermann, C.E., Gorelick, S.M., 1996. Heterogeneity in sedimentary deposits: a review of structure-imitating, process-imitating, and descriptive approaches. Water Resour. Res. doi:10.1029/96WR00025

Kruseman, G.P., de Ridder, N.A., 1991. Analysis and evaluation of pumping test data. doi:10.1016/0022-1694(71)90015-1

Laga, P., Louwye, S., Geets, S., 2001. Paleogene and Neogene lithostratigraphic units (Belgium). Geol. Belgica 4, 135–152.

Lerm, S., Alawi, M., Miethling-Graff, R., Wolfgramm, M., Rauppach, K., Seibt, A., Würdemann, H., 2011. Influence of microbial processes on the operation of a cold store in a shallow aquifer: impact on well injectivity and filter lifetime. Grundwasser 16, 93–104. doi:10.1007/s00767-011-0165-x

Lerm, S., Westphal, A., Miethling-Graff, R., Alawi, M., Seibt, A., Wolfgramm, M., Würdemann, H., 2013. Thermal effects on microbial composition and microbiologically induced corrosion and mineral precipitation affecting operation of a geothermal plant in a deep saline aquifer. Extremophiles 17, 311–27. doi:10.1007/s00792-013-0518-8

Li, H., Caers, J., 2011. Geological modelling and history matching of multi-scale flow barriers in channelized reservoirs: methodology and application. Pet. Geosci. doi:10.1144/1354-079309-825

Lund, J., Sanner, B., Rybach, L., Curtis, R., Hellström, G., 2004. Geothermal (ground-source) heat pumps a world overview. GHC Bull. 10pp.

Lund, J.W., Bertani, R., 2010. Worldwide geothermal utilization 2010, in: Geothermal Resources Council Annual Meeting 2010, Sacramento, 24-27 October 2010. pp. 182–185.

Lund, J.W., Freeston, D.H., Boyd, T.L., 2011. Direct utilization of geothermal energy 2010 worldwide review. Geothermics 40, 159–180. doi:10.1016/j.geothermics.2011.07.004

Maire, P., Blunier, P., Parriaux, A., Tacher, L., 2006. Underground planning and optimization of the underground resources'combination looking for sustainable development in urban areas.

Meyer, C.F., Todd, D.K., 1973. Conserving energy with heat storage wells. Environ. Sci. Technol. 7, 512–516. doi:10.1021/es60078a009

Michel, F.A., 2009. Utilization of abandoned mine workings for thermal energy storage in Canada, in: Effstock Conference - Thermal Energy Storage for Efficiency and Sustainability, Stockholm.

Mikes, D., 2006. Sampling procedure for small-scale heterogeneities (crossbedding) for reservoir modelling. Mar. Pet. Geol. 23, 961–977. doi:10.1016/j.marpetgeo.2005.06.006

Miotliński, K., 2008. Coupled reactive transport modeling of redox processes in a nitrate-polluted sandy aquifer. Aquat. Geochemistry 14, 117–131. doi:10.1007/s10498-008-9028-1

Morton, K., Thomas, S., Corbett, P., Davies, D., 2002. Detailed analysis of probe permeameter and interval pressure transient test permeability measurements in a heterogeneous reservoir. Pet. Geosci. doi:10.1144/petgeo.8.3.209

Mustafa Omer, A., 2008. Ground-source heat pumps systems and applications. Renew. Sustain. Energy Rev. 12, 344–371. doi:10.1016/j.rser.2006.10.003

N.V.O.E., 2006. Werkwijzen en richtlijnen ondergrondse energieopslag. Woerden.

Palmer, C.D., Blowes, D.W., Frind, E.O., Molson, J.W., 1992. Thermal energy storage in an unconfined aquifer: 1. Field Injection Experiment. Water Resour. Res. 28, 2845. doi:10.1029/92WR01471

Palmer, C.D., Cherry, J.A., 1984. Geochemical reactions associated with low-temperature thermal-energy storage in aquifers. Can. Geotech. J. 21, 475–488.

Parkhurst, B.D.L., Appelo, C.A.J., 1999. User's guide to PHREEQC (version 2) - A computer program for speciation, and inverse geochemical calculations.

Peeters, L., 2014. Brusseliaan Aquifer - Sables bruxelliens, in: Dassargues, A., Walraevens, K. (Eds.), Watervoerende Lagen en Grondwater in België - Aquifères et Eaux Souterraines en Belgique. Academia Press, Ghent, p. XXIV + 455 p.

Perlinger, J.A., Almendinger, J.E., Urban, N.R., Eisenreich, S.J., 1987. Groundwater geochemistry of aquifer thermal energy storage: long-term test cycle. Water Resour. Res. 23, 2215. doi:10.1029/WR023i012p02215

Possemiers, M., Huysmans, M., Peeters, L., Batelaan, O., Dassargues, A., 2012. Relationship between sedimentary features and permeability at different scales in the Brussels Sands. Geol. Belgica 15, 156–164.

Postma, D., Boesen, C., Kristiansen, H., Larsen, F., 1991. Nitrate reduction in an unconfined sandy aquifer: water chemistry, reduction processes, and geochemical modeling. Water Resour. Res. 27, 2027–2045.

Prommer, H., Barry, D., Davis, G., 2000. Numerical modelling for design and evaluation of groundwater remediation schemes. Ecol. Modell. 128, 181–195. doi:10.1016/S0304-3800(99)00230-6

Prommer, H., Post, V., 2010. PHT3D - A reactive multicomponent transport model for saturated porous media.

Prommer, H., Stuyfzand, P.J., 2005. Identification of temperature-dependent water quality changes during a deep well injection experiment in a pyritic aquifer. Environ. Sci. Technol. 39, 2200–9.

Pyne, R.D.G., 2005. Aquifer Storage and Recovery — A guide to groundwater recharge through wells, 2nd ed. ASR Systems, Gainesville, Florida, 608p.

Ringrose, P.S., Sorbie, K.S., Corbett, P.W.M., Jensen, J.L., 1993. Immiscible flow behaviour in laminated and cross-bedded sandstones. J. Pet. Sci. Eng. 9, 103–124. doi:10.1016/0920-4105(93)90071-L

Rodrigo-Ilarri, J., Jin, S., Blum, P., Bayer, P., Grathwohl, P., 2010. Geostatistical characterisation of heterogeneous aquifers for the application of open shallow geothermal systems, in: II Congreso de Energía Geotérmica En La Edificación Y La Industria. pp. 75–82.

Rodrigo-Ilarri, J., Reisinger, M., Jaime Gómez-Hernández, J., 2014. Influence of heterogeneity on heat transport simulations in shallow geothermal systems, in: 10th Conference on Geostatistics for Environmental Applications (geoEnv 2014), 9-11 July, Paris, France.

Rybach, L., 2010. Status and prospects of geothermal energy, in: Proceedings of World Geothermal Congress. Bali, Indonesia. p. 5.

Sanner, B., Karytsas, C., Mendrinos, D., Rybach, L., 2003. Current status of ground source heat pumps and underground thermal energy storage in Europe. Geothermics 32, 579–588. doi:10.1016/S0375-6505(03)00060-9

Sanz, E., Ayora, C., Carrera, J., Upstream, E., 2011. Calcite dissolution by mixing waters : geochemical modeling and flow-through experiments 9, 67–77. doi:10.1344/105.000001652

Snijders, A.L., 1991. IEA energy storage programme - Annex VI: "Environmental and chemical aspects of ATES and research and development of water treatment methods," in: Proceedings Thermastock '91, Scheveningen, The Netherlands.

Snijders, A.L., 1994. ATES: water treatment and environmental impacts., in: Proceedings Calorstock '94. Espoo, Finland.

Sommer, W., Valstar, J., van Gaans, P., Grotenhuis, T., Rijnaarts, H., 2013. The impact of aquifer heterogeneity on the performance of aquifer thermal energy storage. Water Resour. Res. 49, 8128–8138. doi:10.1002/2013WR013677

Sommer, W.T., Doornenbal, P.J., Drijver, B.C., Gaans, P.F.M., Leusbrock, I., Grotenhuis, J.T.C., Rijnaarts, H.H.M., 2014. Thermal performance and heat transport in aquifer thermal energy storage. Hydrogeol. J. 22, 263–279. doi:10.1007/s10040-013-1066-0

Sowers, L., York, K.P., Stiles, L., 2006. Impact of thermal buildup on groundwater chemistry and aquifer microbes, in: Proceedings of Ecostock 2006. Pomona, New Jersey, 31st May-2nd June 2006, pp. 1–7.

Strebelle, S., 2002. Conditional simulation of complex geological structures using multiple-point statistics. Math. Geol. 34, 1–21.

Stright, L., 2006. Modeling, upscaling, and history matching thin, irregularly-shaped flow barriers: a comprehensive approach for predicting reservoir connectivity, in: SPE, Student Paper 106528. p. 8.

Stuyfzand, P.J., 1986. A new hydrochemical classification of watertypes: principles and application to the coastal dunes aquifer system of the Netherlands, in: Proceedings 9th Sea Water Intrusion Meeting (SWIM), Delft (The Netherlands). pp. 641–656.

TCB, 2009. Advies Duurzaam gebruik van de bodem voor WKO. Technische Commissie Bodem (TCB), Den Haag.

Theis, C.V., 1935. The relation between the lowering of the piezometric surface and the rate and duration of discharge of a well using groundwater storage. Am. Geophys. Union Trans. 16, 519–524.

Thorne, D., Langevin, C.D., Sukop, M.C., 2006. Addition of simultaneous heat and solute transport and variable fluid viscosity to SEAWAT. Comput. Geosci. 32, 1758–1768. doi:10.1016/j.cageo.2006.04.005

Thullner, M., Schäfer, W., 1999. Modeling of a field experiment on bioremediation of chlorobenzenes in groundwater. Bioremediat. J. 3, 247–267. doi:10.1080/10889869991219352

TNO, 1990. Hydrochemisty and energy storage in aquifers. TNO Committee on Hydrological Research, Den Haag.

Unterberger, W., Hofinger, H., Markiewicz, R., Adam, D., 2005. Running hot and cold in Vienna. Tunnels Tunn. Int. 37, 36–39.

Van Beek, C.G., 2010. Cause and prevention of clogging of wells abstracting groundwater from unconsolidated aquifers. PhD Thesis, Department of Earth Sciences, VU Amsterdam, 203p.

Van Beek, C.G., 2012. Cause and prevention of abstraction well clogging: diagnosing potential supply problems. Water21 14.2, 51–53.

Van Beek, C.G., Kooper, W.F., 1980. The clogging of shallow discharge wells in the Netherlands River Region. Ground Water 18, 578–586.

Van Beek, C.G.E.M., Hiemstra, T., Hofs, B., Nederlof, M.M., Van Paassen, J.A.M., Reijnen, G.K., 2012. Homogeneous, heterogeneous and biological oxidation of iron(II) in rapid sand filtration. J. water supply Res. Technol. 61, 1–13.

Van Halem, D., Heijman, S.G.J., Johnston, R., Huq, I.M., Ghosh, S.K., Verberk, J.Q.J.C., Amy, G.L., van Dijk, J.C., 2010. Subsurface iron and arsenic removal: low-cost technology for community-based water supply in Bangladesh. Water Sci. Technol. 62, 2702–9. doi:10.2166/wst.2010.463

Van Halem, D., Moed, D.H., Verberk, J.Q.J.C., Amy, G.L., van Dijk, J.C., 2012. Cation exchange during subsurface iron removal. Water Res. 46, 307–15. doi:10.1016/j.watres.2011.10.015

Van Halem, D., Vet, W. De, Verberk, J., Amy, G., van Dijk, H., 2011. Characterization of accumulated precipitates during subsurface iron removal. Appl. Geochemistry 26, 116–124. doi:10.1016/j.apgeochem.2010.11.008

Van Oostrom, N., Drijver, B., van Baaren, S., Lieten, S., van Nieuwkerk, E., de Vries, E., Bakr, M., Hartog, N., Krajenbrink, H., Mathijsen, W., Meindertsma, G., Oude Essink, G., Wennekes, R., Woning, M., 2010. Literatuurstudie Meer Met Bodemenergie, Overzicht van kennis en onderzoeksvragen rondom warmte- en koudeopslag. Bioclear, IF Technology, Deltares and Wageningen University, 253p.

Vetter, A., Mangelsdorf, K., Wolfgramm, M., Rauppach, K., Schettler, G., Vieth-Hillebrand, A., 2012. Variations in fluid chemistry and membrane phospholipid fatty acid composition of the bacterial community in a cold storage groundwater system during clogging events. Appl. Geochemistry 27, 1278–1290. doi:10.1016/j.apgeochem.2012.02.022

Wallis, I., Prommer, H., Pichler, T., Post, V., Norton, S.B., Annable, M.D., Simmons, C.T., 2011. Process-based reactive transport model to quantify arsenic mobility during aquifer storage and recovery of potable water. Environ. Sci. Technol. 45, 6924–31. doi:10.1021/es201286c

Ward, J.D., Simmons, C.T., Dillon, P.J., 2007. A theoretical analysis of mixed convection in aquifer storage and recovery: How important are density effects? J. Hydrol. 343, 169–186. doi:10.1016/j.jhydrol.2007.06.011

Willemsen, A., Appelo, C.A.J., 1985. Chemical reactions during heat storage in shallow aquifers in the Netherlands: Laboratory experiments and geochemical modelling, in: Hydrogeology in the Service of Man, Mémoires of the 18th Congress of the International Association of Hydrogeologists, Cambridge. pp. 68–78.

Williamson, M.A., Rimstidt, J.D., 1994. The kinetics and electrochemical rate-determining step of aqueous pyrite oxidation. Geochim. Cosmochim. Acta 58, 5443–5454.

Willis, B.J., White, C.D., 2000. Quantitative outcrop data for flow simulation. J. Sediment. Res. 70, 788–802. doi:10.1306/2DC40938-0E47-11D7-8643000102C1865D

Woodbury, A.D., Sudicky, E.A., 1991. The geostatistical characteristics of the borden aquifer. Water Resour. Res. 27, 533–546. doi:10.1029/90WR02545

Xu, T., Apps, J. a., Pruess, K., 2001. Analysis of mineral trapping for CO2 disposal in deep aquifers. doi:10.2172/789133

Zheng, C., 2010. MT3DMS v5.3 supplemental user's guide. Department of Geological Sciences, The University of Alabama, p.51.

Zheng, C., Gorelick, S.M., 2003. Analysis of solute transport in flow fields influenced by preferential flowpaths at the decimeter scale. Ground Water 41, 142–155.

Zheng, C., Wang, P.P., 1999. MT3DMS: a modular three-dimensional multispecies transport model. Documentation and user's guide. U.S. Army Corps of Engineers.

Zhu, K., Blum, P., Ferguson, G., Balke, K.-D., Bayer, P., 2011. The geothermal potential of urban heat islands. Environ. Res. Lett. 5, 6. doi:10.1088/1748-9326/6/1/019501

Zuurbier, K., 2011. Effecten Warmte-Koude-Opslagsystemen (WKO) op met gechloreerde koolwaterstoffen verontreinigde grondwatersystemen.

Master Thesis, Deltares - VU Amsterdam, 146p.

Zuurbier, K., Hartog, N., Valstar, J., Post, V., van Breukelen, B., 2013. The impact of low-temperature seasonal aquifer thermal energy storage (SATES) systems on chlorinated solvent contaminated groundwater: Modeling of spreading and degradation. J. Contam. Hydrol. 147, 1–13.

FACULTY OF SCIENCE
DEPARTMENT OF EARTH AND ENVIRONMENTAL SCIENCES
GEOLOGY DIVISION
Celestijnenlaan 200E
B-3001 HEVERLEE, BELGIUM
tel. + 32 16 32 78 00
balie@ees.kuleuven.be
www.aow.kuleuven.be